

(NASA-CR-140568) OBSERVATIONS OF HYDROGEN  
AND HELIUM ISOTOPES IN SOLAR COSMIC RAYS  
Ph.D. Thesis (California Inst. of Tech.)  
135 p HC \$9.75

N74-35215

CSSL 03B

G3/29    Unclass  
51068

CALIFORNIA INSTITUTE OF TECHNOLOGY

PASADENA, CALIFORNIA



OBSERVATIONS OF  
HYDROGEN AND HELIUM ISOTOPES IN  
SOLAR COSMIC RAYS

Thesis by  
Gordon James Hurford

SRL 74-3

October 1974

OBSERVATIONS OF  
HYDROGEN AND HELIUM ISOTOPES IN  
SOLAR COSMIC RAYS

Thesis by  
Gordon James Hurford

In Partial Fulfillment of the Requirements  
for the Degree of  
Doctor of Philosophy

California Institute of Technology  
Pasadena, California

1975

(Submitted October 1, 1974)

## ACKNOWLEDGEMENTS

A great many people have contributed their time and talent to the work described in this thesis and to the success of the IMP-7 experiment on which it is based. Although I am indebted to them all, it is to Dr. Edward Stone to whom I owe the most. As principal investigator, the experiment would not have existed without his efforts spanning over eight years. As my supervisor, his unfailing patience has been appreciated many times and his sound judgement has been invaluable.

I am also grateful to Dr. Rochus Vogt, co-investigator, not only for his efforts on behalf of the project, but also for his advice and interest over the years.

Bill Althouse, project engineer, deserves much of the credit for the successful post launch operation of the experiment. I have also valued his insights into the worlds of electronics and administration.

The IMP-7 experiment and this thesis have benefitted in many ways from the comments and contributions of Jim Brown, Tom Garrard, Steward Hartman, John Lupton, Frank Marshall, Dick Mewaldt, Sol Vidor and Mark Wiedenbeck.

One of the pleasures of this work has been the opportunity to work with a succession of enthusiastic and talented undergraduates. The data processing, in particular, has benefitted from the efforts of Mark Bleck, Max Kay, Bob Offerman, Alex Petruncola, Gary Pope,

Kevin Ruddell, Hubert Shen, Bob Sullivan, Pat Tressel and Curt Widdoes. The early stages of the data reduction have been capably handled by Ellen Aguilar and Florence Pickett while Hannah Fox has developed some of the basic software.

The hospitality and assistance of Dr. C. Barnes and Dr. H. B. Mak with the calibrations at the Kellogg Tandem Accelerator is appreciated. I thank Dr. James Mayer for valuable conversations concerning the channeling problem. Dr. Pol Duwez graciously assisted with the Laué diffraction measurements of the detectors. I thank Drs. R. Ramaty and B. Kozlovsky of G.S.F.C. for valuable conversations and a copy of their calculations of the production of rare isotopes.

Analog Technology Corporation was responsible for the detailed design and fabrication of the experiment.

I gratefully acknowledge financial assistance from the National Research Council of Canada and the California Institute of Technology.

Finally I would like to thank my wife, Sheryl, for her patience over the years and critical typing of the rough draft of the manuscript.

This work has been supported by NASA under NAS 5 - 11066 and NGR-05-002-160.

## ABSTRACT

The isotopic composition of hydrogen and helium in solar cosmic rays provides a means of studying solar flare particle acceleration mechanisms since the enhanced relative abundance of rare isotopes, such as  $^2\text{H}$ ,  $^3\text{H}$  and  $^3\text{He}$ , is due to their production by inelastic nuclear collisions in the solar atmosphere during the flare. In this work the Caltech Electron/Isotope Spectrometer on the IMP-7 spacecraft has been used to measure this isotopic composition. The response of the  $dE/dx$ -E particle telescope is discussed and alpha particle channeling in thin detectors is identified as an important background source affecting measurement of low values of  $(^3\text{He}/^4\text{He})$ .

The following flare-averaged results are obtained for the period, October, 1972 - November, 1973:  $(^2\text{H}/^1\text{H}) = 7_{-6}^{+10} \times 10^{-6}$  (1.6 - 8.6 MeV/nuc),  $(^3\text{H}/^1\text{H}) < 3.4 \times 10^{-6}$  (1.2 - 6.8 MeV/nuc),  $(^3\text{He}/^4\text{He}) = (9 \pm 4) \times 10^{-3}$ ,  $(^3\text{He}/^1\text{H}) = (1.7 \pm 0.7) \times 10^{-4}$  (3.1 - 15.0 MeV/nuc). The deuterium and tritium ratios are significantly lower than the same ratios at higher energies, suggesting that the deuterium and tritium spectra are harder than that of the protons. They are, however, consistent with the same thin target model relativistic path length of  $\sim 1 \text{ g/cm}^2$  (or equivalently  $\sim 0.3 \text{ g/cm}^2$  at 30 MeV/nuc) which is implied by the higher energy results. The  $^3\text{He}$  results, consistent with previous observations, would imply a path length at least 3 times as long, but the observations may be contaminated by small  $^3\text{He}$  rich solar events.

During 1973 three " $^3\text{He}$  rich events," containing much more  $^3\text{He}$  than  $^2\text{H}$  or  $^3\text{H}$  were observed on 14 February, 29 June and 5 September.

Although the total production cross sections for  $^2\text{H}$ ,  $^3\text{H}$  and  $^3\text{He}$  are comparable, an upper limit to  $(^2\text{H}/^3\text{He})$  and  $(^3\text{H}/^3\text{He})$  was 0.053 (2.9-6.8 MeV/nuc), summing over the three events. This upper limit is marginally consistent with Ramaty and Kozlovsky's thick target model which accounts for such events by the nuclear reaction kinematics and directional properties of the flare acceleration process. The 5 September event was particularly significant in that much more  $^3\text{He}$  was observed than  $^4\text{He}$  and the fluxes of  $^3\text{He}$  and  $^1\text{H}$  were about equal. The range of  $(^3\text{He}/^4\text{He})$  for such events reported to date is 0.2 to  $\sim 6$  while  $(^3\text{He}/^1\text{H})$  extends from  $10^{-3}$  to  $\sim 1$ . The role of backscattered and mirroring protons and alphas in accounting for such variations is discussed.

## TABLE OF CONTENTS

<u>PART</u>	<u>TITLE</u>	<u>PAGE</u>
I.	INTRODUCTION	1
II.	EXPERIMENT	5
	A. Spacecraft	5
	B. Telescope and Telemetry	5
	C. Nominal Isotope Response	12
	D. Mass Resolution	16
	E. Background	22
	F. Calibration	29
III.	OBSERVATIONS AND RESULTS	37
	A. Introduction	37
	B. List of Solar Active Periods	37
	C. Establishment of Isotopic Ratios	40
	D. Flare Sum--Deuterium and Tritium	43
	E. Flare Sum--Helium 3	49
	F. Helium 3 Rich Flares	53
IV.	DISCUSSION OF RESULTS	60
	A. Comparison of Results	60
	B. Flare Models	70
	C. Interpretation of Flare-Averaged Results	74
	D. Helium 3 Rich Flares	77
V.	SUMMARY AND CONCLUSIONS	85

<u>PART</u>	<u>TITLE</u>	<u>PAGE</u>
Appendix A--	DATA REDUCTION	87
Appendix B--	CALCULATION OF ENERGY SPECTRA	94
Appendix C--	THE EFFECT OF CHANNELING ON THE RESPONSE TO ALPHA PARTICLES	103
	1. Introduction	103
	2. Channeling Experiment	104
	3. Application to Flight Data	114
Appendix D--	ESTIMATE OF BACKSCATTERED PROTON AND ALPHA SPECTRA	119
References		123

## I. INTRODUCTION

In the context of high-energy astrophysics, solar flares provide an opportunity to study at close hand particle acceleration and propagation processes which result in the production of X-ray and radio emission as well as energetic electrons and nuclei. An understanding of these processes in the solar case, where the source and some of the propagation parameters are known, may provide insight into less accessible problems such as galactic cosmic ray production, propagation and modulation.

A "typical" solar cosmic ray (SCR) event can be briefly described as follows. The triggering of a solar flare in an active region of the sun produces a burst of energetic electrons with energies  $\sim$  keV--MeV and nuclei with energies extending up to several 10's of MeV and above. The interaction of the accelerated electrons with the solar atmosphere and magnetic fields results in a variety of X-ray, radio and optical emissions. Ionization energy loss of the accelerated nuclei may also provide a portion of the energy which goes into H $\alpha$  emission characteristic of flares. Within minutes of their acceleration, some SCR's escape into the interplanetary medium where their propagation to earth, dominated by the irregularities in the interplanetary magnetic field, can be as described by a combination of diffusion, convection and adiabatic deceleration. During a large SCR event a heliocentric cavity out to a distance of many AU may be filled for days by these particles. At 1 A.U. the event is observed as a rapid rise in particle flux (of over 6 orders of magnitude in some cases) with large anisotropy

in the incident arrival direction, followed by a smooth turnover and roughly exponential decay with a time constant of 5--30 hours. Thus the particles from a single SCR event may be detectable for many hours or days.

Although the observed chemical composition of SCR's is similar in some respects to the observed solar abundances, there are many detailed, but significant differences whose origin is not understood. For example, the relative abundance of hydrogen and helium, the two main constituents of the solar atmosphere, is found to vary by over 2 orders of magnitude from flare to flare (Anglin et al. 1973a) with somewhat smaller variations observed during the course of an individual flare. The relative abundance of heavier nuclei are found to be enhanced at lower energies in SCR's. The explanation for these observations as well as the acceleration mechanism itself remains an open question.

A new approach to the study of these problems has become available recently with the direct observation of the products of nuclear reactions that occur in the solar atmosphere during flares. These reactions, which can occur only after the particles have been accelerated to energies  $\sim 10^1$ 's of MeV/nuc give rise to gamma rays such as have been detected by Chupp et al. (1973), neutrons and positrons (yet to be directly detected) as well as secondary nuclei.

Isotopic analysis of the SCR's at 1 A.U. provides a means of isolating this secondary component since the rare isotopes of hydrogen and helium ( $^2\text{H}$ ,  $^3\text{H}$  and  $^3\text{He}$ ) do not constitute a significant fraction of the ambient solar atmosphere and so can be attributed to such reactions.

Following pioneering work in the early '60's\* (eg, Schaeffer and Zahringer (1962), Biswas (1964), Waddington and Freier (1964)), Hsieh and Simpson (1970) resolved the isotopes of helium above 15 MeV/nuc after averaging over 7 flares. More recently Anglin et al. (1973b) have detected finite fluxes of deuterium and tritium at 10 MeV/nuc by averaging a large number of solar events.

Garrard, Stone and Vogt (1972) were the first to identify " $^3\text{He}$  rich events" in which the ratio of  $^3\text{He}$  to  $^4\text{He}$  exceeded 20%. Such events are interesting because of the conspicuous absence of  $^2\text{H}$  and  $^3\text{H}$ , presumably produced at the same time as the  $^3\text{He}$  by reactions with comparable cross sections.

In this work, observations of SCR isotopes are extended to lower energies by a high resolution particle telescope, the Caltech Electron/Isotope Spectrometer, flown aboard the IMP-7 satellite. In addition to flare averaged measurements of the rare isotopes, three more ' $^3\text{He}$  rich events' are observed, including one in which the abundance of  $^3\text{He}$  is the highest reported to date. The observations are interpreted in terms of recent calculations (Ramaty and Kozlovsky, 1974) of secondary isotope production in which the reaction kinematics and

---

\*Lingenfelter and Ramaty (1967) review measurements prior to 1967.

directional properties of the flare acceleration mechanisms are found to play a key role in accounting for such <sup>3</sup>He rich flares.

A preliminary account of part of this work has been presented elsewhere (Hurford et al. 1973e).

## II. Experiment

### A. Spacecraft

The observations were made with the Caltech Electron/Isotope Spectrometer (EIS), a cosmic ray telescope aboard the IMP-7 spacecraft. The spacecraft is spin stabilized with its axis of symmetry perpendicular to the ecliptic. The telescope axis is mounted normal to this spin axis and so scans the ecliptic plane as the spacecraft rotates. Selected parameters are listed in Table II-1.

The circular orbit of about 35 earth radii ensures that most of the observations are made from well outside the magnetosphere. About 90% of the flare averaged data and all of the data for  $^3\text{He}$  rich events were acquired outside the magnetotail.

### B. Telescope and Telemetry

Figure II-1 shows a cross section view of the telescope, which consists of a stack of eleven fully depleted silicon surface-barrier detectors, D0-D10, inside a plastic scintillator anticoincidence shield, D11, viewed by a photomultiplier tube. The top of the telescope is covered by an aluminized mylar window. Each detector is connected to a charge sensitive preamplifier, whose output (in the case of D0 thru D9) is pulse height analyzed by a linear analog to digital converter (ADC). D10 and D11 are connected to a single level discriminator. Table II-2 lists the nominal detector and ADC characteristics. Detailed results of the actual ADC calibrations can be found elsewhere (Mewaldt and Vidor, 1974). Except for a few channels just above threshold, where the ADC response is nonlinear, the measured gains and detector thicknesses are within 2% of the nominal values.

Table II-1. Selected IMP-7 Spacecraft Parameters

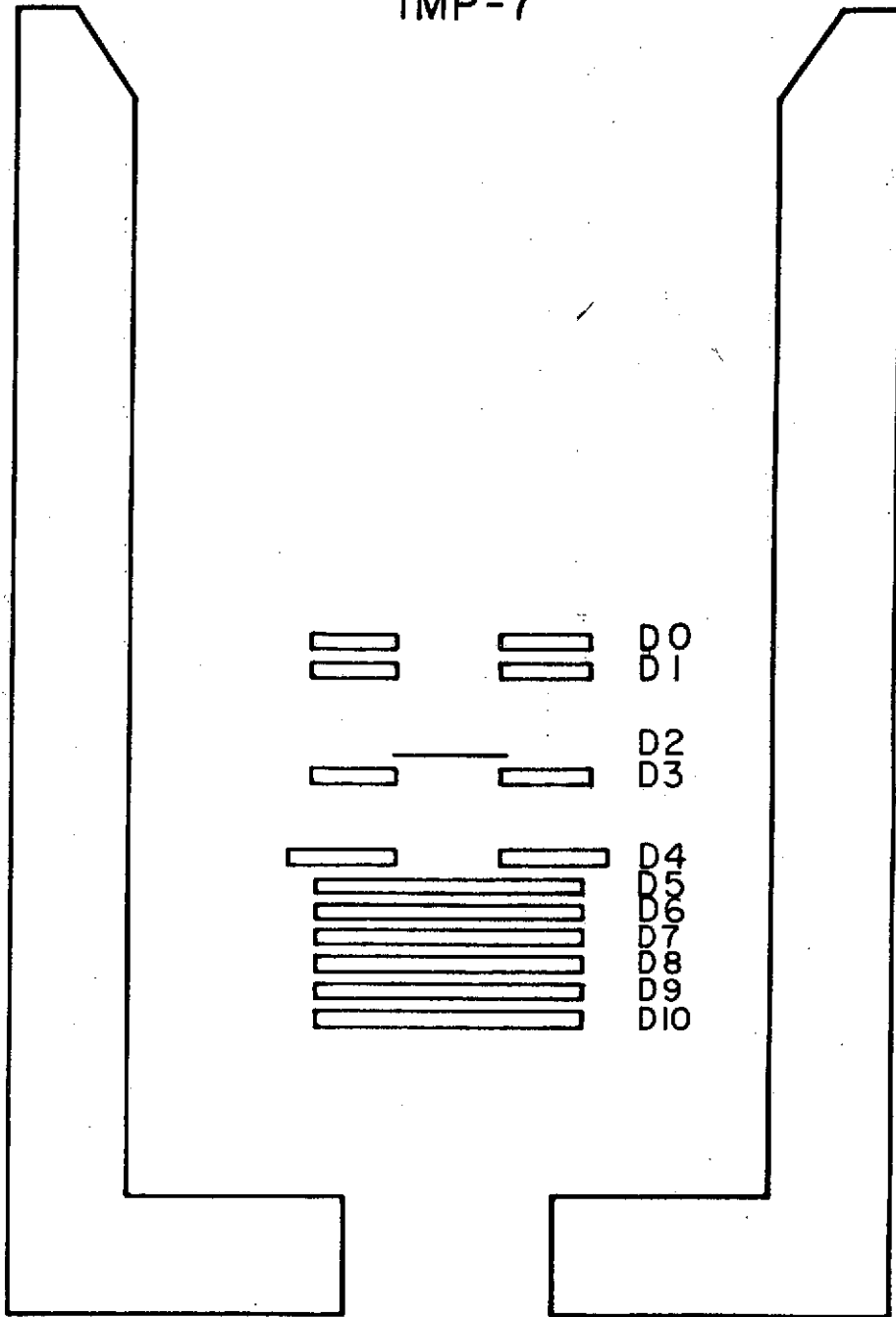
Launch Date	Sept 23, 1972
Apogee	206885 km
Perigee	229978 km
Orbital Period	12.28 days
Spin Rate	45.2 rpm
Spin Axis	$\pm 2$ degrees of south ecliptic pole

Figure II-1

Cross Section of the IMP-7 Electron/Isotope Spectrometer Telescope

# CALTECH ELECTRON/ISOTOPE SPECTROMETER

## IMP-7



SCALE  
1 CM

Table II-2. Nominal Detector and ADC Characteristics

Detector	Type	Thickness <sup>†</sup> (microns)	Outer <sup>+</sup> Diameter (mm)	Inner <sup>+</sup> Diameter (mm)	Discriminator <sup>**</sup> Threshold (MeV)	ADC <sup>**</sup> Resolution (MeV)	Number of ADC Channels
D0, D1, D3	annular	1000	22	8	0.16	0.165	1023
D4	annular	1000	25	8	0.16	0.165	1023
D2	disk	50	9	-	0.16 0.3 (D2H)++	0.0412	1023
D5	disk	1000	21	-	0.16 3.0 (D5H)++	0.0412*	4095
D6, D7, D8, D9	disk	1000	21	-	0.16	0.165	1023
D10	disk	1000	21	-	0.16	-	-
D11	scintillator	-	-	-	~ 0.4	-	-

\* Above channel 1023, effective resolution is only 0.165 MeV since the two least significant bits are deleted from the telemetry.

<sup>+</sup> Wafer diameters (D2 excepted). Fully depleted diameters and physical diameters of the holes are slightly smaller (Hartman, 1973). In the case of D2, the wafer diameter is 25 mm while the active diameter is 9 mm.

<sup>†</sup> Measured thicknesses are discussed elsewhere, (Hurford, 1974b) but fall within 2% of the nominal values.

<sup>\*\*</sup> Detailed results of prelaunch ADC calibrations can be found elsewhere (Mewaldt and Vidor, 1974).

<sup>++</sup> D2H and D5H represent high level threshold levels for the D2 and the D5 ADC's which are used in the experiment logic for a number of purposes, such as distinguishing electrons and nuclei.

The experiment can be used in several different modes for the detection of electrons ( $\sim 0.16$  to  $\sim 5$  MeV) (Hurford et al., 1973a, 1974b), positrons ( $\sim 0.16$  to  $\sim 2$  MeV) (Hurford et al., 1973b, 1973c), and light isotopes through  $^{10}\text{Be}$  (2 to 40 MeV/nuc) with limited isotope capability through  $^{18}\text{O}$  (Hurford et al., 1973d, 1974a).

These varied capabilities are made possible by the use of a five level priority system that determines which events are completely analyzed and included in the telemetry data. The details of the priority system are outlined elsewhere (Garrard, 1974a). Of particular interest for the measurement of flare isotopes is the narrow geometry mode, defined by the logic requirement\*  $(R2H \overline{r10} + R5) \overline{r0} \overline{r1} \overline{r3} \overline{r4} \overline{r11}$ . The annular detectors, D0, D1, D3 and D4, are used as active collimators in this mode, which analyzes nuclei, electrons, positrons and penetrating particles with one of the two highest priorities, which are assigned alternately to electrons and non-electrons. Table II-3 lists some of the different ranges (combinations of triggered detectors) which are included in the narrow geometry mode and indicate which ranges are considered electrons for the purpose of priority assignment.

During each readout period (0.64 seconds) the experiment will fully analyze a particle provided that no previous particle of equal or higher priority has been analyzed during that period. At the end of each period, the datum on the last analyzed particle is included in the telemetry and constitutes one event. Thus, the events in

---

\*  $R_n$  = signal above threshold in detector n  
 $\overline{r_n}$  = no such signal  
 R2H, R5H refer to high level discriminator thresholds in D2 and D5 respectively.

Table II-3. Selected Narrow Geometry Ranges

Range*	'electron'	A pulse height	B pulse height	Nominal Interpretation <sup>†</sup>
D5	yes	D5	D2 offset <sup>+</sup>	Electrons, ~ 0.2 to ~ 1 MeV
D56(789)	yes	D5	D6 (+D7+D8+D9)	Electrons, ~ 1 to ~ 3 MeV
D2	no	D5 offset <sup>+</sup>	D2	Nuclei, 1.0 - 2.4 MeV/nuc**
D25(H)	no	D5	D2	Nuclei, 2.4 - 12.8 MeV/nuc
D5H	no	D5	D2 or D2 offset <sup>+</sup>	Protons that fail to exceed the D2H threshold
D25H6	no	D5	D6	Nuclei, 12.8 - 18.7 MeV/nuc that trigger D2 <span style="float: right;">II</span>

\* Event ranges will be labeled by  $Dn_1, \dots, n_2$  ( $n_3 \dots n_4$ ) where  $Dn_1, \dots, Dn_2$  are in coincidence;  $Dn_3, \dots, Dn_4$  may or may not be triggered and unnamed detectors are assumed to be in anticoincidence. D5 and D5H refer to signals above the low and high D5 ADC thresholds respectively. D2, however, refers to the high level D2 ADC threshold.

\*\* Energy limits refer to alpha particles. See Table II-5 for limits for other nuclei.

<sup>+</sup> The D2 (or D5) 'offset' is the D2 (or D5) ADC response to a zero signal input.

<sup>†</sup> In some cases the dominant contribution to a given range may be caused by background, and so void the 'Nominal Interpretation'. This is particularly true during solar quiet periods. Background contributions that are important during flares are discussed in Section II-E. Note that electrons are distinguished from nuclei by the absence of a D2 or D5H signal.

the telemetry constitute a sample of all particles that would be assigned the same priority for analysis.\*

The telemetry for each analyzed event contains four items of interest. First, there is a range word, which indicates which combination of detectors was triggered. Then there are two pulse heights, A and B, whose interpretation depends on range, as indicated in Table II-3. Finally, there are three sector bits, which indicate in which of eight  $45^\circ$  sectors of the ecliptic plane the telescope axis was pointing when the analyzed particle arrived.

In addition to the event data, an extensive set of rate data, listed in Table II-4 is also included in the telemetry. The rate data are useful for monitoring detector and experiment operation, for studies of the time structure of transient events such as flares and for normalization to compensate for the sampling bias associated with the event data.

### C. Nominal Isotope Response

The principal range used in evaluating SCR isotopic ratios is D25(H). Particles with a shorter range, such as D2 single events, cannot be unambiguously identified since only one parameter (their energy loss in D2) is measured. Particles with a longer range, such as D(2)5H6 can, in principle, be identified, but because of the higher energy threshold for such events and the steep SCR spectrum (typically  $\frac{dN}{dE} \sim E^{-3}$ ), the number of such events is significantly diminished, and

---

\* While this sample is unbiased with respect to particle type, it is not unbiased with respect to time or direction of incidence. For a discussion of this type of biasing, see Roelof, (1974).

Table II-4. Rates

Rate	Logic Requirement	Nominal Physical Significance
ELO	N S $\overline{r2H}$ R5 $\overline{r5h}$ $\overline{r6}$ $\overline{r7}$ b	Electrons, ~ 0.2 to ~ 1 MeV, including Compton recoils
EHI	N S $\overline{r2}$ R5 $\overline{r5h}$ R6	Electrons, ~ 1 to ~ 3 MeV, including Compton recoils
PLO	N S R2H $\overline{r5}$ $\overline{r6}$ $\overline{r7}$ b	Nuclei, 1.2-2.4 MeV <sup>+</sup>
PHI	N S R2 R5H $\overline{r6}$	Nuclei, 4-13 MeV
DO*	R0 S	Electrons, ~ 0.16 to ~ 5 MeV, plus nuclei, 1-43 MeV
DO1*	R0 R1 S	Electrons, ~ 1 to ~ 5 MeV, plus nuclei, 13-43 MeV
PEN	N R5 R6 R10 $\overline{r11}$	Electrons and nuclei that penetrate the telescope (electrons > 3 MeV, nuclei > 30 MeV)
NEUT	N S $\overline{r5}$ R7	Neutral particles, such as $\gamma$ -rays, whose Compton recoil electrons are detected in D7
ADC	R0+R1+...+R9	The 'or' of all pulse-height-analyzed detectors.
HAZ	-	The rate at which the HAZARD flag is set.*
DO, D1, ..., D11	-	Singles rates for individual detectors.

N = narrow geometry =  $\overline{r0}$   $\overline{r1}$   $\overline{r3}$   $\overline{r4}$

S = stopping =  $\overline{r10}$   $\overline{r11}$

B = busy = analysis in progress

<sup>+</sup> Nuclei energy limits are for protons. Limits for other nuclei are given in Table II-5.

\* The HAZARD flag is set whenever a particle triggers an ADC within ~ 16 microseconds of a previous ADC trigger. The second particle is flagged to indicate the possibility of a compromised energy loss measurement. See section II-D.

so a longer time is required to acquire a statistically significant sample. Therefore, in this study, only D25(H) isotopes are discussed. Other ranges are used only to supplement the D25(H) data, as described in the first two appendices. Table II-5 shows the energy threshold associated with each range.

The identification of isotopes is accomplished by the  $dE/dx$ -E technique, which is described briefly below with reference to D25(H) events. In the  $dE/dx$ -E technique, 2 parameters of each incident particle are measured—its energy loss ( $\delta E$ ) in the one detector (D2) and its residual energy ( $E'$ ) after penetrating that detector. In this case, the residual energy is measured by D5. If we consider an incident proton of energy,  $E$ , and a  $\delta E$  detector of known thickness, the expected values of  $\delta E$  and  $E'$  can easily be determined from proton range-energy tables.\* For other particles, the scaling relation,

$$R(M,Z,E) = \frac{M}{Z^2} R_p(E/M)$$

is used where  $R(M,Z,E)$  is the average range of a particle of mass,  $M$  (units of proton mass), charge,  $Z$ , energy,  $E$ , and  $R_p(E/M)$  is the range of a proton of energy,  $(E/M)$ .

---

\*The basic set of range-energy tables used throughout this work are Janni proton tables (Janni, 1966). For  $Z = 2$  incident ions, the tables are corrected for electron-pickup effects using data compiled by Northcliffe and Schilling (1970) for aluminum.

Table II-5. Energy Thresholds for Selected Narrow Geometry Ranges

Range	Thresholds <sup>+</sup> (MeV/nuc)				
	<sup>1</sup> H	<sup>2</sup> H	<sup>3</sup> H	<sup>3</sup> He	<sup>4</sup> He
D2*	1.23	0.79	0.58	1.28	1.07
D25	2.45	1.64	1.22	2.86	2.39
D25H	4.17	2.40	1.75	3.21	2.67
D(2)5H6	12.74	8.55	6.76	14.99	12.77

\* The threshold for D2 events is sensitive to the offset of the D2 ADC. As discussed in section II-F, this offset was subject to shifts. The values at any time, however, are within 0.06 MeV/nuc of the typical values shown here.

+ The relative and absolute accuracies of these threshold values are estimated to be 1 1/2% and 3% respectively.

For each particle species,  $\delta E$  and  $E'$  can be calculated for various values of  $E$  and if plotted, a track for each species is obtained. Figure II-2 shows this nominal isotope response for D25(H) events. In principle, after measuring the energy loss in D2 and D5, any particle can be identified by noting on which track it lies. In practice this is sometimes possible, but for rare isotopes it is complicated by the inherent resolution of the system and background considerations.

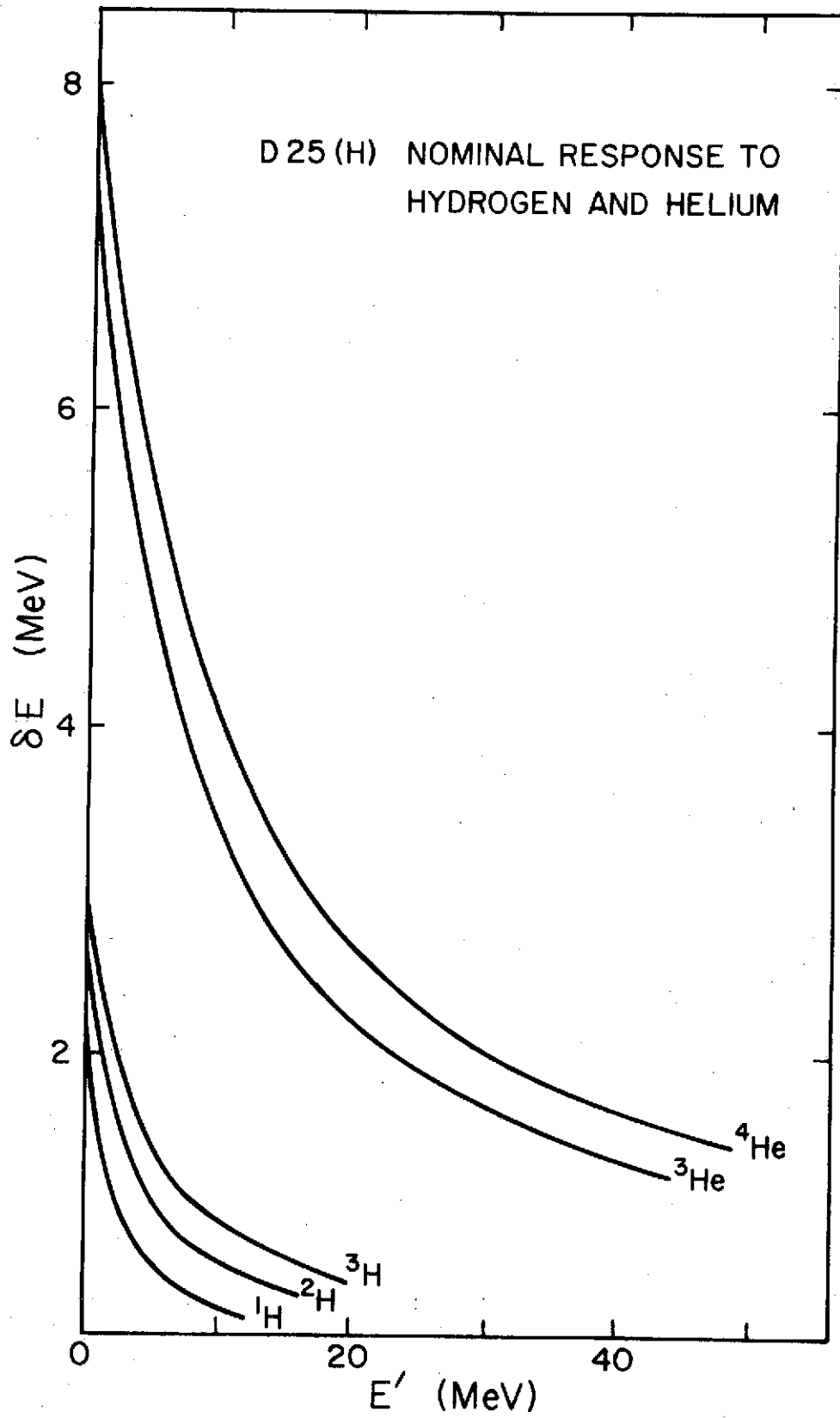
The handling of resolution and background effects is simplified if transformation is made to a mass scale. Figure II-2 shows the tracks calculated for integral masses. The track location for non-integral masses such as 1.1, 1.2, 1.3, etc. can just as easily be evaluated. Then particles falling between these closely spaced tracks can be assigned to corresponding mass bins and so a mass histogram can be formed. The response of the system can then be considered as that of a mass spectrometer. The creation of mass histograms from flight data is discussed in Appendix A. Examples of  $\delta E$ - $E'$  plots and the corresponding mass histograms are shown in Figures II-4 and II-5 and will be discussed in section II-F.

#### D. Mass Resolution

In practice, the observed values of  $\delta E$  and  $E'$  form a distribution about the tracks shown in Figure II-2. The equivalent mass histogram shows a mass distribution, peaked near an integral mass, but with a finite width.

Figure II-2

Nominal response of EIS for hydrogen and helium nuclei detected in range D25(H). The energy loss,  $\delta E$ , in D2 is plotted as a function of energy loss,  $E'$ , in D5, assuming an average path length of 50.8 microns in D2, which corresponds to an incident angle of 12 degrees.



Since the calculated mass,  $M(\delta E, E', t)$  is a function of the energy loss, residual energy and assumed thickness of the first detector, the mass resolution is determined by the uncertainty in  $\delta E$ ,  $E'$  and  $t$ . The sources of error in each of the quantities are now considered.

### 1. Fluctuations in ionization energy loss

The statistical fluctuations in ionization energy loss for protons have been discussed elsewhere (e.g. Seltzer and Berger, 1964). For the particle types and energies considered here, the distribution of energy losses in a silicon detector of about 50 microns is essentially Gaussian with a standard deviation given by

$$\sigma_{\delta E} = 0.435 Z \sqrt{t} D \sqrt{\frac{1 - \beta^2/2}{1 - \beta^2}}$$

where  $\beta c$  = velocity of incident particle  
 $Z$  = charge of incident particle  
 $t$  = thickness (cm Si)

and the additional factor,

$$D = \sqrt{1 - .8705 \left[ 1 + \frac{R}{t} \ln \left( 1 - \frac{t}{R} \right) \right]}$$

is a deceleration factor of order unity that allows for the change of velocity as the particle traverses the detector.  $R$  is the range of the incident particle (cm Si). For example  $\sigma_{\delta E} = .065$  MeV for a 20 MeV alpha which loses about 3 MeV in a 50 micron detector. Note that the fluctuations affect  $\delta E$  but not the measured total energy,  $(\delta E + E')$ .

### 2. Measurement of $\delta E$ and $E'$

Combined detector, amplifier and ADC Gaussian rms noise levels are about 15 and 9 keV for D2 and D5 respectively.

For a pulse height analyzer of channel width,  $w$ , there is an r.m.s. measurement uncertainty of  $w/\sqrt{12}$ . Since the channel widths for both D2 and D5 are 41 kev, this adds another 12 kev to the r.m.s. error. The total measurement error for D2 and D5 is then 19 and 15 kev respectively.

A potential source of error which has affected previous measurements of SCR isotopes (Dietrich, 1973) is the possible dependence of the ADC response on the counting rate. For example, base line shifts might change the ADC response during high rate periods. This problem has been eliminated in the EIS by the use of a hazard flag which identifies those events analyzed within 14-18 microseconds of previous ADC activity. Such 'hazard' events are assigned a low priority and have been excluded from this work.

### 3. Pathlength Uncertainties

The nominal response for D25(H) events shown in Figure II-2 assumes that all particles pass through a thickness,  $t = 50.8$  microns of silicon, which corresponds to an incident polar angle of 12 degrees with respect to the axis of symmetry. Particles arriving with a polar angle greater than 12 degrees have a longer path length,  $t \sec \theta$ , thereby losing additional energy in D2. In addition, thickness variations in the detector are also present. It becomes necessary, therefore, to consider the distribution of pathlengths in D2.

The incident angle effects can easily be estimated from the geometry. The  $24^\circ$  maximum half angle implies that  $\sec \theta$  is bounded by 1.0 and 1.09, with an r.m.s. variation of 2.2% as determined by a Monte Carlo calculation (Hartman, 1973).

The thickness variations in D2 can be considered to consist of two components. The first is a radial thickness variation, in which the thickness increases linearly with increasing radius, while the second component can be considered as a random thickness variation, superimposed on the radial component. A five-point measurement of the thickness of the flight detector yielded a result consistent with a radial gradient of 0.3 microns/mm with an r.m.s. random component of about 0.6 microns.

The radial thickness variation and incident angle effects are not independent, since for example, the geometry implies that particles with large incident angles will tend to go through the thinner, central region of D2, so that some compensation will occur. Evaluating these effects by means of the Monte Carlo program leads to a total r.m.s. uncertainty of 2.5% in path length, including the random effects.

Given a knowledge of the variations in  $\delta E, E'$  and  $t$ , the next step is to convert this to a mass resolution. Assuming a range energy relation of the form,  $R = \frac{k M}{Z^2} \left(\frac{E}{M}\right)^A$ , an explicit solution for  $M$  can be obtained in terms of a  $\delta E - E'$  measurement.

$$M = \left(\frac{tZ^2}{k}\right)^{\frac{1}{1-A}} \left[ (\delta E + E')^A - E'^A \right]^{\frac{1}{1-A}}$$

From this equation and the values  $\sigma_t$ ,  $\sigma_{\delta E}$  and  $\sigma_E$ , discussed above, standard techniques can be employed to estimate the rms error in  $m$ ,  $\sigma_m$ , for each of the error sources identified above. Figure II-3 illustrates the result of such a calculation, showing the relative importance of each component of  $\sigma_m$  for proton mass resolution.

Alternatively the error sources can be incorporated into a Monte Carlo program which simulates the response of the detector system to an isotropic flux with an appropriate energy distribution. Such a procedure not only predicts the width of the mass distribution, but also provides insight into its detailed shape. This approach is discussed in more detail in Appendix C.

#### E. Background

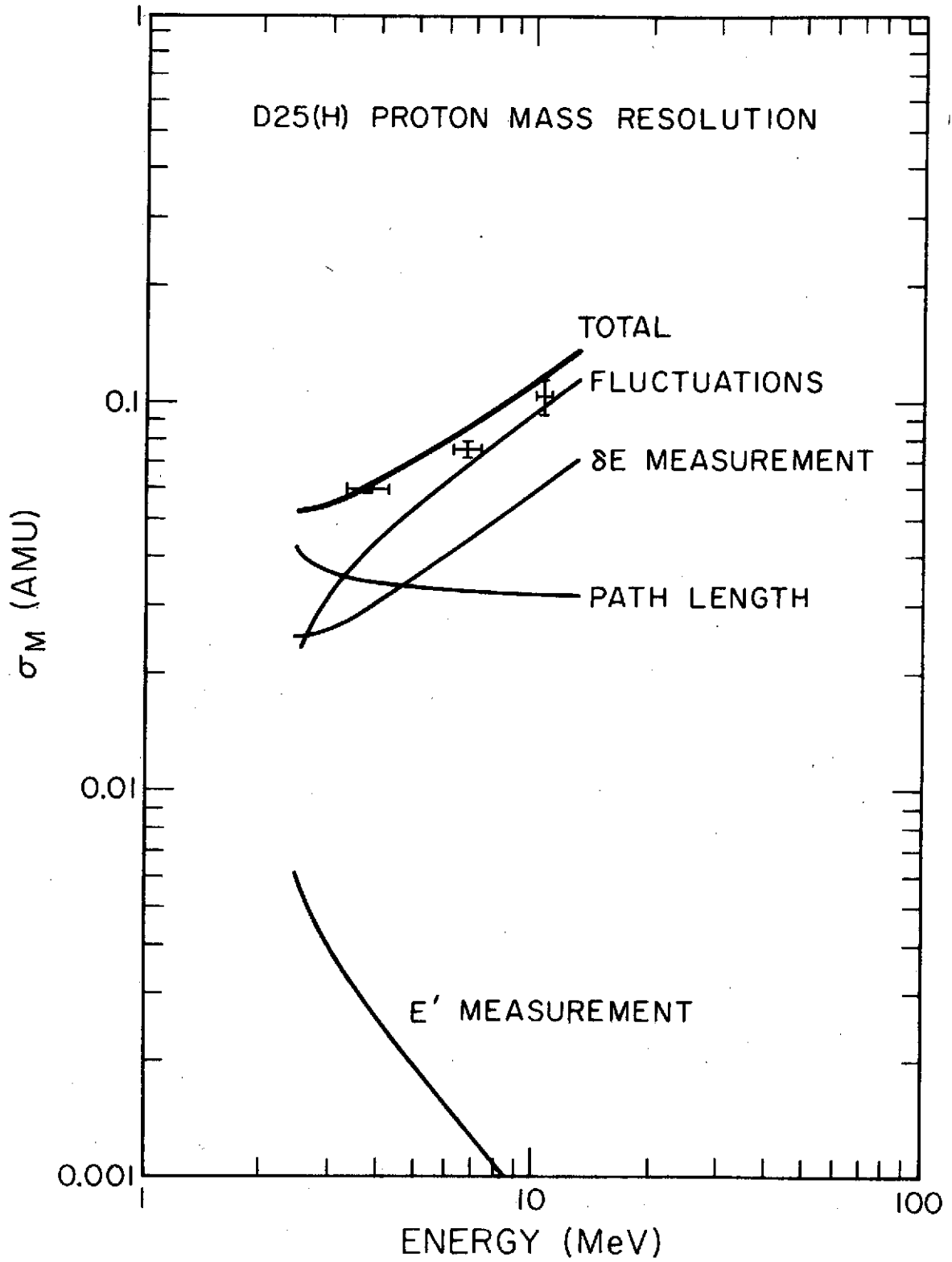
There are numerous potential background sources which can affect the measurement of rare isotopes. Four of these are important in the present study and are discussed below.

##### 1. Nuclear Interactions in D5

While ionization energy loss is the dominant mechanism by which incident ions lose energy in the telescope, a small fraction of incident nuclei are involved in nuclear interactions which can result in spurious values of  $\delta E$  and  $E'$ . At the low energies relevant here, elastic proton-silicon scattering is the principal concern, for if a proton is backscattered in D5 so as to pass through the D4 and D3 apertures and lose energy a second time in

Figure II-3

Proton mass resolution for D25(H) events. The calculated contributions from each error source are added quadratically to get the total. Calculated  $E'$  and  $\delta E$  measurement errors include noise and ADC resolution. Calculated path length variations include  $\sec \theta$  and thickness variations combined for an isotropic flux. Fluctuations refer to the statistical fluctuations in ionization energy loss. The plotted points represent the observed resolution for typical flare data.



D2, the value of  $\delta E$  becomes much higher than normal. As Figure II-2 suggests, such a proton might be interpreted as a higher mass particle.

A rough estimate of the magnitude of this background can easily be made. For an  $E^{-3}$  incident spectrum, the average penetration depth in D5 is 120 microns, and so 60 microns is the average depth within which the interaction must occur. A proton whose range is 120 microns has an average energy of about 3 MeV during its first 60 microns of travel. Although the p-Si elastic cross section near 3 MeV is structured, an average value is about  $10^{-1}$  barns/steradian in the backward hemisphere (Vorona et al., 1959). The D3 aperture and D2 subtend 0.5 steradians at D5. Therefore the effective cross section is about 0.05 barns. Combining the interaction depth and cross sections with the atomic density of silicon, the probability of such a background event is found to be  $\sim 10^{-5}$ . The contribution of such events to the observed  ${}^2\text{H}$  or  ${}^3\text{H}$  flux is somewhat less than this figure, however, since only a fraction of such events appear sufficiently close to the  ${}^2\text{H}$  or  ${}^3\text{H}$  'track' to be misidentified.

## 2. Channeling in D2

The normal value of the ionization energy loss of an incident ion penetrating D2 can be reduced by as much as a factor of 3 if the incident direction closely parallels one of the major crystal planes in the D2 silicon crystal. Particles which 'channel'

in this manner have an abnormally low value of  $\delta E$  and a correspondingly larger value of  $E'$  and so appear to have an abnormally low mass. While channeling protons cannot affect the rare isotope measurement, channeling alphas can give rise to a significant background affecting the  $^3\text{He}$  measurement. As is shown in Appendix C, about 2% of incident 8.785 MeV alphas channel to the extent that their calculated mass is below 3.5 amu, and roughly 1/2% of such alphas fall within the expected  $^3\text{He}$  FWHM peak position.

### 3. Pulse Pileup

Pulse pileup in D2 provides a background mechanism which can affect the  $^2\text{H}$  or  $^3\text{H}$  measurement. The main problem here is the possibility of the coincident arrival of a D25(H) particle and a low energy proton which deposits additional energy in D2. A simple quantitative estimate can be made from the observation that during the peak of the 29 Oct 1972 event, an enhanced fraction of background events (defined as  $M > 1.7$  amu in the hydrogen mass plot) was observed. This enhanced background was present only during the peak of the flare. While a simplified calculation of the pulse pileup problem, (based on a nominal 1 microsecond time constant) predicted 4 such background events during this period the observed number was 5. Thus, this background can be empirically quantified by a time,  $\tau \approx 1.2$  microseconds such that the probability of a significant coincidence occurring with a given D25(H) particle is  $\tau$  times the rate of D2H particles.

#### 4. Galactic Background

Small flares and the late stages of larger events encounter a potential background caused by galactic particles. This background, whose contribution is proportional to 'live time', has 3 components.

- a. Low energy galactic cosmic rays which are detected normally.
- b. Higher energy galactic cosmic rays which suffer nuclear interactions in the detector stack, and trigger only D2 and D5.
- c. Neutrons, produced in the spacecraft by high energy cosmic rays, can pass through D11 undetected, interact in or near D2 and D5 to give D2-D5 coincidence events.

The contribution of the sum of these three components can be estimated empirically by analyzing quiet time data in the absence of solar activity. During  $1.2 \times 10^7$  seconds of quiet time data, a total of 14 particles with  $Z = 1$  and  $M > 1.7$  amu, and 9 particles with  $Z = 2$  and  $2.8 < M < 3.2$  amu were observed. Normalized, this implies a background rate of  $1.2 \times 10^{-6}$ /sec and  $8 \times 10^{-7}$ /sec for  $Z = 1$  and  $Z = 2$  respectively.

Of these four background mechanisms, the effects of the first two (nuclear interactions and channeling) are independent of the intensity of the SCR flux and so ultimately limit the EIS sensitivity to the rare hydrogen and helium isotopes. The latter two (pulse pileup and galactic background) bracket the dynamic range of the SCR flux that can be analyzed to detect the rare

SCR isotopes at a given level of abundance. In chapter III, it is shown how the effects of these latter two background sources are minimized in order to establish flare averaged upper measurements of deuterium and tritium.

In addition to the four background sources discussed above, the following background mechanisms have been considered and found not to play an important role in the present context.

1. Energy loss in the epoxy rim which coats the inner annulus of the annular detectors is not significant for D25(H) events because of the small geometrical factor and steep SCR spectrum.
2. Inefficiency of the surface barrier detectors near their edges is not a factor since the edges of D2 and D5 are shielded by the annular collimators.
3. D25(H) events in which the particle escapes from D5 before stopping do not occur because there is no inactive layer between D5 and D6.
4. Elastic nuclear collisions in D2 are not significant because of kinematical considerations.
5. Inefficiency of the D11 anticoincidence detector during high rate periods is not a factor due to an updating-discriminator feature of the D11 electronics.
6. Pulse pileup involving electron-proton coincidences is small compared to the proton-proton coincidences discussed above.

## F. Calibration

The extensive calibration of the EIS can be conveniently divided into two parts. The first consists of the calibration of individual subsystems, such as the ADC response, detector parameters, etc., while the second consists of determining the response of the experiment as a whole to incident particles. The section that follows discusses those calibrations relevant to the detection of SCR's.

### 1. ADC Calibration

The method and result of the ADC calibration is described by Mewaldt and Vidor (1974). Very briefly, the method consists of depositing a known charge pulse at the preamp input by means of test pulsers built into each ADC, and noting the digital response of the ADC. The threshold of any channel can be determined by varying the magnitude of the charge pulse which is accurately determined by an externally supplied DC voltage. The use of a precision programmable DC power supply and appropriate interfaces permits the entire calibration to be computer controlled.

Calibration of the ADC test pulsers was established by means of an external test pulser whose normalization in turn was fixed by comparison to 5.486 MeV alphas from an  $^{241}\text{Am}$  source detected in a laboratory-standard silicon surface-barrier detector.

Prelaunch ADC calibrations over 10 months and a wide range of environmental conditions indicated that the D2 and D5 ADC gains were stable to within 0.1%. Significant shifts, however, were noted in the offset of the D2, and to a minor extent, D5 ADC's.

For the analysis of postlaunch data, correction can be made for these shifts by using the D2 and D5 ADC offsets which are included in the telemetry when D5 or D2 singles events are analyzed, as shown in Table II-3 (Mewaldt and Vidor, 1974). The uncertainty in this correction is about 10 keV.

## 2. D11 Threshold

The threshold of the D11 scintillator-PM tube single-level discriminator combination is set to ensure the efficient detection of minimum ionizing particles (Murray, 1970). Its stability during prelaunch testing was verified by a  $^{106}\text{Ru}$  calibration source. Postlaunch behavior has indicated no significant changes to date.

## 3. Window Thickness

The thickness of the aluminized mylar window was determined to be equivalent to  $2.43 \pm 0.06 \text{ mg/cm}^2$  mylar by exposing the window to a beam of 8.875 MeV alphas from a  $^{212}\text{Pb}$  source, and measuring their residual energy after penetration (S. Vidor, private communication).

## 4. D2 Thickness

The thickness of D2 was sampled in a similar manner at 5 separate positions, yielding a range of values of 49.2 to 50.3 microns and a mean result of 49.7 microns. The variations in thickness are discussed in section II-3. Since the effective thickness of D2 for use in analyzing postlaunch data is a weighted average over the active area of D2 with a weighting function determined by the convolution of the D2 radial thickness variations

with the angular and radial distribution of the collimated incident flux, the simple mean quoted above cannot be used. The effective value of D2 thickness for postlaunch data was determined by requiring that the alpha peak in the flare averaged helium mass plot be in the correct position. This value, 50.8 microns, is consistent with the 49.7 microns quoted above since it includes the  $\sec \theta$  factor and is used for analysis of all postlaunch hydrogen and helium data.

#### 5. Response to Beams of Light Nuclei

The overall response of the experiment to light nuclei was checked by calibrations at the Caltech Tandem van der Graff accelerator. Details of this calibration are described elsewhere (Hurford, 1974b). Very briefly, the telescope was exposed to broad beams of  $^1\text{H}$ ,  $^2\text{H}$ ,  $^3\text{H}$ ,  $^3\text{He}$  and  $^4\text{He}$ , produced from primary  $^3\text{He}$  and  $^4\text{He}$  beams by a variety of elastic and inelastic reactions and rigidity analyzed by the 48 inch magnetic spectrometer. Output energies from 3 to 24 MeV were available and were set at a series of discrete values as well as varied during a run so that the response to both discrete and continuous energy distributions would be verified. The response to beams incident from off-axis directions was also measured.

A typical experiment response is shown in Figure II-4 where data from separate  $^3\text{He}$  and  $^4\text{He}$  energy scans are combined. The separation of  $^3\text{He}$  and  $^4\text{He}$  is clean, except for 5 individual  $^4\text{He}$  points, indicated by the hand drawn circles. The same data, expressed in the form of a mass histogram, are shown in Figure II-5.

Figure II-4

Combined data from two separate Tandem calibration runs. Variable energy  $^3\text{He}$  and  $^4\text{He}$  beams were incident parallel to the axis of the telescope and detected in the D25(H) range. The data points represent the number of events as a function of their D2 and D5 pulse heights. The separation is clean except for events represented by hand drawn circles. Letters are used when the number of events exceeds 10.

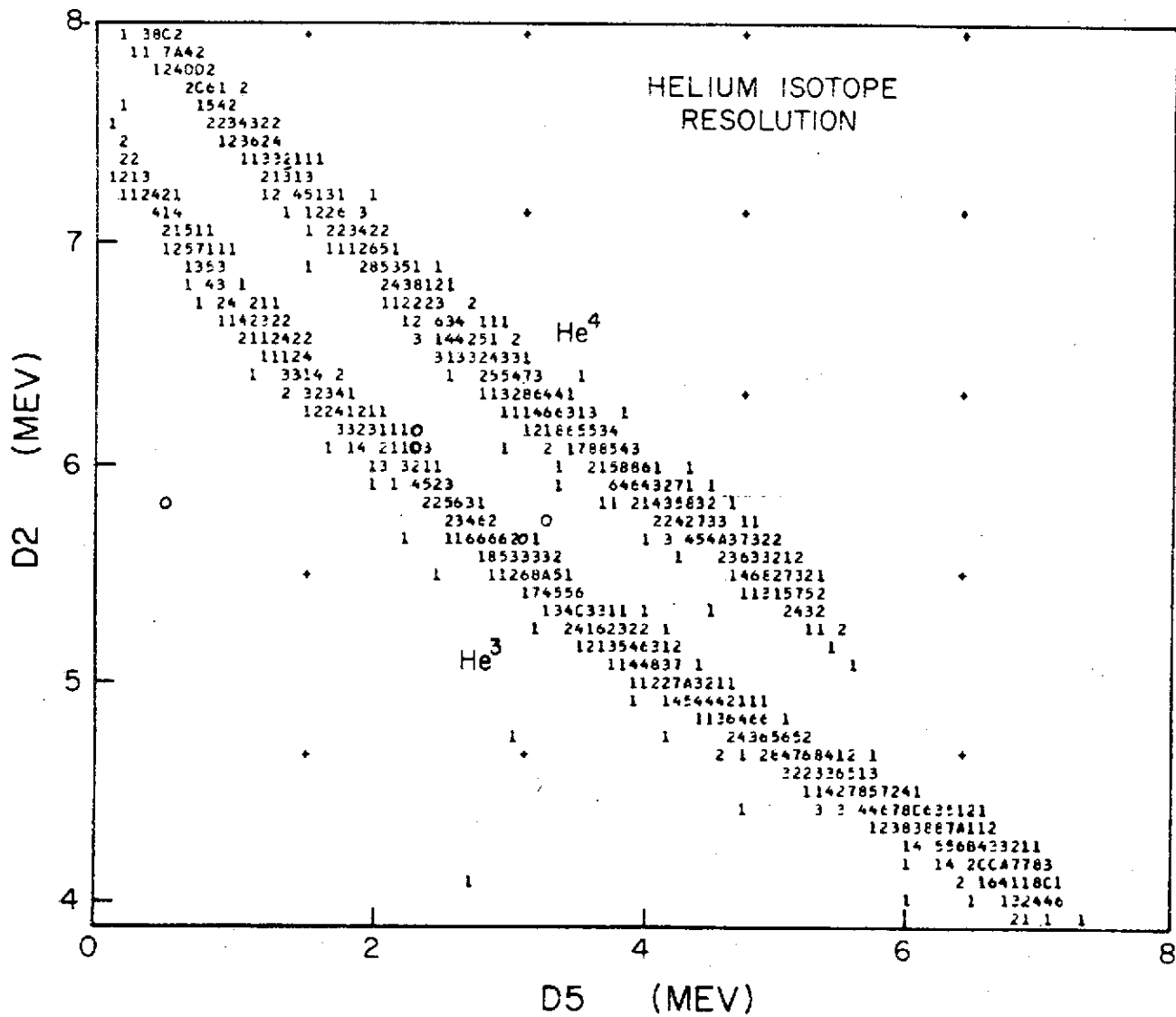
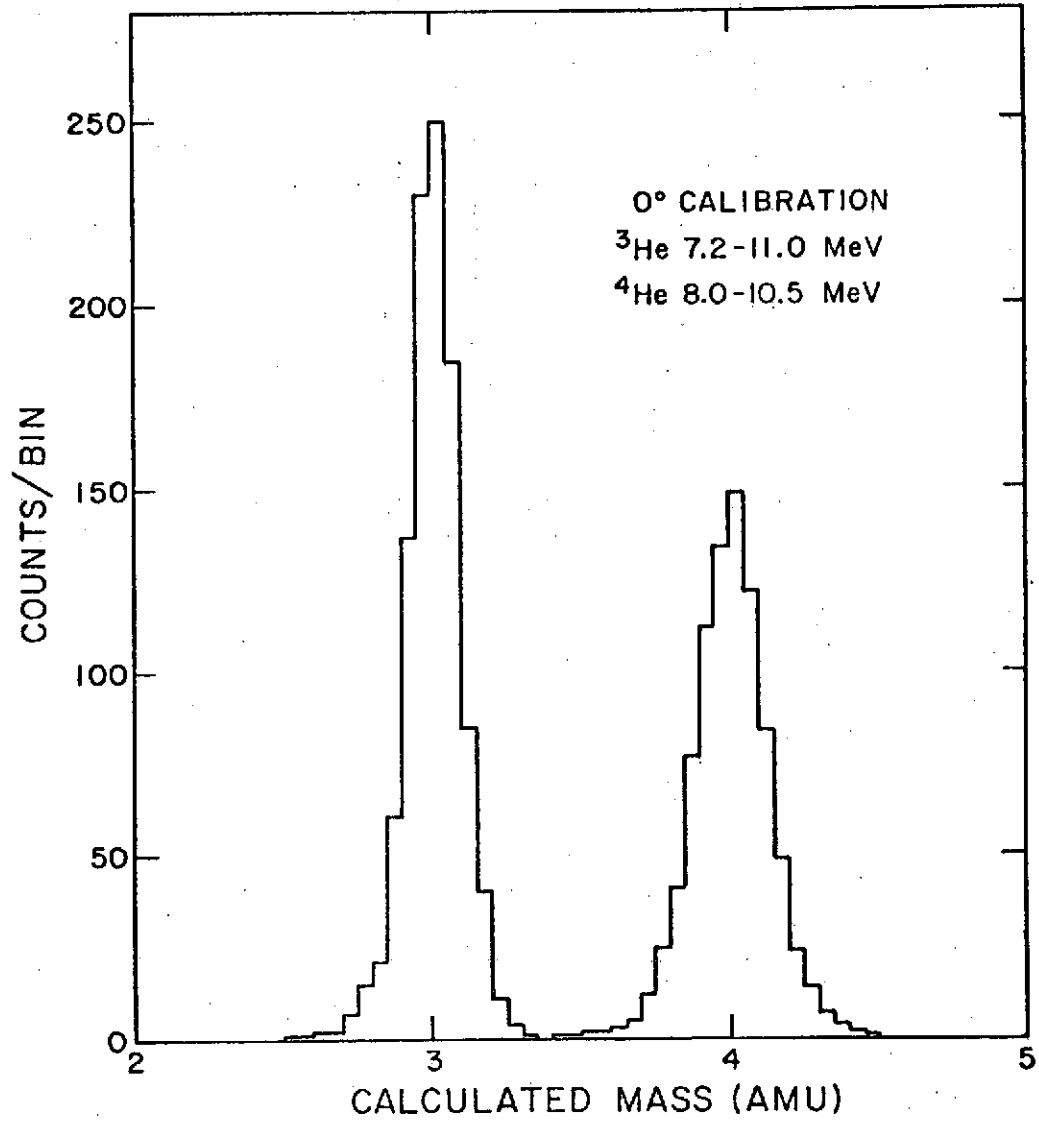


Figure II-5

The same data as shown in Figure II-4 converted to a mass histogram. The observed standard deviations are 0.082 and 0.12 amu for  $^3\text{He}$  and  $^4\text{He}$  respectively.



The observed standard deviations of 0.082 and 0.12 amu can be compared to expected values of 0.077 and 0.10 amu respectively, from predictions using techniques outlined in section II-3.

In this case the resolution is determined largely by the random thickness variations in D2 as discussed in section II-D, since the statistical fluctuations and measurement errors are proportionately less and the incident beam eliminates the  $\sec \theta$  path length variations.

### III Observations and Results

#### A. Introduction

Chapter II and Appendix A have indicated the method used to determine mass spectra for particles detected in a given time interval. In Section B of this chapter, a list of solar active periods between October 1972 and November 1973 is presented, along with the observed number of isotopes for each period. It shows that in three flares, finite fluxes of  $^3\text{He}$  were measured. These " $^3\text{He}$  rich flares" are discussed in more detail in Section F. For all other individual flares, only upper limits to deuterium, tritium and  $^3\text{He}$  could be established. The calculation of flare-averaged ratios for these isotopes is discussed in Sections D and E.

In all cases, the determination of upper limits and isotopic ratios requires certain corrections to be applied to the mass histograms. These corrections are outlined in Section C.

#### B. List of Solar Active Periods

To establish a data base from which to begin analysis of SCR isotopes, time intervals between October 1972 and November 1973 were identified during which the six hour average rate of 2.4-13 MeV/nuc nuclei exceeded  $0.03/\text{cm}^2 \text{ sr sec}$ . This level corresponds to  $\sim 10$  times greater than the rate used to establish 'solar quiet time' intervals for the study of low energy galactic cosmic rays (Hurford et al., 1973d). The criteria thus exclude all periods during which galactic particles might contribute more than  $\sim 10\%$  to the observed events, while retaining all but the smallest solar events. A systematic search for

interesting small solar events is described in Section F.

Minor editing was next employed to eliminate statistically marginal or isolated intervals, as well as to cut off the late stage of the decay phases, in order to further minimize galactic background. This reduced the number of events in the data base by less than 2%. Also purged at this point was data acquired between 30 April and 17 May 1973 during which detector D4 was disabled. Such data had a much higher than normal background rate, due to the compromised geometry. The remaining data, representing 98 days of observations, were grouped into 29 solar active periods. These periods, along with 2 additional periods identified in Section F are listed in Table III-1.

Where possible, each solar active period was associated with the corresponding optical flare (Leighton, 1973). In most cases, the basis for this association is the time of the onset of the solar electron flux. Table III-1 also lists the optical flare parameters, when known. For each of the 31 solar active periods, D2 and D25(H) events were summed and a fluence and spectral index for protons were estimated as described in Appendix B. Mass histograms of D25(H) events were produced for each period and from these, the event count for each isotope was determined and listed. In the absence of a prominent mass peak, any event occurring within  $\pm 2$  (predicted) standard deviations of the expected peak location was included. Otherwise the equivalent criteria of 95.4% of the observed counts in the peak was adopted. For the three  $^3\text{He}$  rich flares, for which all the peaks were well defined, the entries in Table III-1 represent the total of the observed D25(H) events. For each period, these counts were converted to iso-

Table III-1. List of Solar Active Periods\*\*

Dates	-----Optical-----				Proton Fluence >2 MeV (/cm <sup>2</sup> sr)	V <sub>p</sub> <sup>+</sup>	Notes	D25(H) Event Counts Corrected Isotopic Ratios <sup>†</sup> in equal MeV/nuc Intervals									
	Flare Peak	Imp.	Location	D25(H) Event Counts					Corrected Isotopic Ratios <sup>†</sup>								
				<sup>1</sup> H				<sup>2</sup> H	<sup>3</sup> H	<sup>3</sup> He	<sup>4</sup> He	( <sup>2</sup> H/ <sup>1</sup> H) 1.6-8.6	( <sup>3</sup> H/ <sup>1</sup> H) 1.2-6.8	( <sup>3</sup> He/ <sup>4</sup> He) 2.9-15.0	( <sup>3</sup> He/ <sup>4</sup> He) 2.9-15.0	( <sup>4</sup> He/ <sup>1</sup> H) 2.4-12.7	
29 Oct - 7 Nov '72	1747, 29 Oct	2F	S10 E05	1 x 10 <sup>8</sup>	3.1		29795	≤ 2	≤ 2	≤ 1	201	< 7x10 <sup>-5</sup>	< 2x10 <sup>-5</sup>	< 2x10 <sup>-6</sup>	< 0.03	0.010	
24 - 27 Nov '72	0830, 25 Nov	1B	S06 W46	7 x 10 <sup>6</sup>	3.1		1783	0	0	≤ 2	241	< 5x10 <sup>-6</sup>	< 2x10 <sup>-6</sup>	< 5x10 <sup>-7</sup>	< 0.03	0.16	
28 Nov - 1 Dec '72	0403, 28 Nov	1B	S08 W80	4 x 10 <sup>5</sup>	3.1		7399	0	0	0	57	< 1x10 <sup>-4</sup>	< 6x10 <sup>-5</sup>	< 5x10 <sup>-6</sup>	< 0.04	0.010	
16 - 17 Dec '72	0349, 16 Dec	1B	N12 W57	4 x 10 <sup>6</sup>	2.3		1658	0	0	≤ 4	199	< 8x10 <sup>-6</sup>	< 5x10 <sup>-6</sup>	< 8x10 <sup>-7</sup>	< 0.04	0.17	
7 Jan '73	*	*	*	8 x 10 <sup>3</sup>	3.7	C	186	0	0	≤ 1	5	< 3x10 <sup>-3</sup>	< 2x10 <sup>-3</sup>	< 4x10 <sup>-2</sup>	< 1	0.03	
14 - 15 Feb '73	2054, 14 Feb	*	*	1 x 10 <sup>6</sup>	3.1	NRV	403	0	0	12	83	< 2x10 <sup>-3</sup>	< 1x10 <sup>-3</sup>	0.05	0.21	0.27	
18 - 22 Feb '73	*	*	*	1 x 10 <sup>5</sup>	3.3	C	2681	≤ 1	0	≤ 2	96	< 5x10 <sup>-4</sup>	< 1x10 <sup>-4</sup>	< 3x10 <sup>-3</sup>	< 0.08	0.063	
12 - 14 Mar '73	1113, 12 Mar	1B	S19 W21	2 x 10 <sup>6</sup>	3.2		634	0	0	≤ 1	12	< 1x10 <sup>-3</sup>	< 6x10 <sup>-4</sup>	< 1x10 <sup>-2</sup>	< 0.4	0.03	
19 - 25 Mar '73	*	*	*	5 x 10 <sup>5</sup>	4.5	C	5695	0	0	≤ 2	232	< 8x10 <sup>-5</sup>	< 3x10 <sup>-5</sup>	< 2x10 <sup>-3</sup>	< 0.04	0.043	
30 Mar - 1 Apr '73	*	*	*	7 x 10 <sup>6</sup>	1.7		1768	0	0	0	2	< 8x10 <sup>-4</sup>	< 7x10 <sup>-4</sup>	< 2x10 <sup>-3</sup>	*	0.001	
11 - 22 Apr '73	*	*	*	1 x 10 <sup>7</sup>	3.2		31540	0	0	≤ 18	900	< 3x10 <sup>-5</sup>	< 1x10 <sup>-5</sup>	< 1x10 <sup>-3</sup>	< 0.04	0.036	
24 - 26 Apr '73	1445, 24 Apr	--N	S04 E57	4 x 10 <sup>6</sup>	3.0		931	0	0	≤ 2	58	< 9x10 <sup>-6</sup>	< 5x10 <sup>-6</sup>	< 9x10 <sup>-3</sup>	< 0.1	0.09	
29 - 30 Apr '73	2100, 29 Apr	1B	N13 W73	2x 10 <sup>5</sup>	~1.4	D	3185	0	0	0	67	< 9x10 <sup>-6</sup>	< 1x10 <sup>-3</sup>	< 8x10 <sup>-6</sup>	< 0.02	0.03	
17 - 21 May '73	*	*	*	>2 x 10 <sup>5</sup>	2.2	D	5943	≤ 1	0	≤ 5	244	< 4x10 <sup>-4</sup>	< 3x10 <sup>-4</sup>	< 2x10 <sup>-3</sup>	< 0.04	0.050	
21 - 24 May '73	*	*	*	4 x 10 <sup>6</sup>	1.7		1228	0	0	≤ 1	53	< 1x10 <sup>-3</sup>	< 9x10 <sup>-6</sup>	< 4x10 <sup>-3</sup>	< 0.07	0.05	
10 - 12 June '73	*	*	*	2 x 10 <sup>5</sup>	4.0	C	3583	0	0	≤ 2	161	< 2x10 <sup>-4</sup>	< 7x10 <sup>-5</sup>	< 3x10 <sup>-3</sup>	< 0.05	0.044	
13 - 17 June '73	*	*	*	1 x 10 <sup>5</sup>	2.8		3185	0	0	≤ 2	128	< 3x10 <sup>-4</sup>	< 2x10 <sup>-4</sup>	< 3x10 <sup>-3</sup>	< 0.05	0.052	
20 June '73	*	*	*	4 x 10 <sup>3</sup>	3.0		115	0	0	0	10	< 7x10 <sup>-3</sup>	< 4x10 <sup>-3</sup>	< 3x10 <sup>-2</sup>	< 0.3	0.11	
29 June '73	0150, 29 June	-N	S13 W48	7 x 10 <sup>3</sup>	3.7	SV	199	0	0	9	10	< 3x10 <sup>-3</sup>	< 1x10 <sup>-3</sup>	0.09	~ 2	0.06	
12 - 15 July '73	*	*	*	2 x 10 <sup>3</sup>	3.1	C	4553	0	0	≤ 2	144	< 2x10 <sup>-4</sup>	< 1x10 <sup>-4</sup>	< 2x10 <sup>-3</sup>	< 0.05	0.041	
28 July '73	*	*	*	2 x 10 <sup>3</sup>	2.9	A	94	0	0	0	4	< 9x10 <sup>-3</sup>	< 5x10 <sup>-3</sup>	< 3x10 <sup>-2</sup>	< 1	0.06	
29 July - 6 Aug '73	1329, 29 July	3B	N14 E45	4 x 10 <sup>6</sup>	2.9		33349	≤ 2	0	≤ 2	98	< 7x10 <sup>-5</sup>	< 2x10 <sup>-5</sup>	< 2x10 <sup>-6</sup>	< 0.08	0.043	
24 - 27 Aug '73	*	*	*	6 x 10 <sup>4</sup>	4.0	C	1307	0	0	≤ 1	57	< 4x10 <sup>-4</sup>	< 2x10 <sup>-4</sup>	< 5x10 <sup>-3</sup>	< 0.1	0.05	
5 Sept '73	*	*	*	~5 x 10 <sup>2</sup>	~3.6	ABV	16	0	0	12	2	< 4x10 <sup>-2</sup>	< 2x10 <sup>-2</sup>	1.0 <sup>+0.5</sup> <sub>-0.4</sub>	~ 6	~ 0.1	
7 - 15 Sept '73	1212, 7 Sept	2B	S18 W46	5 x 10 <sup>7</sup>	3.1		31837	≤ 3	0	≤ 4	296	< 7x10 <sup>-5</sup>	< 1x10 <sup>-5</sup>	< 4x10 <sup>-4</sup>	< 0.04	0.013	
17 - 20 Sept '73	1521, 17 Sept	*	*	3 x 10 <sup>6</sup>	1.8	R	894	0	0	≤ 1	2	< 2x10 <sup>-3</sup>	< 1x10 <sup>-3</sup>	< 6x10 <sup>-3</sup>	*	0.005	
27 - 28 Sept '73	*	*	*	2 x 10 <sup>6</sup>	3.7	C	477	0	0	≤ 1	10	< 1x10 <sup>-3</sup>	< 6x10 <sup>-4</sup>	< 1x10 <sup>-2</sup>	< 0.3	0.03	
4 - 7 Oct '73	*	*	*	8 x 10 <sup>6</sup>	2.9	A	2377	≤ 1	0	≤ 1	81	< 7x10 <sup>-4</sup>	< 2x10 <sup>-4</sup>	< 2x10 <sup>-3</sup>	< 0.06	0.04	
20 - 21 Oct '73	*	*	*	3 x 10 <sup>6</sup>	4.8	C	462	0	0	0	18	< 9x10 <sup>-4</sup>	< 3x10 <sup>-4</sup>	< 9x10 <sup>-3</sup>	< 0.2	0.05	
25 - 29 Oct '73	*	*	*	4 x 10 <sup>6</sup>	3.3	C	1311	≤ 1	0	0	24	< 1x10 <sup>-3</sup>	< 3x10 <sup>-4</sup>	< 5x10 <sup>-3</sup>	< 0.1	0.02	
3 - 6 Nov '73	0034, 3 Nov	2B	S18 W85	2 x 10 <sup>6</sup>	2.3		23720	0	0	0	166	< 5x10 <sup>-5</sup>	< 3x10 <sup>-5</sup>	< 1x10 <sup>-4</sup>	< 0.02	0.009	

A--Association with a specific optical event not possible since several subflares occurred within a few hours.

C--Possible corotating event.

D--Detector, D4, was disabled during part of this flare so that the quoted particle fluence should be considered a lower limit.

N--No optical flare patrol.

R--Flare peak time determined from radio data.

S--SCR event identified as described in Section III-F.

V--<sup>3</sup>He rich event.

---Least squares fit to proton spectrum of form  $\frac{dN}{dE} = A \cdot E^{-V_p}$  between 1.3 and 10.2 MeV. See Appendix B.

†--Estimated errors not shown may be inferred from the event counts.

\*\*--Except for the optical data which is from Solar-Geophysical Data, all entries in this table are from this work, as described in the text.

topic ratios as described in the next section. Ratios in which the observed counts of  $^2\text{H}$ ,  $^3\text{H}$  or  $^3\text{He}$  were likely to include significant background contributions are listed in Table III-1 as 84% confidence level upper limits.

### C. Establishment of Isotopic Ratios

In order to convert the number of isotopes observed in the D25(H) mass histograms to isotopic ratios, two corrections must be applied.

The first is to compensate for the crosstalk problem discussed in Appendix B, whereby an average of about 15% of real D25(H) events are excluded from the original D25(H) mass histograms. The relative effect on various isotopes can be estimated by using simulated data and a semi-empirical model of the crosstalk process. Table III-2 shows the average correction factor applicable to a differential  $E^{-3}$  D25(H) spectrum of various isotopes. The observed crosstalk fractions for protons and alphas shows that over the range of spectra encountered in the periods listed in Table III-1, the correction factors listed in Table III-2 can be considered to have an R.M.S. accuracy of 2% and 11% for hydrogen and helium respectively. With the exception of ( $^4\text{He}/^1\text{H}$ ) whose crosstalk correction is handled as in Appendix B, the expected correction to the isotopic ratios is much smaller than the corresponding statistical error.

As shown in Table II-5, the energy thresholds for range D25(H) events are unique to each isotope. In order to take full advantage of the EIS sensitivity to rare isotopes in the D25(H) range the energy

Table III-2. Average Crosstalk Correction Factor for  $E^{-3}$   
D25(H) Isotopes

	Correction Factor †
$^1\text{H}$	1.10*
$^2\text{H}$	1.12
$^3\text{H}$	1.14
$^3\text{He}$	1.45
$^4\text{He}$	1.47**
$(^2\text{H}/^1\text{H})$	1.02
$(^3\text{H}/^1\text{H})$	1.04
$(^3\text{He}/^1\text{H})$	1.32
$(^4\text{He}/^1\text{H})$	1.34 <sup>+</sup>
$(^2\text{H}/^3\text{He})$	0.77
$(^3\text{H}/^3\text{He})$	0.79
$(^3\text{He}/^4\text{He})$	0.99

\* Estimated RMS accuracy is 2%.

\*\* Estimated RMS accuracy is 11%.

<sup>+</sup> The crosstalk correction for  $(^4\text{He}/^1\text{H})$  was done on an individual flare basis as described in Appendix B. The value quoted here is typical.

† The correction factor is the ratio of the number of events (or ratio) that would have been observed in the absence of crosstalk to the number (or ratio) that were actually observed.

limits for the rare isotopes are used as the basis for establishing ratios. As the energy spectra for the more numerous primary particles (protons or alphas) are known, this implies that the primary spectra must be integrated between the rare isotope energy/nucleon limits. A convenient way of performing this integration is to define a 'Spectral Correction Factor',

$$S \equiv \frac{E_{R1}^{-\gamma+1} - E_{R2}^{-\gamma+1}}{E_{P1}^{-\gamma+1} - E_{P2}^{-\gamma+1}}$$

where  $(E_{R1}, E_{R2})$  are the energy/nucleon limits for D25(H) events for the rare isotope in question,  $(E_{P1}, E_{P2})$  are the D25(H) energy/nucleon limits for the primary isotope, and  $\gamma$  is the primary differential spectral index.  $S$  is then just the ratio of the integrated primary flux between  $(E_{R1}, E_{R2})$  to the integrated primary flux between  $(E_{P1}, E_{P2})$ . Note that the value of  $\gamma$ , upon which the calculation of  $S$  is dependent, is in most cases measured over the full range of  $(E_{R1}, E_{R2})$ . The only extrapolations involve  ${}^3\text{He}$ , where the primary flux must be extrapolated above 12.7 MeV to 15 MeV. No significant error is introduced, however, because of the steep primary spectra.

The corrected isotopic ratio,  $(R/P)$ , between  $(E_{R1}$  and  $E_{R2})$  is then given by:

$$\frac{R}{P} = \frac{N_R}{N_P \cdot S} \cdot C_{XT} \quad (\text{III-1})$$

where  $N_R$  and  $N_P$  are the number of observed D25(H) rare isotope and

primary events in the D25(H) range respectively, and  $C_{XT}$  is the crosstalk correction factor listed in Table III-2.

#### D. Flare Sum - Deuterium and Tritium

Since no deuterium or tritium was observed in a single flare, it is of interest to estimate the flare averaged values of the ratios ( ${}^2\text{H}/{}^1\text{H}$ ) and ( ${}^3\text{H}/{}^1\text{H}$ ). A sum over the flare periods in Table III-1 shows that up to 11  ${}^2\text{H}$ -like and 2  ${}^3\text{H}$ -like events were observed. Most of these events are, however, background from pulse pileup and events of galactic origin (Section II-E). A disproportionately large fraction of these background events occur either during the peaks of large flares, or during very small flares when the ratio of solar to galactic particles is relatively low.

If the assumption is made that the ratios of ( ${}^2\text{H}/{}^1\text{H}$ ) and ( ${}^3\text{H}/{}^1\text{H}$ ) are constant, then the ratio of real events (including  ${}^2\text{H}$  and  ${}^3\text{H}$ ) to background events (viz, the signal to noise ratio, S/N) can be improved by deleting the lowest and highest rate periods from consideration. For each six hour period originally considered, the expected background contribution can be calculated using the numerical parameters discussed in Section II-E. Next, the 515 six hour periods are ordered in terms of their predicted S/N ratios. The optimum choice of periods in a flare sum includes those periods with relatively high S/N, with a sufficient number of periods so that adequate statistics can be obtained. This is equivalent to determining an optimum cutoff point in the ordered list, and including only those periods above that cutoff. Minor editing then eliminated 8 marginal periods

which were either isolated in time or whose qualification was conditional on the choice of numerical background parameters. The resulting optimum set of 115 six hour periods, shown in Table III-3, is not unduly sensitive to the numerical parameters used to estimate the background.

It should be noted that the optimization procedure used is based on the ratio of observed protons to predicted background, and is not influenced by the number of "deuterons" or "tritons" that were actually observed in any one six hour solar active period.

The mass histogram resulting from this optimized sum is shown in Figure III-1. It shows that 132274 protons, up to 3 deuterons and no tritons were observed. In the case of tritium, this enables an upper limit at the 84% confidence level to be established at  $3.4 \times 10^{-6}$  for ( ${}^3\text{H}/{}^1\text{H}$ ) between 1.2 and 6.8 MeV/nuc.

The deuterium requires a more detailed discussion since the possibility cannot be excluded that at least one of these events is background. The expected  $\sigma_m$  for  ${}^2\text{H}$  ranges from 0.10 to 0.20 amu depending on energy. By associating each event with the  $\sigma_m$  appropriate to its energy, each event falls within  $1 \sigma_m$  of  $M = 2$  and the total  $\chi^2$  for these three events is found to be 1.3. This corresponds at the 72% confidence level to the hypothesis that all three events are part of a deuterium 'peak'.

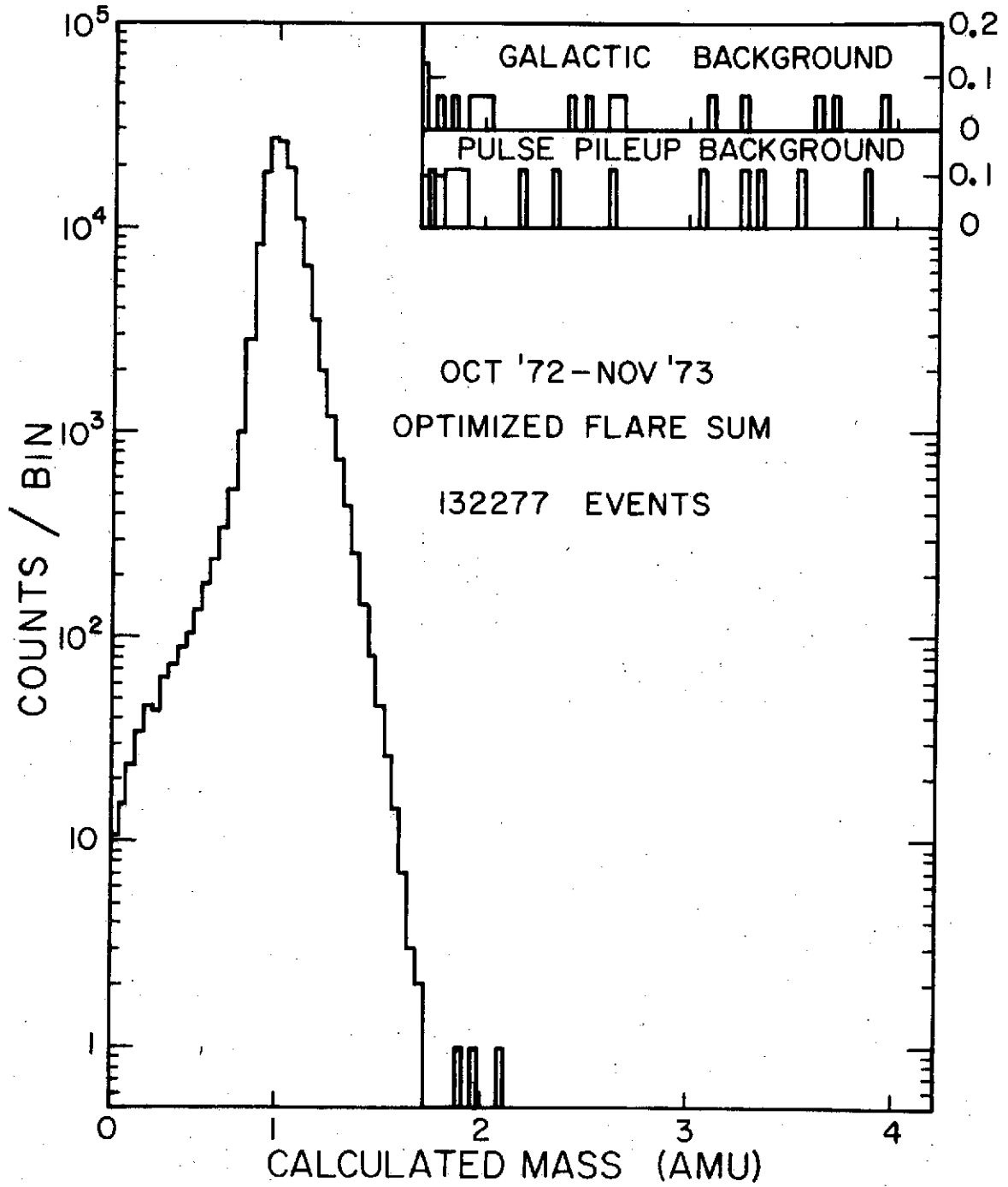
To evaluate the possibility of a background origin of these events, the inset in Figure III-1 shows two observed background spectra

Table III-3. Time Periods in Optimized Flare Sum

Time Period	D25(H) Hydrogen Event Count
2023, 29 Oct.--0304, 30 Oct. '72 0823, 1 Nov.--1421, 4 Nov. '72	14678
1100, 28 Nov.--2259, 29 Nov. '72	6361
0519, 20 Mar.--2317, 22 Mar. '73	4381
0000, 12 Apr.--2358, 12 Apr. '73 1200, 14 Apr.--1157, 20 Apr. '73	24877
2120, 29 Apr.--1459, 30 Apr. '73	3336
0551--1750, 18 May '73	1077
1201, 11 June--1759, 12 June '73	2987
0000--2358, 14 July '73	2931
1800, 29 July--1759, 3 Aug. '73	32108
1200, 7 Sept.--0559, 8 Sept. '73 2052, 10 Sept.--2044, 12 Sept. '73	15474
0000, 3 Nov.--1801, 5 Nov. '73	24067
Total	132277

Figure III-1

Hydrogen mass histogram for the optimized flare sum. The insets show the individual galactic and pulse pileup background events measured during solar quiet times and the peaks of large flares respectively. The vertical background scales normalize these events to the level expected for the optimized flare sum. Note that the background levels of  $\sim 0.1$  are offscale on the semi-logarithmic plot of the flare sum data.



acquired during solar quiet times (galactic background) and during the peaks of three flares (pulse pileup), normalized to correspond to the flare sum. The flat spectral shape in each case is in contrast to the observed group at  $M = 2$ .

Based on the observed background which is mainly low energy with  $\sigma_m \approx 0.1$ , the number of expected background events within  $\pm 2 \sigma_m$  of the  $^2\text{H}$  peak is 0.3 and 0.4 for galactic and pulse pileup respectively, compared to the 3 observed. Including an estimate of backscattered protons (see Section II-E) brings the expected background within  $\pm 2 \sigma_m$  to 1.0 events. The probabilities of observing 0, 1, 2 or 3 background events within  $\pm 0.2$  amu given an expectation of 1.0 and the fact that no more than 3 were observed are 0.375, 0.375, 0.188 and 0.062 respectively. Thus there is a 94% probability that at least 1 of the three events is real, based on a background expectation of 1.0.

That background estimate in turn is based on 9 events in the Figure III-1 inset which fall within  $\pm 2 \sigma_m$  of the  $^2\text{H}$  peak, plus a conservative estimate of the backscattering component. A 95% upper limit to the background (corresponding to 1.6 background events expected in Figure III-1) still yields an 85% probability that at least 1 of the three events is real. Such a significant underestimate of the background near  $M = 2$  is not likely in view of the observed shape of the expected background and the lack of background events elsewhere in Figure III-1.

Taking into account the large statistical uncertainty in background subtraction, a deuterium/proton ratio can be established between 1.6 and 8.6 MeV/nuc with 68% confidence limits. This value,  $7_{-6}^{+10} \times 10^{-6}$  corresponds to a level of  $2_{-1.6}^{+3}$  real  ${}^2\text{H}$  events in Figure III-1.

#### E. Flare Sum--Helium 3

With the exception of the three events of 14 February, 29 June and 5 September 1973, no Helium 3 was positively identified during any single solar active period. To establish a flare-averaged abundance of  ${}^3\text{He}$ , the helium mass histograms for all other periods listed in Table III-1 were summed. Preliminary analysis of this histogram indicated that a significant background existed near  $M = 3$  from a low mass tail to the alpha peak at  $M = 4$ . As discussed in Section II-E and Appendix C, such a tail is caused by alpha particles channeling in D2. In Appendix C a channeling calibration experiment is described which permits the response of the D2-D5 system to be evaluated for an isotropic flux of 8.785 MeV alphas. Because of the complex energy dependence of the channeling and dechanneling effects, these calibration results cannot be readily extended to other energies.

Thus, the channeling calibration data cannot be applied to the full D25(H) mass histogram which includes alpha particles with energies from 8 to 51 MeV. In the more limited range of detected energy\* of

---

\* Detected energy is the sum of the energy losses in D2 and D5. It does not include the energy loss in the mylar window.

8 - 10 MeV, which brackets the calibration energy of 8.785 MeV, the energy dependence of the channeling process can be neglected and the calibration data applied directly.

The top panel of Figure III-2 shows the mass histogram for 8 - 10 MeV particles and the corresponding level of channeling background. A peak at  $M = 3$  is observed with 12 counts within a FWHM (0.28 amu). The channeling background (known to high statistical accuracy) in the same mass interval is 4.6. Since the difference of 7.4 counts includes only those within a FWHM (ie. 76% of the total), this should be compared to 76% of the corresponding alpha count. Equation III-1 can then be used to determine a corrected isotopic ratio with a spectral correction factor,  $S = 0.78$  (for  $\gamma = 3$ ) and  $C_{XT} = 1.31$ .\* The result is  $({}^3\text{He}/{}^4\text{He}) = 0.011 \pm 0.006$  in the restricted velocity interval of 3.1 - 3.7 MeV/nuc which corresponds to the 8 - 10 MeV limits on the detected energy for  ${}^3\text{He}$ .

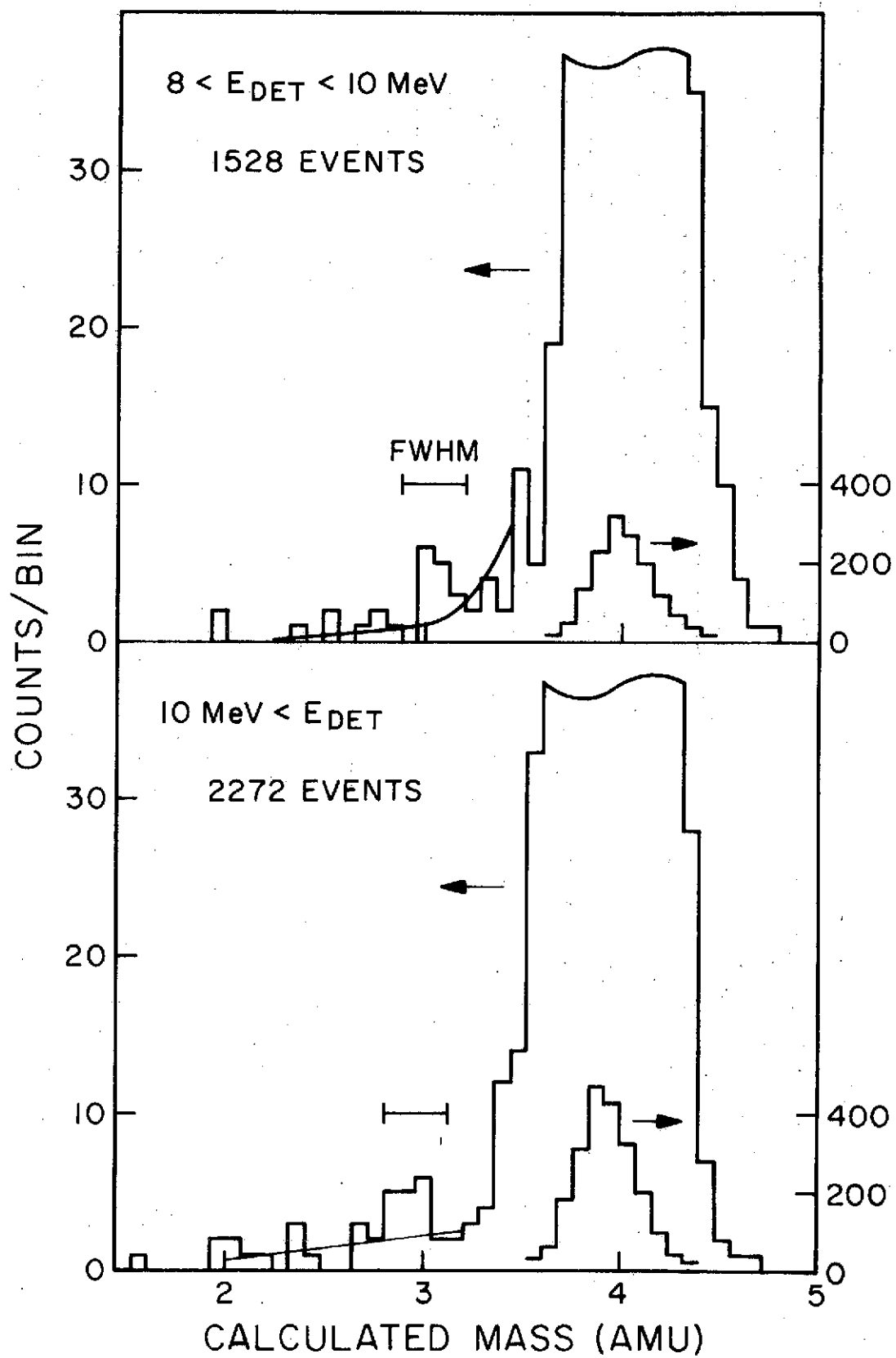
Since this flare sum represents a total of  $4 \times 10^6$  seconds of live time, the contribution of galactic  ${}^3\text{He}$  to this result should be evaluated. D25(H) solar quiet time measurements shows that in this restricted energy interval the galactic  ${}^3\text{He}$  contribution is negligible ( $< 1\%$  of the observed  ${}^3\text{He}$ ).

---

\*This value of  $C_{XT}$ , calculated from simulated data, differs from that quoted in Table III-2 since only part of the D25(H) matrix is used here.

Figure III-2

Helium mass histograms for the sum over all periods listed in Table III-1 excluding the  $^3\text{He}$  rich events of 14 February, 29 June and 5 September, 1973. The top panel shows particles with detected energies in the range 8 - 10 MeV. For alphas in this energy range, the channeling background near  $M = 3$  is known and is represented by the light smooth curve. The lower panel shows D25(H) particles with detected energies greater than 10 MeV. Since the channeling background is not known in this case, the smooth curve represents an empirical estimate of the background near  $M = 3$ .



The lower panel of Figure III-2 shows the helium mass histogram for D25(H) events with detected energy greater than 10 MeV. Again a statistically significant  $^3\text{He}$  peak is observed. Although the background level cannot be quantitatively determined from the channeling data, an empirical background estimate, normalized to the data outside the  $^3\text{He}$  peak location can be drawn as shown and can account for 8 out of the 16 events within a FWHM.

To improve the statistical accuracy, the data in both panels of Figure III-2 are combined to yield 28 events within a FWHM of the expected  $^3\text{He}$  peak positions with 13 of these estimated to be background. Evaluating the corrected ratio as described above, with  $S = 0.61$  and  $C_{\text{XT}} = 0.99$ , yields a value of  $(^3\text{He}/^4\text{He}) = 0.009 \pm 0.004$  in the velocity interval 3.1 - 15.0 MeV/nuc. The corresponding ratio of  $(^3\text{He}/^1\text{H})$  in the same interval is  $1.7 \pm 0.7 \times 10^{-4}$ . The galactic contribution to the observed  $^3\text{He}$  is less than 10% in this case.

#### F. Helium 3 Rich Flares

Previously reported work by Garrard et al. (1973a,b), Hurford et al. (1973e) and Anglin et al. (1974) have shown the existence of small solar particle events in which the  $^3\text{He}/^4\text{He}$  ratio is relatively large. The 14 February event in Table III-1 is one such event. Since the criteria described in Section III-B to establish a data base tends to discriminate against very small solar events, a check was made to ensure that no small events, rich in the rare isotopes, were overlooked.

Individual mass histograms of D25(H) events were constructed for each day between 30 September 1972 and 9 January 1974 that was not

included in the original six hour averages. For each day, the number of  $^2\text{H}$ ,  $^3\text{H}$  and  $^3\text{He}$  events\* were noted with resulting daily averages of 0.01, 0.01 and 0.1 respectively. While the " $^2\text{H}$ " and " $^3\text{H}$ " were randomly distributed over the 330 days included in this study, over half (23) of the total of 43 " $^3\text{He}$ " were observed on 29 June and 5 September, 1973. Using the PHI rate to further restrict the time intervals to periods of enhancement on these days the results presented in Table III-1 were obtained. The mass spectra for the three  $^3\text{He}$  rich events are shown in Figure III-3.

The most remarkable of these three is the 5 September, 1973 event in which the  $^3\text{He}$  was the dominant species of helium observed. The fact that the observed ( $^3\text{He}/^4\text{He}$ ) ratio is  $\gg 1$  rather than  $\ll 1$  raises the spectre of an undetected ADC gain or offset shift as the cause of the high " $^3\text{He}$ " component. The possibility of a D5 ADC anomaly is discounted by the fact that the maximum energy loss for D2 singles (the 'endpoint') corresponds to  $^3\text{He}$ , not  $^4\text{He}$ . Thus the dominance of  $^3\text{He}$  over  $^4\text{He}$  is supported by the D2 data alone, independent of D5. A D2 gain shift of 10% or an offset shift of 20 channels would be the only remaining possibility. Such an occurrence would shift the proton peak down by  $\sim 15\%$  or  $\sim 50\%$  respectively, which is inconsistent with the simultaneously measured proton mass spectrum. A solar as opposed to galactic origin for the observed  $^3\text{He}$  particles is supported by their

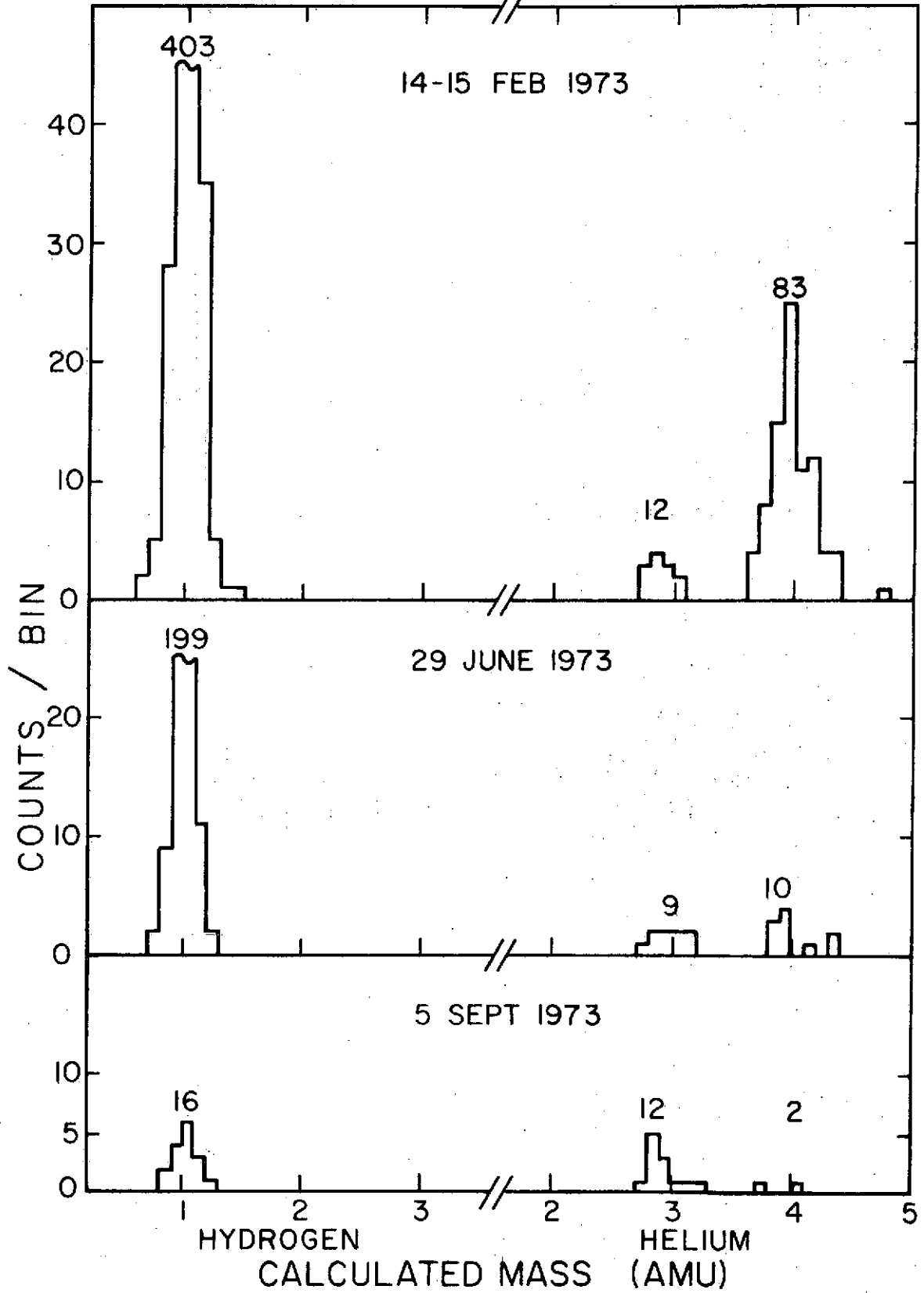
---

\* Such events included background, if any.

Figure III-3

Hydrogen and helium mass histograms for the  $^3\text{He}$  rich events of 14 February, 29 June and 5 September, 1973. The total counts in each peak are shown.

(The mass histogram for the 14 February event corresponds to the D25(H) matrix shown in Figure A-2.)



steep spectrum, their time profile and their arrival direction, which was strongly anisotropic in the direction of the average magnetic field line from the sun.

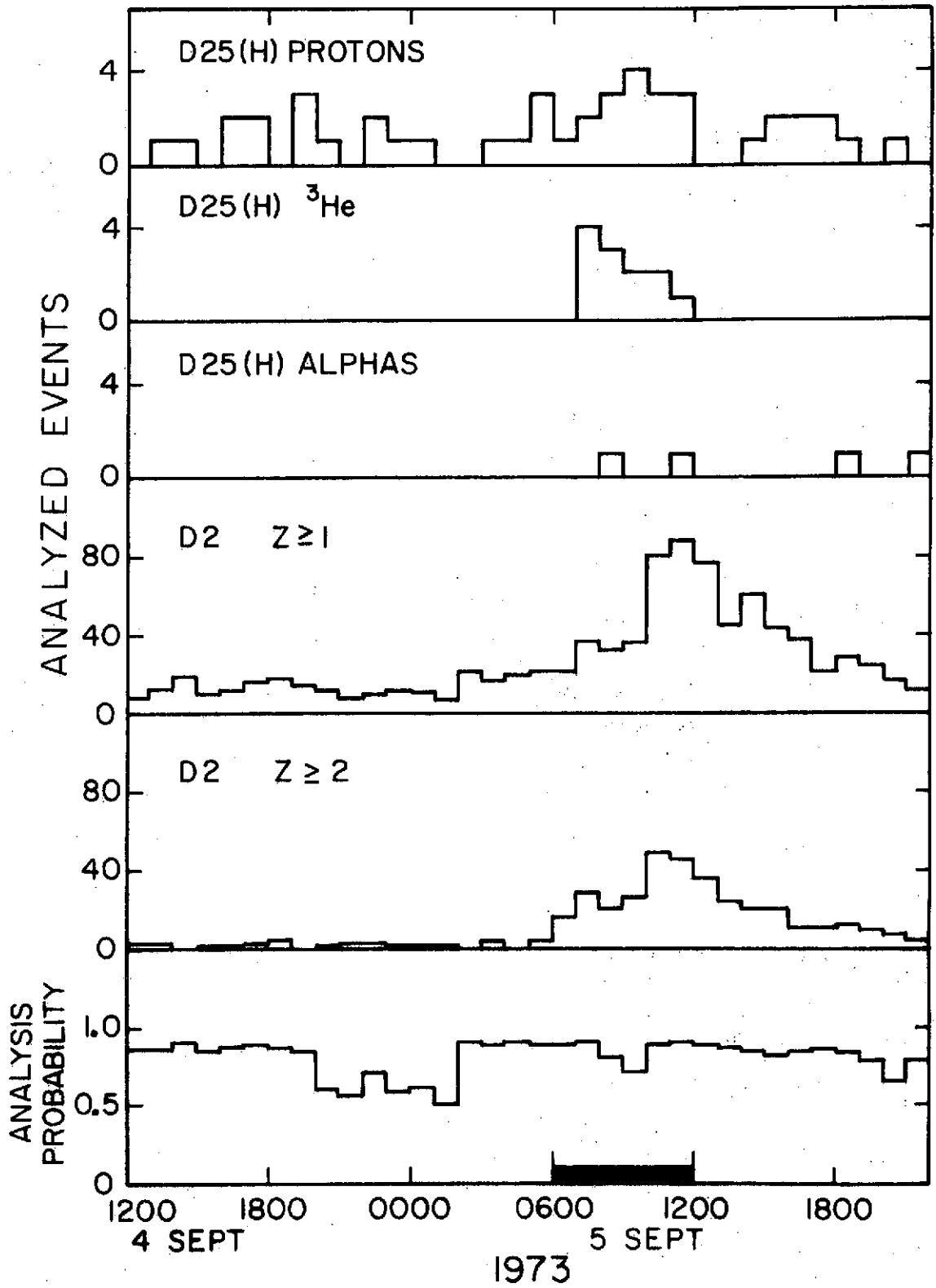
Figure III-4 shows the time profile of the 5 September event. It shows that the group of  $^3\text{He}$  nuclei detected on 5 September occurred during a period of constant proton flux, somewhat enhanced over quiet time levels of  $\lesssim 5$  D25(H) events/day. The  $^3\text{He}$  nuclei were accompanied by a small increase in the D25(H) proton flux as well as by lower energy nuclei detected by D2. Note that in the abundance ratios quoted in Table III-1, no allowance was made for the 'steady state' proton activity. The EIS did not detect any accompanying electron activity during this period. In the hours preceding this event, there were several subflares observed, so that the association of any particular subflare with the  $^3\text{He}$  flux is not possible.

Figure III-3 shows that a common characteristic of all 3 events is the absence of a detectable deuterium or tritium flux, compared to the 33  $^3\text{He}$  observed. In the restricted energy interval of 2.9 - 6.8 MeV/nuc, common to all three isotopes, 27  $^3\text{He}$  nuclei were observed. This sets an 84% upper limit of 0.053 to the ratios ( $^2\text{H}/^3\text{He}$ ) and ( $^3\text{H}/^3\text{He}$ ), averaged over these three events.

A second common characteristic is their relatively small proton fluence as shown in Table III-1. The  $^3\text{He}$  fluence for each of these events is similar at about  $3 \times 10^2/\text{cm}^2$  sr between 3.2 and 15 MeV/nuc. This is about a factor of 3 above the threshold for detectability in this study.

Figure III-4

Time profile of the 5 September 1973 SCR event. The first five panels show the number of events analyzed in each one hour period. The analysis probability, plotted in the last panel, can be considered the fraction of the hour in which the experiment was 'live' to such nuclei. The D2  $Z \geq 1$  events are predominantly protons (1.23 - 1.87 MeV) with some contamination by alphas (1.06 - 1.17 MeV/nuc) and  $^3\text{He}$  (1.06 - 1.22 MeV/nuc). The D2  $Z \geq 2$  events are  $^3\text{He}$  (1.36 - 2.86 MeV/nuc) and alphas (1.26 - 2.39 MeV/nuc). The energy limits for D25(H) events are 2.45 - 12.74, 2.86 - 14.99, and 2.39 - 12.77 MeV/nuc for protons,  $^3\text{He}$  and alphas respectively. The geometrical factors for D2 and D25(H) events are 0.2 and 0.07 cm<sup>2</sup> sr respectively. The bar along the time axis indicates the period included in the mass histogram in Figure III-3.



#### IV. DISCUSSION OF RESULTS

##### A. Comparison of Results

In this section the isotopic ratios obtained above will be compared to previous observations of SCR's by other workers. Table IV-1 summarizes these observations along with current values of the ambient solar abundances. All of the SCR results were obtained by satellite-borne dE/dx-E telescopes, with the exception of the four earliest measurements which have been reviewed by Lingenfelter and Ramaty (1967). The data summarized in Table IV-1 will be considered below in three groups.

##### 1. Deuterium and tritium observations

The flare averaged results of ( $^2\text{H}/^1\text{H}$ ) and ( $^3\text{H}/^1\text{H}$ ) reported by Anglin et al., Garrard et al., and the present work are summarized in Figure IV-1, along with the Rothwell et al. upper limits for the 30 October 1972 event. The most striking feature of this comparison is the fact that the upper limits of Rothwell et al. and the present results are significantly below the ratios reported by Anglin et al. at 10 MeV/nuc. Since the lower results were obtained with average proton energies less than 10 MeV, this suggests that ( $^2\text{H}/^1\text{H}$ ) and ( $^3\text{H}/^1\text{H}$ ) decrease with decreasing energy below 10 MeV/nuc. If differential power law spectra are assumed for all the isotopes, Figure IV-1 then shows that the softer proton spectrum must have a spectral index which differs by at least 1 from that of the deuterium or tritium spectra below 10 MeV/nuc.

Table IV-1. Isotopic Ratios Measured in Equal Velocity Intervals

Flare	Energy (MeV/nuc)	( <sup>2</sup> H/ <sup>1</sup> H)	( <sup>3</sup> He/ <sup>4</sup> He)	( <sup>12</sup> C/ <sup>13</sup> C)	( <sup>3</sup> He/ <sup>4</sup> He)	( <sup>3</sup> He/ <sup>1</sup> H)	( <sup>3</sup> He/ <sup>4</sup> He)	Vehicle	Reference
11 Nov '60	25-50	< 10 <sup>-3</sup>						rocket	Biswas et al., as reported by Biswas, 1964 Schauffer & Zahringer, 1962 Biswas, 1964 Waddington & Freier, 1964
12 Nov '60	~70						0.2	Discoverer 17	
12 Nov '60	>30							Discoverer 17	
18 July '61	>50	< 2.10 <sup>-3</sup>						balloon	
7 flare average	10-100 10-15 15-100	< 8.10 <sup>-5</sup>	< 8.10 <sup>-3</sup>	< 4.10 <sup>-3</sup>	< 4.10 <sup>-3</sup>	2.10 <sup>-4</sup>	0.021±0.004	IMP-4	Heich & Simpson, 1970
May-Dec '67							< 0.01		
17 flare average							0.06		
7 flare average '69*	4-5	< 7.10 <sup>-4</sup>		< 1.10 <sup>-4</sup>		(6±1).10 <sup>-4</sup>	0.10±0.02	IMP-4	Anglin, et al., 1973a
14 Oct '69	4-5	< 5.10 <sup>-4</sup>		< 5.10 <sup>-4</sup>		(3±1).10 <sup>-3</sup>	0.26±0.08		
6 Nov '69	4-5	< 7.10 <sup>-4</sup>		< 7.10 <sup>-4</sup>		< 1.10 <sup>-3</sup>	< 0.06		
14 Oct + 24 Nov '69	4-5						0.24±0.07		
5 flare average '69	4-5						< 0.02		
2 Nov '69	10-50						0.077±0.020	IMP-5	Dietrich, 1973 also Anglin et al., 1973a
25 Jan '71	10-50		< 0.5				0.020±0.010		
5 'He3 Rich' flares†	10-50						0.033		
7 'He3 Poor' flares	10-50		< 0.024				< 0.015*		
10 Oct '72	3.1-30.6 2.4-23.0	< 1.4.10 <sup>-5</sup>		< 9.10 <sup>-6</sup>				S72-1	Rothwell et al., 1973
Sept '69	10.5-13.5	(6.8±3.0).10 <sup>-5</sup>	(8.0±3.5).10 <sup>-3</sup>	(1.2±0.7).10 <sup>-5</sup>	(1.3±0.8).10 <sup>-3</sup>			IMP-5	Anglin et al., 1973b
-Nov '72	7.1-9.9			< 2.10 <sup>-3</sup>	< 2.10 <sup>-3</sup>				
sum	6.7-13.5	(6.7±2.6).10 <sup>-5</sup>	(7.3±2.8).10 <sup>-3</sup>						
Mar '71	5.3-9.9								
-Aug '72	10.9-13.2	(6.3±1.5).10 <sup>-5</sup>	(1.0±0.2).10 <sup>-2</sup>	(1.8±0.3).10 <sup>-5</sup>	(2.7±0.7).10 <sup>-3</sup>				
sum	7.9-10.6							IMP-6	
Sept '69-Nov '72 average	8.1-13.2	(1.3±0.3).10 <sup>-4</sup>	(1.9±0.5).10 <sup>-2</sup>	(3.2±0.7).10 <sup>-5</sup>	(4.6±1.1).10 <sup>-3</sup>				
30 July '70	17.2-22.1 10.5-22.1						0.14±0.05 0.54±0.09	IMP-5	Anglin et al., 1974
Aug '72	-7 -60						0.002 0.02	Pioneer 10	Webber, et al., as reported by Kamaty and Koslovsky, '74
Oct '72-Nov'73 sum	1.6-8.6 1.2-6.8 3.1-3.7 3.1-15.0	(7 <sup>+10</sup> <sub>-6</sub> ).10 <sup>-6</sup>		< 3.4.10 <sup>-4</sup>			(1.7±0.7).10 <sup>-4</sup> 0.011±0.006 0.009±0.004	IMP-7	this work
16 Feb '73	1.6-8.6 1.2-6.8 2.9-15.0	< 0.002		< 0.001			0.05 ± 0.02 0.21±0.07		
29 June '73	1.6-8.6 1.2-6.8 2.9-15.0	< 0.003		< 0.001			0.09±0.04 ~2		
5 Sept '73	1.6-8.6 1.2-6.8 2.9-15.0	< 0.06		< 0.02			1.0 <sup>+0.5</sup> <sub>-0.4</sub> ~6		
photosphere solar wind solar wind		< 5.10 <sup>-6</sup> < 3.10 <sup>-6</sup>					4.10 <sup>-4</sup>		

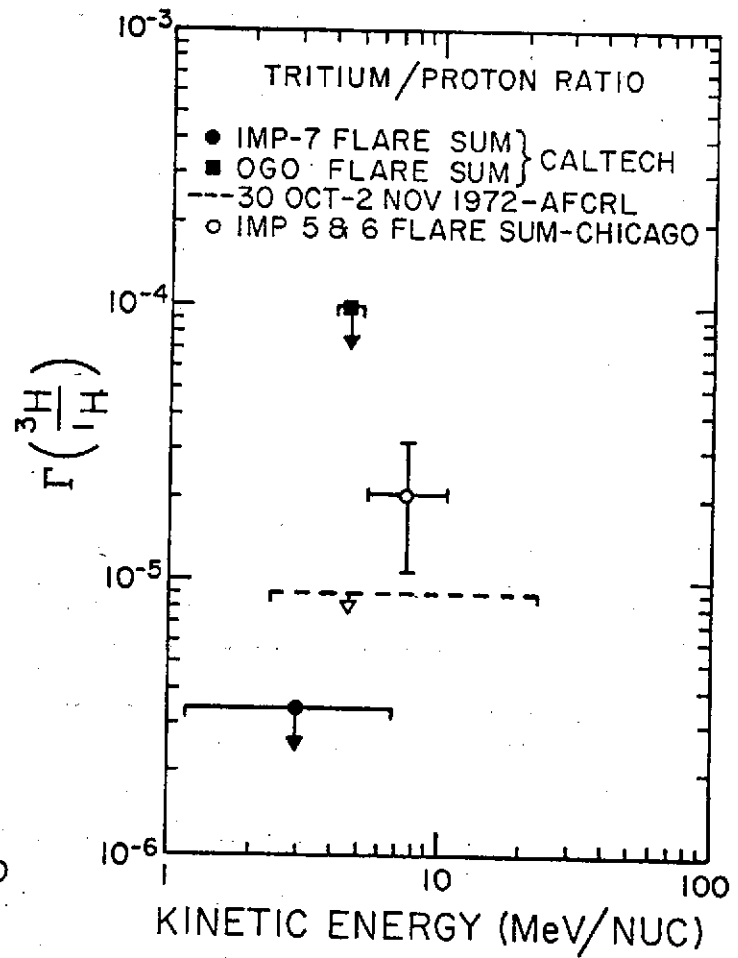
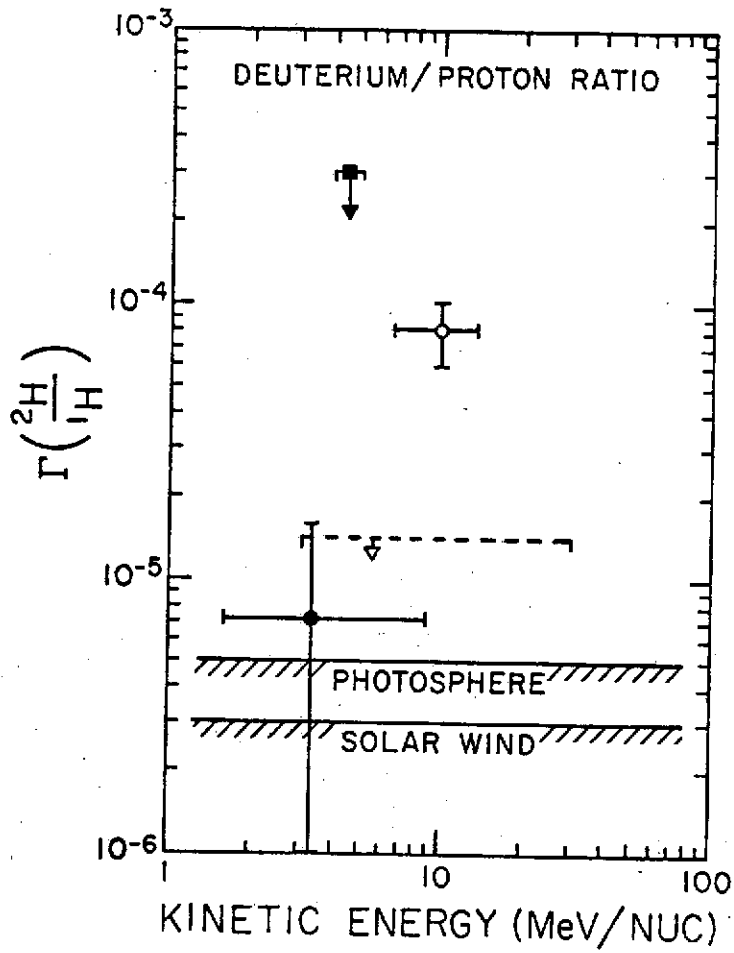
\* Reported as a finite flux, but should be regarded as an upper limit. See text.

† Average includes 2 flares whose finite <sup>3</sup>He content is shown separately.

REPRODUCIBILITY OF THE ORIGINAL PAGE IS POOR

Figure IV-1

Summary of selected ( $^2\text{H}/^1\text{H}$ ) and ( $^3\text{H}/^1\text{H}$ ) observations. The dashed upper limits were obtained by Rothwell et al. (1973) for the 29 October 1972 flare. The solid squares, open and closed circles are flare averages reported by Garrard et al. (1973a), Anglin et al. (1973b) and this work respectively. The photospheric and solar wind results of Grevesse (1970) and Epstein and Taylor (1972) are upper limits.



It should be noted that the different observations shown in Figure IV-1 refer to different flares.\* However both the present results and those of Anglin et al., refer to flare averages which should minimize the effects of flare-to-flare variations.†

Another possibility which cannot be excluded is that experimental error has contributed to the observed differences. The observational differences are sufficiently significant‡, however, to require gross experimental errors to account for the full range of reported ratios.

## 2. Flare averaged $^3\text{He}$ observations

The wide flare-to-flare variation in the relative abundance of  $^3\text{He}$  has been independently established by Dietrich, Garrard et al. and the present results. Table IV-1 shows that the observed values of  $(^3\text{He}/^4\text{He})$  for individual flares varies over 3 orders of magnitude from 0.002 for the large August 1972 events to  $\sim 6$  for the small event of 5 September, 1973. Thus the same cautionary note applied to comparisons of flare average ratios based on different sets of flares. In particular,

---

\* The 30 October 1972 event, measured by Rothwell et al. and presumably included in Anglin et al.'s IMP-5 flare sum constitutes only 11% of the data used in the present work.

† The extent of flare-to-flare variation in the deuterium or tritium abundances is difficult to estimate since observations of finite fluxes have previously been reported for only two flare averages. The two sets of data were consistent to a factor of 2. The present results for deuterium are at least a factor of 4 below the average of those higher energy measurements.

‡ If the present experiment had measured ratios of  $(^2\text{H}/^1\text{H})$  and  $(^3\text{H}/^1\text{H})$  at the same levels as observed by Anglin et al., then in Figure III-1, the deuterium and tritium peaks would have contained 23 and 11 counts respectively instead of the 3 and 0 observed.

flare averages which contain known "<sup>3</sup>He rich events" are discounted below. Below 15 MeV/nuc then, the present result of  $(^3\text{He}/^4\text{He}) = 0.9\%$  can be compared to the remaining flare-averaged upper limits of 1% of Hsieh and Simpson, 2% of Garrard et al. and the value of  $1\frac{1}{2}\%$  for 7 <sup>3</sup>He poor flares, reported by Anglin et al. (1973a). This value of  $1\frac{1}{2}\%$  should also be considered an upper limit since it is based on 5 <sup>3</sup>He events, and "some or all of these five events could be background" according to Dietrich (1973). Thus, the present result is consistent with previous measurements of flare-averaged  $(^3\text{He}/^4\text{He})$  below 15 MeV/nuc but is higher than the Webber et al. result for the August 1972 flare.

The present result must be regarded with great caution, however, since the possibility exists of significant contamination by small <sup>3</sup>He rich events discussed below. The inherently poor spatial and temporal resolution of SCR observations would permit such contamination to occur undetected, particularly during complex solar active periods.

### 3. Individual <sup>3</sup>He rich flares

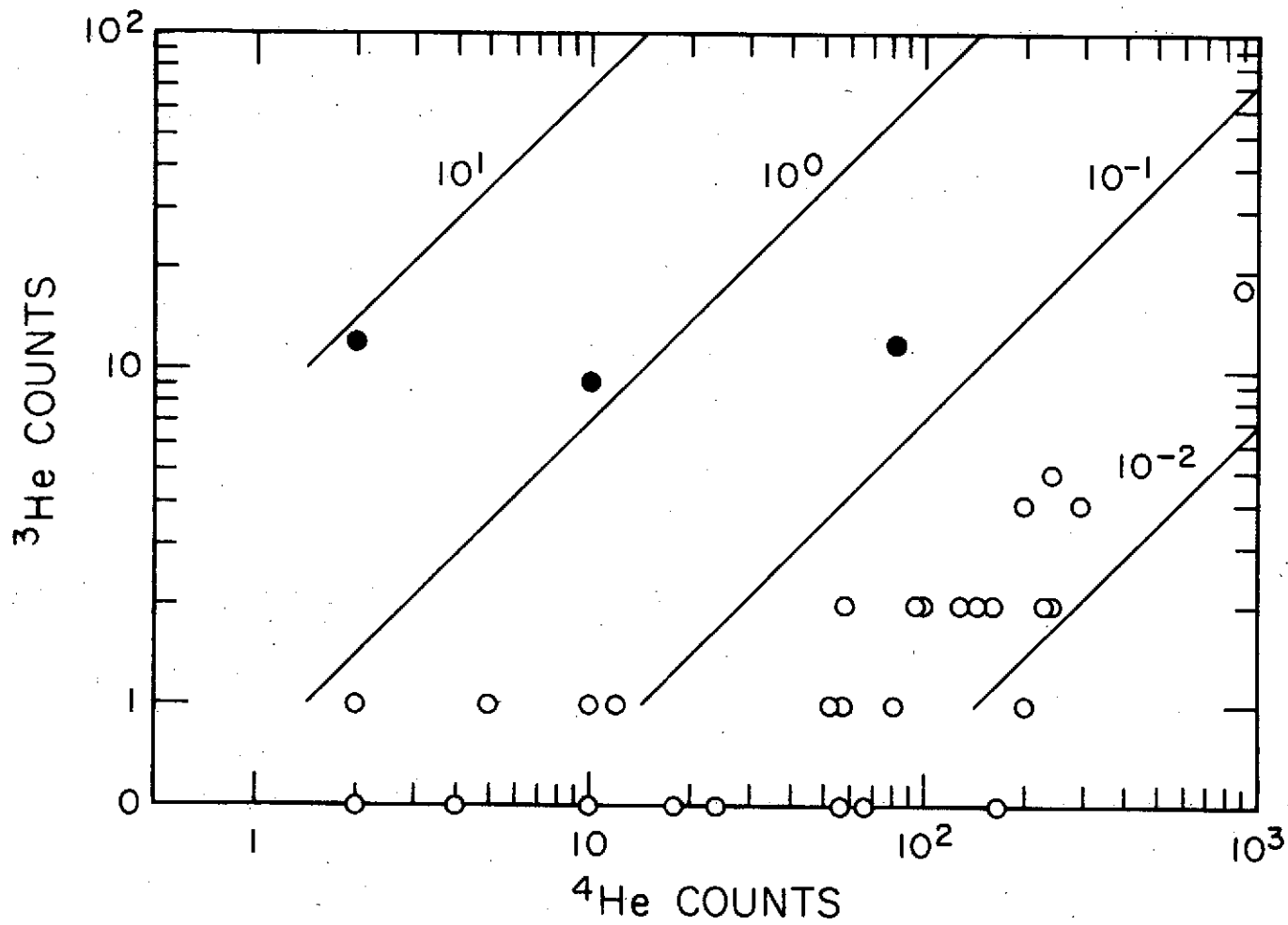
The raw helium observations from Table III-1 are presented in Figure IV-2 to correlate the number of observed <sup>3</sup>He nuclei in each solar event with the corresponding alpha count. With the exception of the largest solar flares, the relative event count provides an indication of the relative fluence. The effect of channeling is seen by the trend of the data parallel to the  $(^3\text{He}/^4\text{He}) \sim 10^{-2}$  line.\*

---

\* Note that since a  $\pm 2\sigma$  criteria was used to identify "<sup>3</sup>He" in Table III-1, the channeling background will be greater than the  $1\frac{1}{2}\%$  suggested by the results in Section III-E, where a more restrictive FWHM criteria was used.

Figure IV-2

Correlation of the number of  ${}^3\text{He}$  and  ${}^4\text{He}$  counts in each solar event listed in Table III-1. The solid circles represent the  ${}^3\text{He}$  rich events of 14 February, 29 June and 5 September, 1973. The diagonal lines suggest the corrected ( ${}^3\text{He}/{}^4\text{He}$ ) ratio assuming an  $E^{-3}$  spectrum, which is not appropriate in all cases. Channeling effects are reflected in the trend of data parallel to the  $10^{-2}$  line.



The four events with  $(^3\text{He}/^4\text{He}) > 0.1$  but only 1 " $^3\text{He}$ " count might contain a significant  $^3\text{He}$  component but cannot be so identified here because of statistical limitations. The events of 14 February, 29 June and 5 September 1973 represented by the solid circles are seen to be distinctive not only on the basis of their high  $(^3\text{He}/^4\text{He})$  ratios, but also because of the large absolute number of  $^3\text{He}$  counts. In fact the number of  $^3\text{He}$  counts observed in each of the  $^3\text{He}$  rich flares was comparable to the 15 real  $^3\text{He}$  events observed in the sum over the remaining flares in Table III-1.<sup>+</sup> Because of their  $(^3\text{He}/^4\text{He})$  ratio ( $> 0.1$ ), and observable number of  $^3\text{He}$  events these flares are similar to the 14 October and 24 November 1969 SCR events reported by Garrard et al. (1973a, 1973b) and the 30 July 1970 event discussed Anglin et al. (1974).

Although significant amounts of  $^3\text{He}$  was observed in each of these  $^3\text{He}$  rich events,  $^2\text{H}$  and  $^3\text{H}$  were conspicuously absent. Averaging over the 1973 events, upper limits to  $(^2\text{H}/^3\text{He})$  and  $(^3\text{H}/^3\text{He})$  are set at 0.053. Anglin et al. have set corresponding limits of 0.05 for the 30 July '70 event at 10 MeV/nuc.

The relative abundances for the events are compared in Table IV-2.  $(^3\text{He}/^1\text{H})$  varies over 3 decades from event to event from  $9 \times 10^{-4}$  to the order of unity for the 5 September 1973 event. That is, up to half of

---

\*The term " $^3\text{He}$  rich events" has also been used by Dietrich (1973) to refer to the 5 out of 12 large SCR events in which 3 or more  $^3\text{He}$  nuclei were detected by the University of Chicago telescope on IMP-5. None of these events would have been detected as " $^3\text{He}$  rich" by the present experiment since at 10 MeV/nuc, Dietrich found that  $(^3\text{He}/^4\text{He})$  was significantly less than 0.1.

<sup>+</sup>Dead time effects significantly reduced the number of observed events during the large flares of 29 October 1972, 11-22 April and 7 September, 1973.

Table IV-2. Selected  $^3\text{He}$  Rich Events

Date	$(^3\text{He}/^1\text{H})$	$(^3\text{He}/^4\text{He})$	$(^4\text{He}/^1\text{H})$	Reference
14 Oct. '69	$0.003 \pm 0.001$	$0.26 \pm 0.08$	$0.013 \pm 0.002$	Garrard et al., 1973a
24 Nov. '69	$0.0009 \pm 0.0004$	$0.28 \pm 0.14$	$0.0032 \pm 0.0007$	Garrard (private communication, 1974)
30 July '70	$0.14 \pm 0.05$	$0.54 \pm 0.09$	0.2	Anglin et al., 1974
14 Feb. '73	$0.05 \pm 0.02$	$0.21 \pm 0.07$	$0.27 \pm 0.03$	} this work
29 June '73	$0.09 \pm 0.04$	~ 2	$0.06 \pm 0.02$	
5 Sept. '73	$1.0^{+.5}_{-.4}$	~ 6	~ 0.1	

the observed SCR's in such an event can be  ${}^3\text{He}$ . The ( ${}^3\text{He}/{}^4\text{He}$ ) and ( ${}^4\text{He}/{}^1\text{H}$ ) ratios also vary over  $1\frac{1}{2}$  decades. The data in Table III-1 and Figure IV-2 suggest that a significant part of this variation is due to the range of proton and alpha fluences, with the  ${}^3\text{He}$  component remaining relatively constant. Further systematic observations are needed, however, to evaluate the importance of selection effects in this regard.

Anglin (1974) has established that at least for the 14 October 1969 and 30 July 1970 events, the ratio of ( ${}^3\text{He}/{}^4\text{He}$ ) is not strongly energy dependent.<sup>+</sup>

Table IV-3 summarizes the current status of SCR isotope observations discussed in this section and Chapter III.

#### B. Flare Models

Table IV-1 shows that the abundance of  ${}^2\text{H}$  and  ${}^3\text{He}$  in SCR's can be significantly greater than the ambient abundance of these isotopes in the chromosphere or solar wind. The easiest way to account for this enhancement is in terms of models in which primary SCR's (reflecting the ambient solar abundances) are accelerated to sufficiently high energies ( $> 30$  MeV/nuc) that they undergo inelastic nuclear collisions with the ambient atmosphere to produce secondary  ${}^2\text{H}$ ,  ${}^3\text{H}$  and  ${}^3\text{He}$ . The relevant reactions, listed in Table IV-4 are discussed by Lingenfelter and Ramaty (1967). Assuming ambient solar abundances of

---

<sup>+</sup>This is in contrast to the 2 November 1969 and 25 January 1971 events discussed by Dietrich in which the  ${}^3\text{He}$  spectrum was significantly harder than that of  ${}^4\text{He}$ .

Table IV-3. Current Status of SCR Isotope Observations

Flare Averages: \*  $(\frac{2}{\text{H}}/\frac{1}{\text{H}}) = (8 \pm 2) \times 10^{-5}$  } 10 MeV/nuc  
 \*  $(\frac{3}{\text{H}}/\frac{1}{\text{H}}) = (2.1 \pm 1.0) \times 10^{-5}$  }

with ratios dropping at lower energies to

\*  $(\frac{2}{\text{H}}/\frac{1}{\text{H}}) = 7^{+10}_{-6} \times 10^{-6}$  1.6 - 8.6 MeV/nuc  
 \*  $(\frac{3}{\text{H}}/\frac{1}{\text{H}}) < 3.4 \times 10^{-6}$  1.2 - 6.8 MeV/nuc  
 \*  $(\frac{3}{\text{He}}/\frac{4}{\text{He}}) = 0.009 \pm 0.004$  } 3.1 - 15.0 MeV/nuc<sup>+</sup>  
 \*  $(\frac{3}{\text{He}}/\frac{1}{\text{H}}) = 1.7 \pm 0.7 \times 10^{-4}$  }  
 \*  $(\frac{3}{\text{He}}/\frac{4}{\text{He}}) \approx 0.04$  15 - 100 MeV/nuc

+ (These  $^3\text{He}$  results should be viewed with caution since contributions from small  $^3\text{He}$  rich events may have been included in the flare average.)

$^3\text{He}$  Rich Events: \*  $(\frac{3}{\text{He}}/\frac{4}{\text{He}})$  in the range 0.2 to  $\sim 6$  } not strongly  
 \*  $(\frac{3}{\text{He}}/\frac{1}{\text{H}})$  in the range  $10^{-3}$  to  $\sim 1$  } energy dependent  
 \*  $(\frac{2}{\text{H}}/\frac{3}{\text{He}}) < 0.05$  } 10 MeV/nuc and below  
 \*  $(\frac{3}{\text{H}}/\frac{3}{\text{He}}) < 0.05$  }  
 \*  $^3\text{He}$  Fluence in range  $10^2 - 10^3/\text{cm}^2 \text{sr}$ )\*,  $> 3 \text{ MeV}$   
 \* No analagous  $^2\text{H}$  or  $^3\text{H}$  rich flares detected.

$^3\text{He}$  in Other Individual Flares:

\*  $(\frac{3}{\text{He}}/\frac{4}{\text{He}})$  in the range  $10^{-3}$  to 0.03 below 10 MeV/nuc and rising to the range 0.02 to 0.3 at  $\sim 50 \text{ MeV/nuc}$ .  
 (2 Nov. '69, 25 Jan. '71, Aug. '72)

+ See Tables IV-1 and IV-2 for references.

Table IV-4. Selected\* Nuclear Reactions Yielding  ${}^2\text{H}$ ,  ${}^3\text{H}$  and  ${}^3\text{He}$ .

Reaction	Threshold (MeV/nuc) <sup>+</sup>	$\sigma^{\ddagger}$ (mb)
$p + \alpha \rightarrow {}^2\text{H} + {}^3\text{He}$	23.0	40
$p + \alpha \rightarrow {}^3\text{H} + p + p$	24.9	17
$p + \alpha \rightarrow {}^3\text{He} + p + n$	25.8	46
$p + \alpha \rightarrow {}^2\text{H} + {}^2\text{H} + p$	29.8	5
$p + \alpha \rightarrow {}^2\text{H} + p + p + n$	32.7	10
$p + p \rightarrow {}^2\text{H} + \pi^+$	286.5	0

<sup>+</sup>In all cases either primary nucleus can be stationary in the lab frame.

\*In addition to these cases, there are many channels by which ( $\alpha + \alpha$ ), ( $p + \text{CNO}$ ) and ( $\alpha + \text{CNO}$ ) can yield  ${}^2\text{H}$ ,  ${}^3\text{H}$  and  ${}^3\text{He}$ .

<sup>‡</sup>Total cross section at 50 MeV/nuc (Meyer, 1971).

$H:He:CNO = 1:0.07:10^{-3}$  (Cameron, 1973), the dominant reactions involve alpha-proton collisions, with alpha-alpha and CNO-proton interactions playing a lesser role. Among the alpha-proton reactions in Table IV-4, the first reaction dominates below incident energies of  $\sim 50$  MeV/nuc, with the other four reactions becoming important at higher energies. The  ${}^1_0H(p, \pi^+) {}^2_1H$  reaction, although important in the production of  ${}^2_1H$  in galactic cosmic rays, is not significant in this case due to the high threshold energy. Cross section data have been reviewed recently by Meyer (1971), but in a context of galactic cosmic rays where  ${}^3_1H$  production can be assimilated into  ${}^3_2He$  production. Jung et al. (1973) have developed a theoretical treatment of the differential cross sections for alpha-proton reactions and have presented the results as semi-empirical formulae. Finally, Ramaty and Kozlovsky (1974) (R&K) have reevaluated the production of  ${}^2_1H$ ,  ${}^3_1H$  and  ${}^3_2He$  in the solar atmosphere paying due attention to the reaction kinematics.

Calculations of expected yields of  ${}^2_1H$ ,  ${}^3_1H$  and  ${}^3_2He$  generally take the form of propagating a known primary spectrum of particles through a 'slab' of solar material. Given the nuclear cross sections, the production spectrum of secondary isotopes can be calculated. In thick target models, the primary beam loses energy due to ionization energy loss and the production of secondaries is summed over its entire range. In thin target models, the primary beam passes through a thin target

(or travels for a short time)\* so that there is no appreciable change in energy of the primary beam. The observations are then interpreted in terms of the thickness of the slab required to produce the observed fraction of secondary isotopes.<sup>†</sup>

A factor which is not taken into account in comparisons of observations with such models is the adiabatic energy loss of the SCR's during their propagation from the sun to the earth. The magnitude of this energy loss, which may be  $\sim 50\%$ , is strongly dependent on the radial dependence of the diffusion coefficient used to describe the propagation process, (Palmer 1973, Marshall 1974a). The neglect of such factors suggests the caution with which numerical results of model calculations should be treated.

### C. Interpretation of Flare-Averaged Results

Using a thin target model and an  $E^{-s}$  primary spectrum, with  $2 \leq s \leq 3$ , R&K can account for the abundance of  ${}^2\text{H}$  and  ${}^3\text{H}$  at 10 MeV/nuc by a path length of 0.08 to 0.2  $\text{g}/\text{cm}^2$  for 10 MeV/nuc particles, or equivalently  $x_1 = 0.5$  to 1.5  $\text{g}/\text{cm}^2$ . Figure IV-3 shows the R&K predictions for  $s = 2$  and  $s = 3$  and an assumed path length,  $x_1 = 1 \text{ g}/\text{cm}^2$

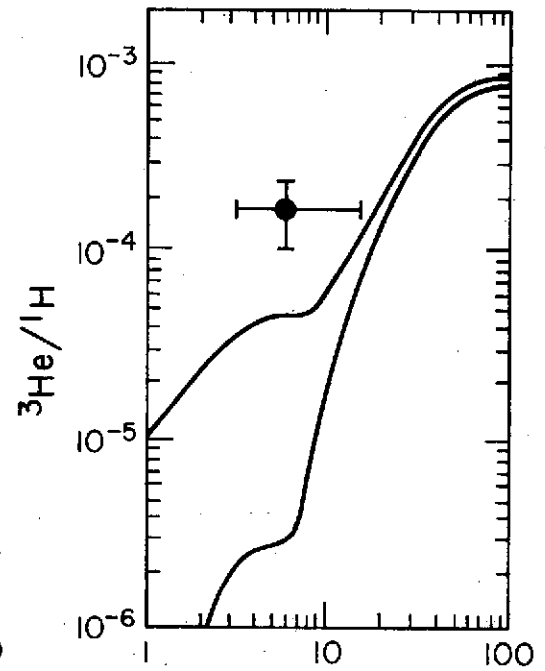
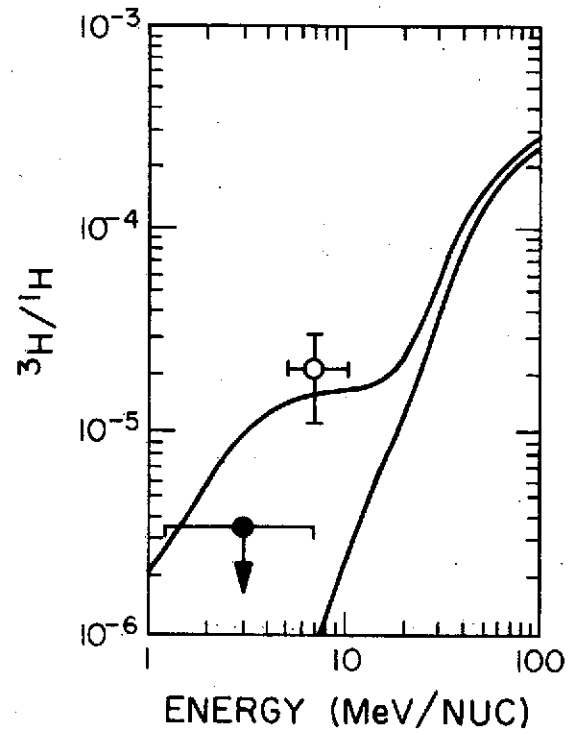
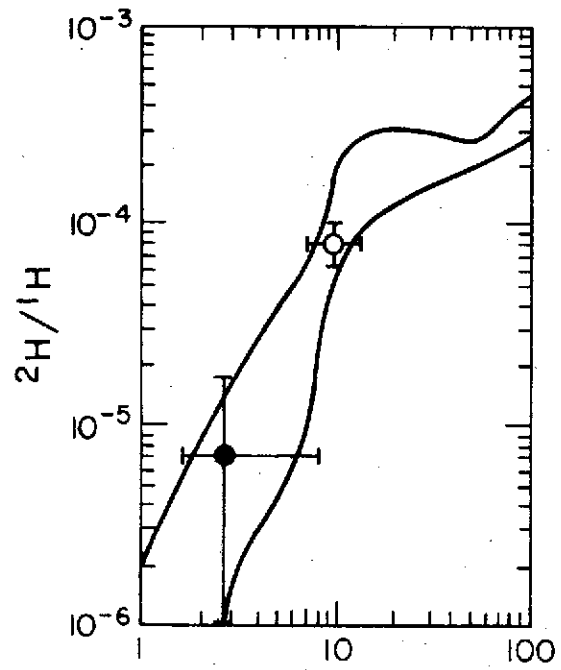
---

\* Note the distinction. In case of a 'time slab' higher energy particles pass through more matter. The path length of a particle of velocity,  $\beta c$ , is  $x = \beta x_1$ , where  $x_1$  is the path length for relativistic particles.

<sup>†</sup> See for example Anglin et al., 1973a.

Figure IV-3

Isotopic ratios predicted by R&K using a thin target 'time slab' model and a path length for relativistic particles,  $x_1 = 1 \text{ g/cm}^2$  (or  $x \approx 0.3 \text{ g/cm}^2$  at 30 MeV/nuc. The  $({}^3\text{He}/{}^1\text{H})$  curve is adopted from their calculated  $({}^3\text{He}/{}^4\text{He})$  curve by using their assumed value of  $({}^4\text{He}/{}^1\text{H}) = 0.07$ . In each panel the upper and lower smooth curves assume  $E^{-2}$  and  $E^{-3}$  differential primary spectra respectively. The open circles are the flare-averaged results of Anglin et al. (1973b). The solid circles are the present results for the flare sums discussed in the text which do not include the  ${}^3\text{He}$  rich events of 14 February, 29 June or 5 September, 1973.



(or  $x \approx 0.3 \text{ g/cm}^2$  at 30 MeV/nuc), which is appropriate for the 10 MeV/nuc results. Such a pathlength is also consistent with the present  $^2\text{H}$  and  $^3\text{H}$  results, but the  $^3\text{He}$  observations suggest a pathlength at least 3 times longer. This discrepancy may be due to the contamination of the flare averaged data by small  $^3\text{He}$  rich events, as discussed in Section III-E. In all cases the observations were made a 1 A.U. whereas the calculated curves refer to the solar surface. The effect of adiabatic deceleration would be to shift the calculated curves to the left and smooth the spectral features. Such effects might also account in part for the  $^3\text{He}$  discrepancy. Finally, the possibility cannot be excluded that the R&K thin target model is not appropriate in this context.

#### D. Helium-3 Rich Flares

The  $^3\text{He}$  rich flares provide a somewhat more interesting test for flare models. The reaction cross sections predict a total yield of  $^2\text{H}$ ,  $^3\text{H}$  and  $^3\text{He}$  roughly in the ratio, 2:1:3 (R&K, thick target). While these ratios are not independent of the assumed shape of the primary energy spectrum, inspection of the total cross sections (Jung et al., 1973) shows that the total yield of  $^2\text{H}$  must be at least  $\frac{1}{2}$  that of  $^3\text{He}$ . This contrasts to the observed ratio,  $(^2\text{H}/^3\text{He}) < 0.05$ . Since alpha-proton reactions are the dominant source of both  $^2\text{H}$  and  $^3\text{He}$ , sensitivity to the assumed solar abundances cannot account for this discrepancy.

R&K have proposed an explanation in terms of the angular distribution of the secondary products. They point out that the yield of  $^3\text{He}$  in the backward lab hemisphere greatly exceeds the backward yield of  $^2\text{H}$  or  $^3\text{H}$ , especially at secondary energies below  $\sim 2 \text{ MeV/nuc}$ .

Figure IV-4

Production spectra of secondary nuclei in the backward lab hemisphere. The primary beam, containing 93% hydrogen and 7% helium, is incident on a target of similar composition. The energy spectrum of the primary beam, normalized to 1 proton above 30 MeV, is either exponential in rigidity with characteristic rigidity of 150 MV, or a kinetic energy power law. The  $^2\text{H}$  and  $^3\text{He}$  curves are from R&K. The proton curves are for elastic alpha-proton scattering (Equation D-1). The dashed curves neglect the secondary protons produced in the first  $\text{g/cm}^2$ . In all cases the curves represent the energy spectra before any reacceleration of the secondary nuclei occurs.

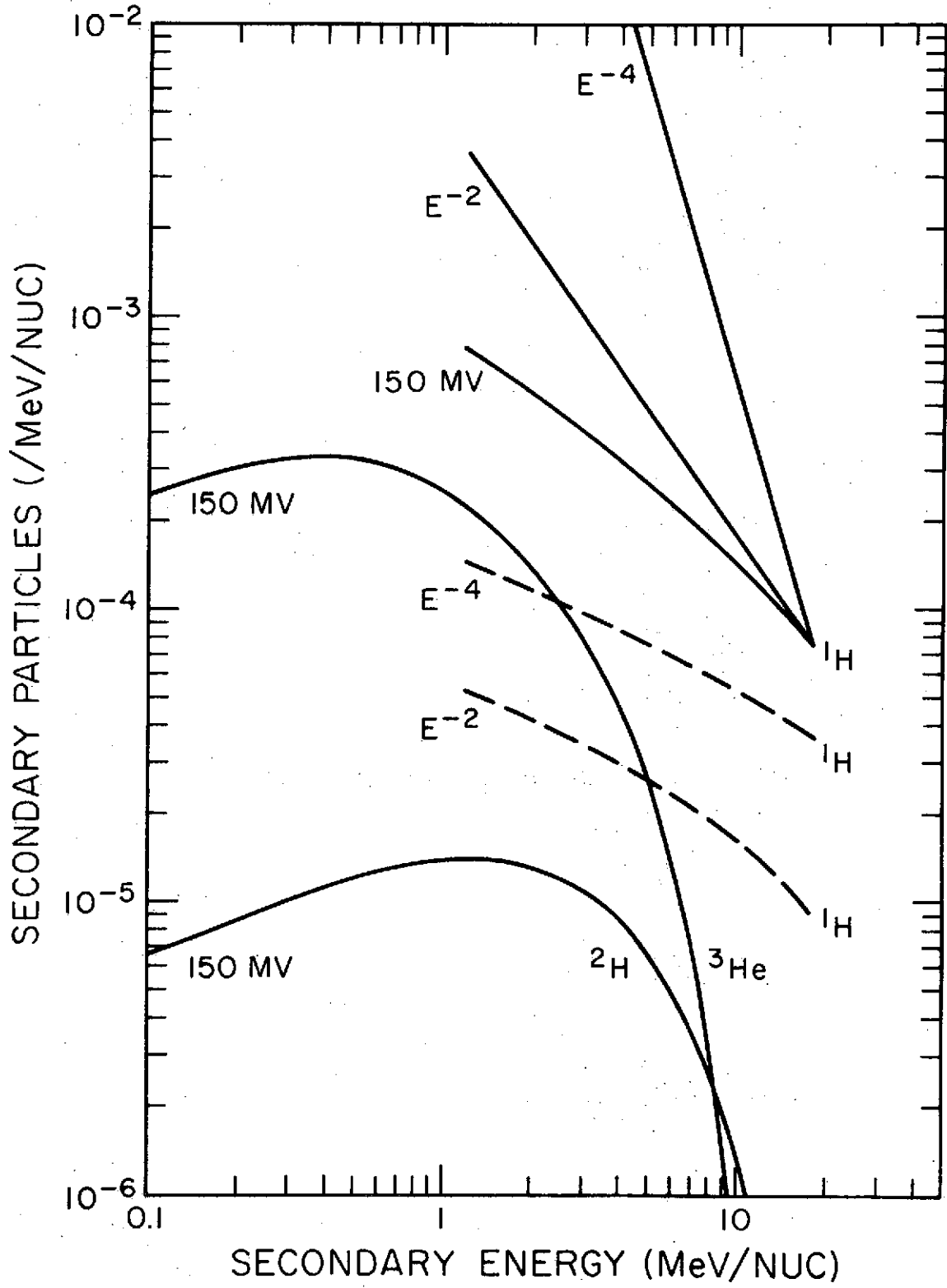


Figure IV-4 shows the spectrum of backward moving  $^2\text{H}$  and  $^3\text{He}$ . (R&K do not explicitly calculate the backward spectrum of  $^3\text{H}$ , but argue that it is small and easily destroyed by the  $^3\text{H}(p,n)^3\text{He}$  reaction). Thus the absence of  $^2\text{H}$  and  $^3\text{H}$  in  $^3\text{He}$  rich flares can be explained if the primary beam is directed down toward the sun, and only upward moving secondaries are subsequently accelerated and escape. An additional upward directed acceleration mechanism is essential to this model since the range of the secondary isotopes when they are produced is small compared to their average depth in the solar atmosphere. Note that such a three stage process (acceleration, interaction and reacceleration) would be much less efficient than if the primary beam were simply directed upward, so that the total  $^3\text{He}$  fluence of such events would tend to be small, in agreement with observations.

If the  $^3\text{He}$  are produced and accelerated as described by R&K, then there must be a proton component which is backscattered into the backward lab hemisphere and reaccelerated along with the secondary  $^3\text{He}$ . In Appendix D an estimate is made of such a backscattered proton spectrum, assuming a thick target model, with a result of the form:

$$N_s(E_s) = 2.6 \times 10^{-4} E_s^{-0.43} N(>E_s/0.6) \quad (\text{D-2})$$

where  $N_s$  is the differential spectrum of backscattered protons,  $E_s$  is the energy of the backscattered protons,  $N(>E)$  is the integral number of primary protons above energy,  $E$ , normalized so that  $N(>30 \text{ MeV}) = 1$ . Assuming the same exponential rigidity primary spectrum ( $R_0 = 150 \text{ MeV}$ ) used by R&K to calculate the flux of  $^3\text{He}$ , the corresponding proton spectrum can be estimated from equation D-2. Also plotted in Figure

IV-4, it shows that at a few MeV/nuc the backscattered proton spectrum is about a factor of 4 greater than the  $^3\text{He}$ . Note, however, that 2 MeV backscattered protons are produced by 3 MeV primaries, whereas 2 MeV/nuc  $^3\text{He}$  secondaries are made by protons above 23 MeV. Thus the ( $^1\text{H}/^3\text{He}$ ) ratio at 2 MeV can be expected to be dependent on the shape of the primary spectrum. Since the results shown in Figure IV-4 are normalized to the integral primary spectrum above 30 MeV/nuc, the estimated proton spectrum plotted in Figure IV-4 will be much more sensitive to the shape of the primary spectrum than will the  $^3\text{He}$  calculation. To illustrate this sensitivity, Equation D-2 was re-evaluated for the cases of  $E^{-2}$  and  $E^{-4}$  power law primary spectra. These results are also shown in Figure IV-4 along with additional cases in which backscattered proton secondaries produced in the first  $\text{g/cm}^2$  are excluded.\* Such cases might be relevant if the reacceleration mechanism operated only after the primary beam had passed through  $\sim 1 \text{ g/cm}^2$  (ie, only in the photosphere) so that backward moving secondaries produced in the chromosphere would be lost.

---

\* Given an  $E^{-s+1}$  incident integral spectrum and a proton range-energy relation of the form  $R \sim E^{1.8}$ , it is easy to show that after passing through  $1 \text{ g/cm}^2$ , the integral spectrum becomes

$$N(>E) = \left( E^{1.8} + E_0^{1.8} \right)^{\frac{-s+1}{1.8}}, \quad \text{where } E_0 = 50 \text{ MeV is the proton energy corresponding to a range of } 1 \text{ g/cm}^2. \text{ Substitution in Equation D-2 is equivalent to neglecting the secondaries produced in the first } \text{g/cm}^2.$$

Note that these estimates neglect the protons and neutrons produced along with the  $^3\text{He}$  by inelastic proton-alpha reactions and which will also contribute to the observed SCR proton flux. These estimates do, however, illustrate that the backscattered proton yield is indeed sensitive to the assumed primary spectrum and can be made to approach the range of observed  $^3\text{He}/^1\text{H}$  ratios.

These estimates should also be considered only as lower limits to the proton SCR flux, since a fraction of the downward moving primary beam will be redirected upward due to mirroring in the solar magnetic fields. In addition the primary beam may not fully satisfy the assumption that it is completely directed downward. Therefore the observed SCR's will consist of an admixture of primary and backscattered or secondary particles. The proportions of this admixture will undoubtedly vary from flare-to-flare, and along with the shape of the primary spectrum, provide a mechanism which could account for the wide variation in the observed ( $^3\text{He}/^1\text{H}$ ) ratios. In such a picture, the 5 September 1973 event, in which this ratio was of the order of unity, would be a case in which the primary beam component was largely absent. Other events, such as the 14 February 1973 flare, would require a contribution from the primaries in order to account for the abundance of alpha particles, for as is shown in Appendix D, backscattered alphas alone could not suffice.

To summarize then, the R&K model provides an explanation of the  $^3\text{He}$  rich events which are characterized by a relative absence of  $^2\text{H}$  and  $^3\text{H}$ . Inclusion of backscattered and mirroring protons in the reacceleration process can also account, in a fairly natural manner, for the

flare-to-flare variability of ( $^3\text{He}/^1\text{H}$ ).

There are some potential difficulties, however. First the cross section data used as input to these calculations are not in a completely satisfactory state (Jung et al., 1973), so that the numerical results of such models may be subject to revision. In the case of a 150 MV exponential rigidity primary spectrum, the model can explain an integrated ratio of  $\sim 0.1$  for  $^2\text{H}/^3\text{He}$ . While this is significantly less than the total cross sections alone can account for, it is still a factor of  $\sim 2$  higher than the upper limit to the observed ratio of 0.05. While the factor of 2 is not significant in itself, R&K do show that the enhancement is sensitive to the shape of the primary spectrum. Spectra that are softer than 150 MV or  $E^{-2}$  are not as effective in enhancing the ( $^3\text{He}/^2\text{H}$ ) ratio. Further SCR measurements to establish the actual ratio of ( $^3\text{He}/^2\text{H}$ ) and ( $^3\text{He}/^3\text{H}$ ) would provide a particularly useful test of this point.

A further difficulty is the need for two distinct acceleration stages to be operable for these  $^3\text{He}$  rich flares: the first to accelerate primaries downward with very little upward leakage; the second to reaccelerate the backward moving secondaries upward, with good rejection of downward moving particles. While such a tandem acceleration process cannot be excluded a priori, there is no other evidence at present to support it. Perhaps the X-ray or radio characteristics of such events can provide an insight into whether these events have unique characteristics which would be consistent with such a process. In addition optical observations might illuminate the magnetic configurations which could be associated with this type of flare.

Finally R&K have shown that for each  ${}^3\text{He}$  nucleus released into the interplanetary medium,  $\sim 1$  2.2 MeV  $\gamma$  ray would be produced by the reaction,  $p + n \rightarrow {}^2\text{H} + \gamma$ . Observation of such  $\gamma$  rays for these  ${}^3\text{He}$  rich flares would provide important confirmation of the source of these rare isotopes.

## V. SUMMARY AND CONCLUSIONS

The Caltech Electron/Isotope Spectrometer has been used to measure the isotopic composition of SCR's. As part of an evaluation of the response of the dE/dx-E charged particle telescope, alpha particle channeling in thin detectors was identified as a background mechanism which can affect the measurement of low values of ( $^3\text{He}/^4\text{He}$ ).

Observation of 31 solar active periods between October 1972 and November 1973 failed to yield an observable  $^2\text{H}$  or  $^3\text{H}$  flux in any single period, but the following flare-averaged results were obtained:  
 $(^2\text{H}/^1\text{H}) = 7_{-6}^{+10} \times 10^{-6}$  (1.6 - 8.6 MeV/nuc),  $(^3\text{H}/^1\text{H}) < 3.4 \times 10^{-6}$   
 (1.2 - 6.8 MeV/nuc),  $(^3\text{He}/^4\text{He}) = (9 \pm 4) \times 10^{-3}$  and  $(^3\text{He}/^1\text{H}) =$   
 $(1.7 \pm 0.7) \times 10^{-4}$  (3.1 - 15.0 MeV/nuc). The relative  $^2\text{H}$  and  $^3\text{H}$  abundances were somewhat below previous observations at higher energies suggesting that the  $^2\text{H}$  and  $^3\text{H}$  spectra are harder than that of the protons. The results were consistent with the thin target pathlength for relativistic particles of  $\sim 1 \text{ g/cm}^2$  (or equivalently  $\sim 0.3 \text{ g/cm}^2$  at 30 MeV/nuc). The  $^3\text{He}$  result, which is consistent with previous observations, would suggest a pathlength at least 3 times as long, but the flare-averaged  $^3\text{He}$  measurement may be contaminated by small " $^3\text{He}$  rich events," thus voiding such an interpretation. In addition the effects of adiabatic deceleration may also account for part of the discrepancy. It is also possible that the thin target model, used to calculate the effective pathlengths, is not appropriate for such flare averages.

During 1973 three "<sup>3</sup>He rich events" containing much more <sup>3</sup>He than <sup>2</sup>H or <sup>3</sup>H were observed on 14 February, 29 June and 5 September. The latter event was particularly significant in that much more <sup>3</sup>He than <sup>4</sup>He was observed and the fluxes of <sup>3</sup>He and protons were about equal. The three events were compared to three previously reported <sup>3</sup>He rich events and the ratios of (<sup>3</sup>He/<sup>4</sup>He) and (<sup>3</sup>He/<sup>1</sup>H) were found to range from 0.2 to ~ 6 and from 10<sup>-3</sup> to ~ 1 respectively. Averaging over the three 1973 events, an upper limit to the ratios (<sup>2</sup>H/<sup>3</sup>He) and (<sup>3</sup>H/<sup>3</sup>He) was set at 0.053. This is marginally consistent with the calculation by Ramaty and Kozlovsky of (<sup>2</sup>H/<sup>3</sup>He) ≈ 0.1, in which only the backward moving secondaries in the lab frame are reaccelerated and escape after being created by a downward moving primary beam. Such a downward moving primary beam would also result in protons backscattering from the ambient helium and being reaccelerated along with the secondary <sup>3</sup>He. Estimates of the backscattered proton component show it to be sensitive to the spectral shape of the primary beam, but it can be made as small as the <sup>3</sup>He component in some cases, and so might account for similar proton and <sup>3</sup>He fluxes of the 5 September 1973 event. Other <sup>3</sup>He rich events can be accounted for by the inclusion of a larger backscattering proton component as well as contributions from primary protons and alphas that mirror in the solar magnetic field.

## APPENDIX A. DATA REDUCTION

This appendix describes stages of the data reduction process which are unique to the present study. A guide to the routine analysis procedures followed for the EIS experiments on IMP-7 and IMP-8 can be found elsewhere (Garrard, 1974c). This routine analysis results in the production of Abstract Tapes (Garrard, 1974b), which are analyzed by a program, ATS (Hurford, 1974a) to provide an overview of experiment operation and to identify transient events. This appendix describes the subsequent steps, outlined in Figure A-1, which result in the mass histograms from which isotopic ratios can be obtained as described in Chapter III.

Using the ATS output and criteria discussed in Section III-B, time periods are chosen in which there is an enhancement of 2-12 MeV/nuc particles. For these periods, a set of five 'Strip Tapes' (Garrard and Petruncola, 1973) are produced from the Abstract Tapes. Each file of a Strip Tape contains all relevant rate information, averaged over a six hour period, a list of events\*, plus appropriate time and status information, all in Fortran compatible form.

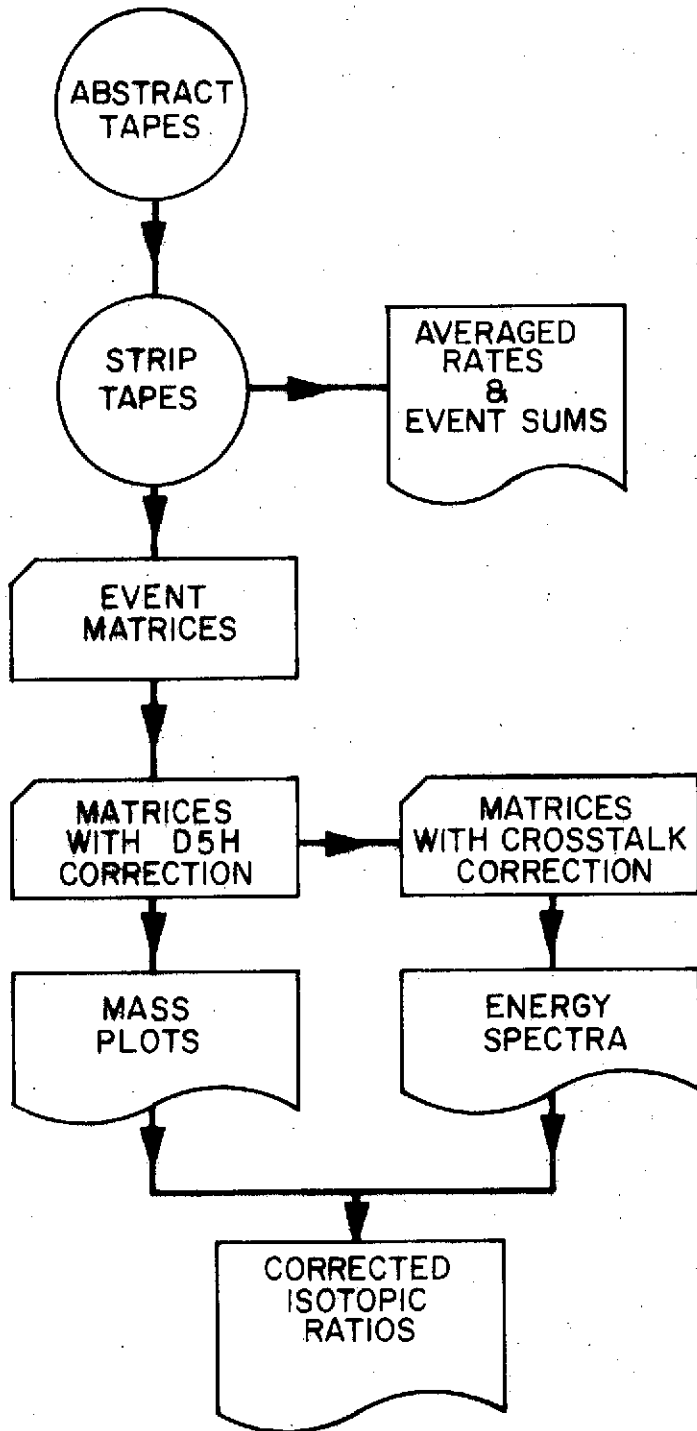
The Strip Tapes are produced on the SRL PDP-11, but analyzed by the campus IBM 370/158 batch processor, by a program, HARVEST. The HARVEST program sums over any combination of files (for example, those

---

\*The choice of events is under operator control, so the program which produces the Strip Tapes is not limited to this type of study. In this case, events with ranges such as D2, D25(H), D25(H)6, etc. were included.

Figure A-1

Flow of IMP-7 data processing associated with the present work. Except for Strip Tape production, all computing shown here is done on the campus IBM 370/158. The crosstalk correction and energy spectra are discussed in Appendix B. The corrections to the isotopic ratios are discussed in Section III-C.



C-2

corresponding to a single flare or those chosen by criteria such as discussed in Section III-D). In addition to averaging rates, HARVEST sums all events of a given range on the basis of their A and B pulse heights to form a matrix,  $N(A,B)$ . An example of such a D25(H) matrix is shown in Figure A-2. The non-zero elements of such matrices are encoded on punched cards or disk for use as input to subsequent programs.

The D2 and D5H singles matrices yield values for the D5 and D2 offsets, respectively, which are used to correct the prelaunch calibration data, as described in Section II-F.

Protons above  $\sim 12$  MeV which almost reach D6 will occasionally fail to leave sufficient energy in D2 to be identified as a D25H event. Instead they have a range D5H, but the B register still contains a valid D2 pulse height. These events are easily distinguished from true D5H singles since the B (D2) pulse height is several channels above the D2 offset. At this stage such events are transferred from the D5H to the D25H matrix.

Next the D25(H) matrix is converted to a mass histogram by a program, MASH. For a given pair of pulse heights, (A,B), the minimum and maximum possible energy loss (neglecting ADC and detector noise) in D2 and D5 are determined from the corrected calibration data. Then for a given  $(\delta E, E')$  pair, values of M and Z are calculated\* using an

---

\*Assuming  $Z=1, 2, \text{etc}$ , corresponding values of M are calculated. Only one of these (M,Z) pairs is reasonable and so M and Z are 'uniquely' determined.

Figure A-2

Part of the D25(H) matrix for a 24 hour period including the flare of 14 February, 1973. The digitized A and B pulse heights, along with an approximate energy calibration for D5 and D2 form the X and Y axes respectively. Distinct  $^1\text{H}$ ,  $^3\text{He}$  and  $^4\text{He}$  tracks can be seen. The corresponding mass plot is shown in Figure III-3.



iterative scheme<sup>†</sup>. This M characterizes that mass contour which passes through the  $(\delta E, E')$  coordinate. This is done for  $(\delta E_{\min}, E'_{\min})$  and  $(\delta E_{\max}, E'_{\max})$  to yield  $M_{\min}$  and  $M_{\max}$ . If both values of M lie within the same predetermined mass bin of the final mass histogram, that bin is incremented appropriately. If the (A,B) channel pair could correspond to more than one mass bin, counts are divided among the bins with the assumption that all values of  $(\delta E, E')$  compatible with (A,B) are equiprobable.

Before incrementing the bins, a 'range test' is performed. Since the energy, charge and mass are assumed known at this stage, the expected range in silicon can be calculated. The test is to verify that this calculated range is physically possible, considering the thickness of D2, D5 etc. If it is, the appropriate mass bins are incremented. If not, the events are disregarded.

Note that with the scheme described above, integral masses are not favoured in any way. In addition, mass histograms from different flares can now be summed without further regard to calibration shifts, etc.

The calculation of energy spectra from the D2 and D25(H) matrices is described in Appendix B.

---

<sup>†</sup>The iterative scheme assumes a range-energy power law to speed convergence, but the final M value is consistent with Z=1 or Z=2 range-energy tables, as appropriate.

## APPENDIX B. CALCULATION OF ENERGY SPECTRA

In this appendix the calculation of proton and alpha energy spectra from the raw D2 and D25(H) matrices is discussed. The method used is not designed to take full advantage of the excellent energy resolution potentially available in the data, nor to give an unbiased flare-averaged energy spectrum. Rather the purpose is to provide an energy spectrum that can be integrated over the velocity limits that are appropriate for  $^2\text{H}$ ,  $^3\text{H}$  and  $^3\text{He}$ , as indicated in Table II-5 so that meaningful isotopic ratios can be determined.

As indicated in Section II-3, the analyzed events constitute a sample of those detected during a flare. The effective live time is dependent upon the instantaneous particle flux, but is the same for D25(H) isotopes with similar time dependence and anisotropy. The relevant energy spectrum for this work is one which reflects the energy spectrum of analyzed particles rather than detected particles. For this reason the D2 and D25(H) matrices are not corrected for the sampling bias which results in the analysis of larger fraction of particles arriving during the later stages of a flare when the rates are lower. Thus, the spectrum calculated below is not an unbiased flare-averaged spectrum, but rather is the one which is most appropriate for the analyzed isotopic sample. The flare-averaged analysis probability is taken into account in the estimate of the fluence values shown in Table III-1.

Before proceeding with the calculation, it is necessary to correct for an instrumental crosstalk problem. Occasionally, during analysis

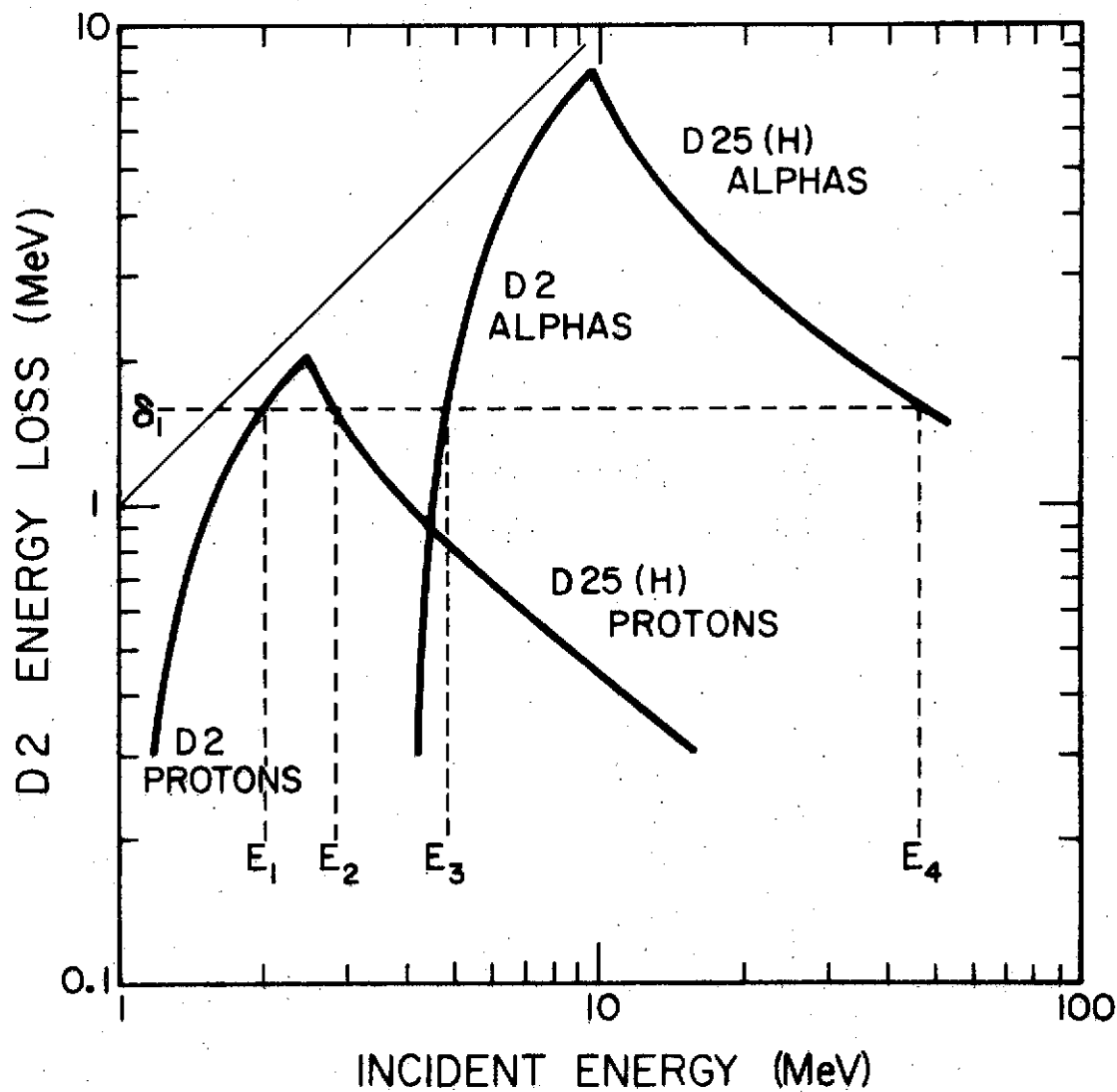
of a normal D25(H) particle that stops in D5, the D6 ADC will be triggered electronically. The event in the telemetry then appears with a D25(H)6 range, a correct A pulse height (D5), and a B pulse height (D6) of zero. Although these events are readily identifiable by the zero B pulse height, the information on the energy loss in D2 is lost. For typical flare spectra, about 15% of D25(H) events are affected. In limited energy regions, characterized by approximately equal D2 and D5 pulse heights, up to ~ 50% of the events are affected. For example up to 50% of protons between 2.8 and 4.1 MeV trigger D6 whereas less than 5% of D25(H) protons outside this interval are affected. Since the condition of equal A and B pulse heights corresponds to the same range in silicon for the various isotopes, the crosstalk does not, to first order, seriously bias the isotopic ratios (see Section III-C). Nevertheless, to establish meaningful energy spectra, allowance must be made. The problem is qualitatively understood so that a semi-empirical correction, normalized to the data itself, is straightforward (Garrard, 1974a). The correction process transfers the crosstalk events from the D25(H)6 matrix back to the D25(H) matrix.

Figure B-1 shows the response of D2 to protons and alphas. There are three factors which complicate this response.

1. The energy loss in the window. This is illustrated in Figure B-1 by the vertical separation of the diagonal line (representing the case of no window energy loss) and the D2 curve for protons or alphas. This window energy loss

Figure B-1

Average energy loss in D2 as a function of incident proton and alpha kinetic energy. The discontinuities in the curves occur when particles just penetrate D2 so that the curves to the left of the discontinuities correspond to particles which stop in D2, while the curves to the right correspond to particles which penetrate D2. The light diagonal line is the response for D2 protons and alphas in the absence of a mylar window. The light dashed lines relate the labeled energies discussed in the text.



dominates near the D2 threshold.

2. Alpha-proton ambiguity below 5 MeV. Figure B-1 shows that the maximum energy loss in D2 produced by a proton is the same as the energy loss in D2 by a 5 MeV alpha. If a D2 event has a pulse height corresponding to a smaller energy loss, such as  $\delta_1$ , it could have been due to either a proton of energy,  $E_1$ , or an alpha of energy,  $E_3$ .
3. Foldback of penetrating proton or alpha spectra. In most cases, if a proton or alpha has sufficient energy to penetrate D2, it will either trigger D3 or D4 and be rejected by the experiment logic, or trigger D5 and so not affect the D2 singles response. If, however, a proton ( $E_2$ ) penetrates D2 and stops in the epoxy on the inner annulus in D3 or D4 without triggering any other detector, it can be misinterpreted as a lower energy proton ( $E_1$ ). Since the lowest energy stopping protons are affected by the highest energy penetrating protons the 'penetrating' spectrum is, in effect, folded back and added to the stopping spectrum. This "foldback" of the proton spectrum is most serious near the highest energy in the D2 range where it can account for up to  $\sim 25\%$  of the observed events. In the same way, the alpha spectrum can foldback upon itself with similar consequences. The energy dependence and geometrical factor for this effect has been determined from tandem calibration data (R. A. Mewaldt, private communication) so that a correction can

easily be made. In principle, high energy alphas ( $E_4$ ) might also affect D2 protons ( $E_1$ ) but in this case the correction is negligible ( $< 1\%$ ) and so is neglected here.

The steps involved in the calculation of the energy spectra are now outlined.

1. The first step is to preselect the boundaries of incident energy bins into which the D2 and D25(H) protons and alphas are stored. Separate bins for protons and alphas are used and energies near the maxima or minima for each range are avoided, as are alpha energies below 5 MeV.
2. Events in the D25(H) matrix are sorted into bins on the basis of their detected energy. The boundaries of these detected energy bins correspond to the boundaries of the incident energy bins when the energy loss in the mylar window is taken into account. The identification of protons and alphas is simplified by the assumption that no other isotopes were present (except for the  $^3\text{He}$  rich flares, which are dealt with by hand).
3. Separate fits\* to the D25(H) proton and alpha spectra are then made.

---

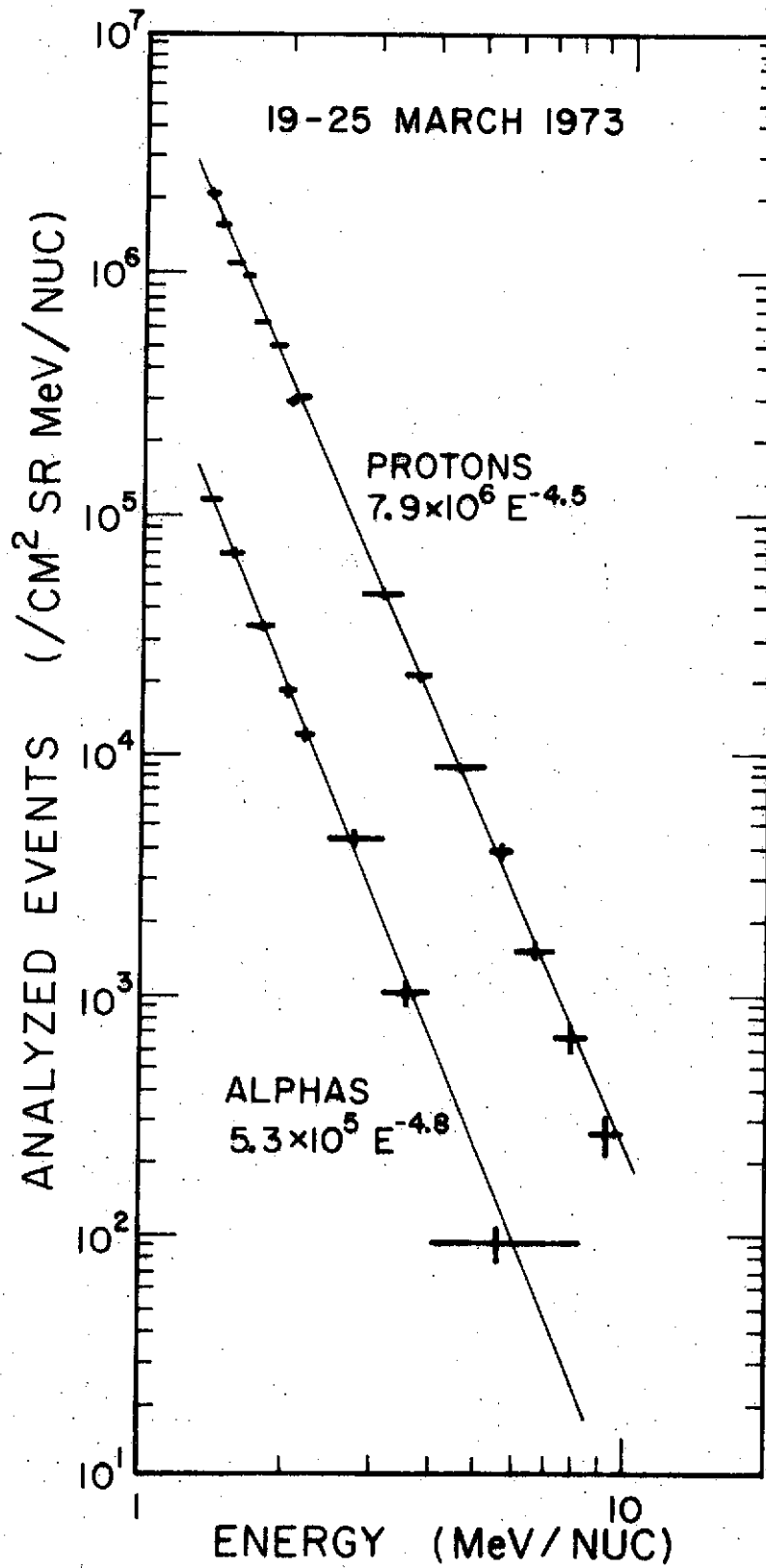
\*Throughout this discussion, "fit" refers to a least square fit of a kinetic energy power law,  $\frac{dN}{dE} = K \cdot E^{-\gamma}$ . Two successive fits are made such that the power law index,  $\gamma$ , found in the first fit determines the effective average energy for each bin used in the final fit.

4. The D2 events are sorted into energy bins on the basis of their detected energies.
5. The foldback corrections to the D2 alphas and protons are made using the fitted D25(H) spectra obtained in step 3.
6. A fit is made to the D2 alpha spectrum.
7. The alpha spectrum obtained in step 6 is extrapolated to energies below 5 MeV to correct the D2 protons for the proton-alpha ambiguity.
8. A fit is made to the D2 proton spectrum.
9. Finally, combined fit is made to the D25(H) and corrected D2 data for protons and also for alphas.

To illustrate the resolution of the resulting fits, the energy spectra for the 19 March, 1973 event are shown in Figure B-2 along with the least squares fits.

Figure B-2

Energy spectrum of analyzed events during the 19-25 March, 1973 SCR event. Points above 2.4 MeV/nuc are measured with range D25(H). Points below that energy are from the D2 data.



## APPENDIX C. THE EFFECT OF CHANNELING ON THE RESPONSE TO ALPHA PARTICLES

## 1. Introduction

The phenomenon of channeling of fast moving charged particles in a crystal lattice is well known. (See for example, Morgan, 1973, Gemmel, 1974). The aspect of channeling relevant to this work is the large reduction (up to  $\sim 65\%$ ) in the rate of ionization energy loss of an incident ion that penetrates a thin crystal along a path parallel to an important crystal axis or plane. For an isotropic alpha flux incident on D2, it will be shown that  $\sim 2\%$  have an abnormally low energy loss in D2. Figure III-2 shows that this may provide a significant background affecting the measurement of low values of ( ${}^3\text{He}/{}^4\text{He}$ ).

There are several reasons why this phenomenon has generally been neglected in previous work on the response of cosmic ray telescopes.

- a. It is of concern only for the measurement of rare isotopes with a mass (or charge) slightly less than that of an abundant specie (e.g,  ${}^3\text{He}$ ,  ${}^4\text{He}$ ).
- b. Channeling is more important for the low energies and thin detectors considered here than for higher energies where thicker  $\delta E$  detectors are used.
- c. Unless the resolution and background levels of the telescope are sufficiently good, channeling may not provide the dominant background source.

As a result of these factors, the basic data required to evaluate the role of channeling for this application are not available in the literature.

Figure C-1 shows the pattern of planes and axes of a face-centred-cubic lattice such as silicon. The small circle at the centre indicates the standard orientation of the axis of symmetry of the detectors. This orientation was verified for several detectors by a Laue X-ray transmission measurement. The large circle indicates the range of incident directions of particles which can have range D25(H). The problem to be solved is to determine the distribution of energy losses for incident alpha particles whose directions of incidence form a smoothly varying distribution within the large circle in Figure C-1.

Section C-2 describes an experiment whose purpose is to measure the response of a 50 micron detector to an 'isotropic' flux of monoenergetic alpha particles. In Section C-3 the application of these results to D25(H) events is discussed.

## 2. Channeling Experiment

The approach taken in this experiment is to measure the response of a 50 micron detector to 8.785 MeV alphas from a  $^{212}\text{Pb}$  source, whose directions of incident are uniformly distributed in the azimuthal component, but collimated in the polar ( $\theta$ ) component. After measuring the response to several different  $\theta$  distributions, weighted averages of these responses can be made to simulate the D25(H) response to an isotropic flux.

Figure C-2 shows a sketch of the experimental setup. B1 and B2 are two baffles, which collimate alphas from a source, S, along the edge of an imaginary cone of half angle,  $\theta$ . D' and D'' are flight spare detectors similar to D2 and D5 respectively. By

Figure C-1

The pattern of planes and axes in silicon within  $30^\circ$  of the  $\langle 110 \rangle$  axis with Miller indices of 3 or less. The small circle at the centre indicates the orientation of the D2 axis of symmetry. The large circle of radius,  $23^\circ$ , indicates the range of incident directions of particles which can have range D25(H).

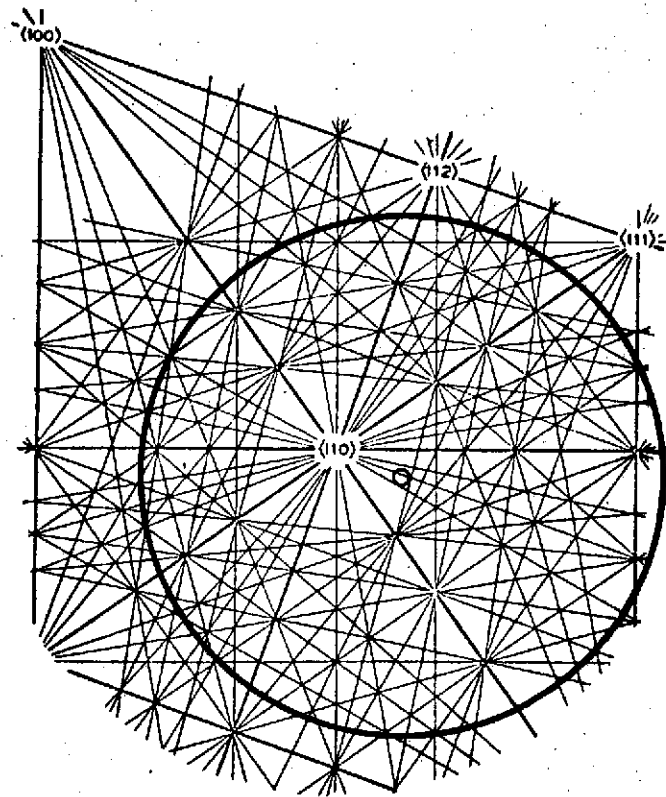
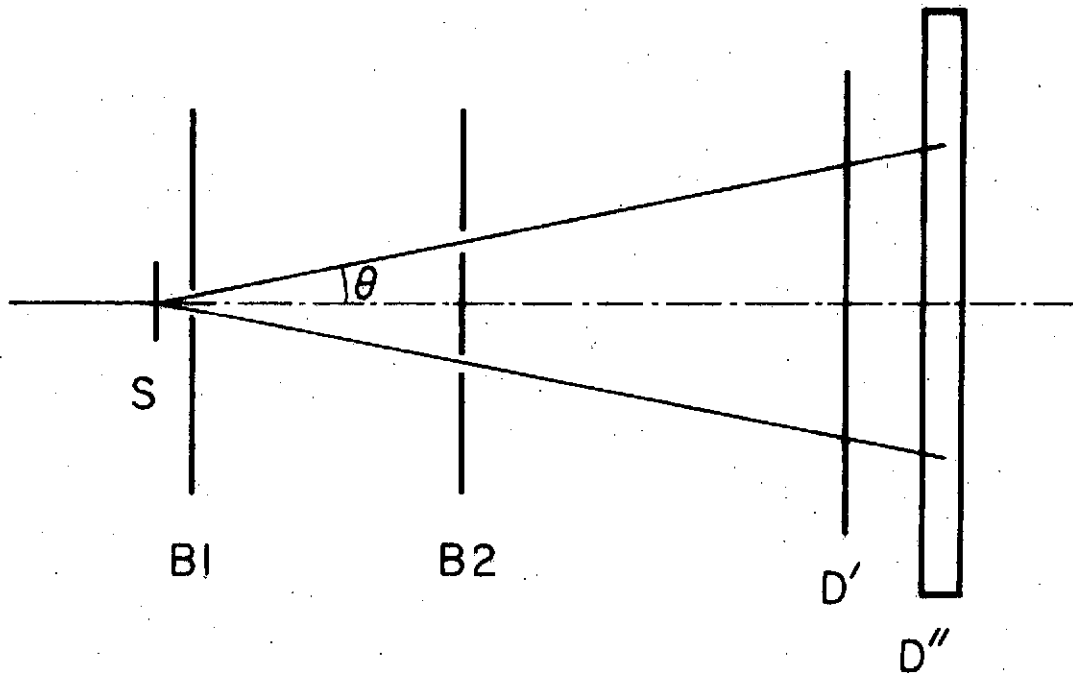


Figure C-2

Schematic cross section of channeling experiment setup, showing alpha source, S, baffles B1 and B2 and detectors D' and D". The entire setup is cylindrically symmetric about the horizontal axis.



varying the distance between B1 and B2, the angle  $\theta$  can be adjusted. By removing the solid centre of baffle, B2, all angles up to  $\theta$  can be included in the beam. In all cases the beam illuminates only the fully active areas of D' and D". D' and D" are simultaneously pulse height analysed by the 'PACE system' electronics (Marshall, 1974b), with individual pulse height pairs recorded on tape. The effective channel widths of 40 kev are similar to those used for D2 and D5.

Figure C-3 shows a typical raw plot of the observed number of events as a function of the D' and D" energy loss. By restricting further consideration to those events which fall between the double diagonal lines (i.e., particles whose total detected energy is  $8.785 \pm 0.12$  MeV), background events such as those due to scattering off the collimator,  $\alpha - \alpha$ ,  $\beta - \alpha$  and  $\gamma - \alpha$  coincidences are eliminated. The remaining data can be expressed as a mass histogram.

Such histograms for typical runs are shown in Figure C-4. Since the histograms for all runs are calculated assuming a fixed average D' thickness, the peak position for a given run will depend on the D' pathlength appropriate to that run. The peak shift to higher masses as  $\theta$  increases merely reflects the longer pathlength in D' due to both secant  $\theta$  and the thicker part of the D' radial profile that is sampled. More significant, however, is the rise of the low mass background due to alphas which channel along one of the planes. As Figure C-1 suggests, larger values of  $\theta$  permit more of the major crystal planes to be illuminated.

Figure C-3

Raw plot of the number of observed events as a function of the D' and D'' energy loss. Letters\* are used in a logarithmic scale when the number of events exceeds 9 so that the highest letter, X, represents almost 5000 events out of the total of 21276 plotted.  $\theta$  was constrained to the range 6.4-8.6 degrees. The double diagonal lines represent constant values of the (D' + D'') energy loss sum of  $8.785 \pm 0.12$  MeV. Events outside these limits are disregarded in subsequent analysis steps. Channeling extends the distribution of energy losses in D' down to 2 MeV compared to an average energy loss of almost 6 MeV.

---

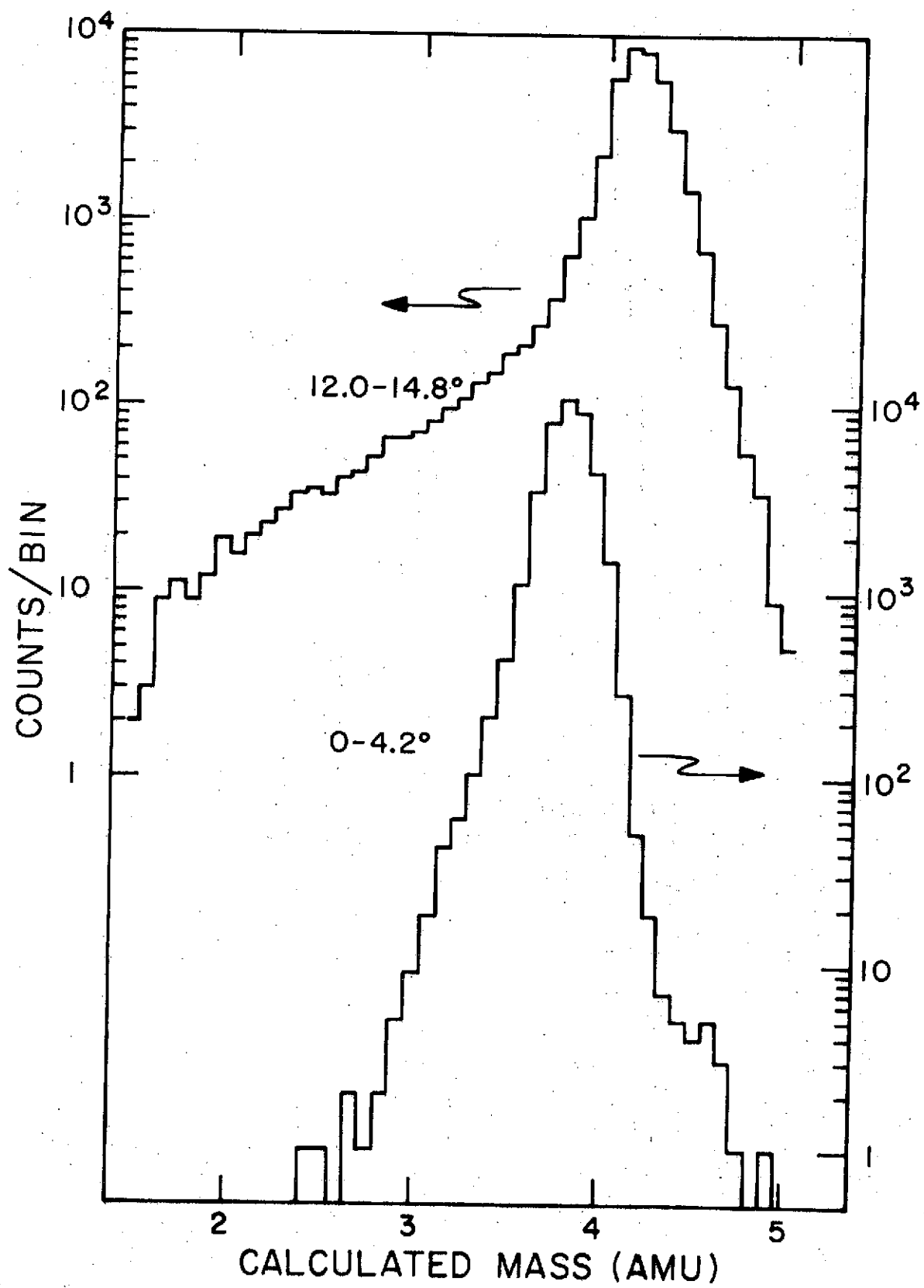
\*The average number of events associated with each letter is as follows:

A $\approx$ 11	D $\approx$ 27	G $\approx$ 65	K $\approx$ 150	R $\approx$ 874	V $\approx$ 2766
B $\approx$ 15	E $\approx$ 37	H $\approx$ 87	M $\approx$ 277	S $\approx$ 1166	W $\approx$ 3689
C $\approx$ 20	F $\approx$ 49	J $\approx$ 116	Q $\approx$ 656	U $\approx$ 2074	X $\approx$ 4919



Figure C-4

Mass histograms for typical channeling experiment runs. Only the events with total detected energy between  $8.785 \pm 0.12$  MeV are included. The  $\theta$  limits associated with each histogram are shown.



Constructing a weighted average of 11 such histograms for angles from 0 to  $24^\circ$  leads to the mass histogram shown in Figure C-5, which represents the D'-D'' response to an isotropic flux of 8.785 MeV alphas, with collimation similar to that provided by D0 and D4.

### 3. Application to Flight Data

The alpha stimulus of a 50 micron detector whose response is shown in Figure C-5 differs from that for flight data in two respects. First, Figure C-5 represents the response to 8.785 MeV alphas whereas the corresponding energy for flare particles varies from 8 to 51 MeV. Second the mass resolution of the laboratory experiment (Figure C-5,  $\sigma_m = 0.25$  amu) is noticeably worse than that for flight data (Figure III-2,  $\sigma_m = 0.17$  amu). This is due to the combined effects of secant  $\theta$  and the radial thickness dependences of D2 or D'. Whereas in Section II-D it was seen that these effects tend to cancel for the flight configuration, in the laboratory experiment they tend to combine linearly (viz, at larger  $\theta$ 's, the thicker part of D' is sampled).

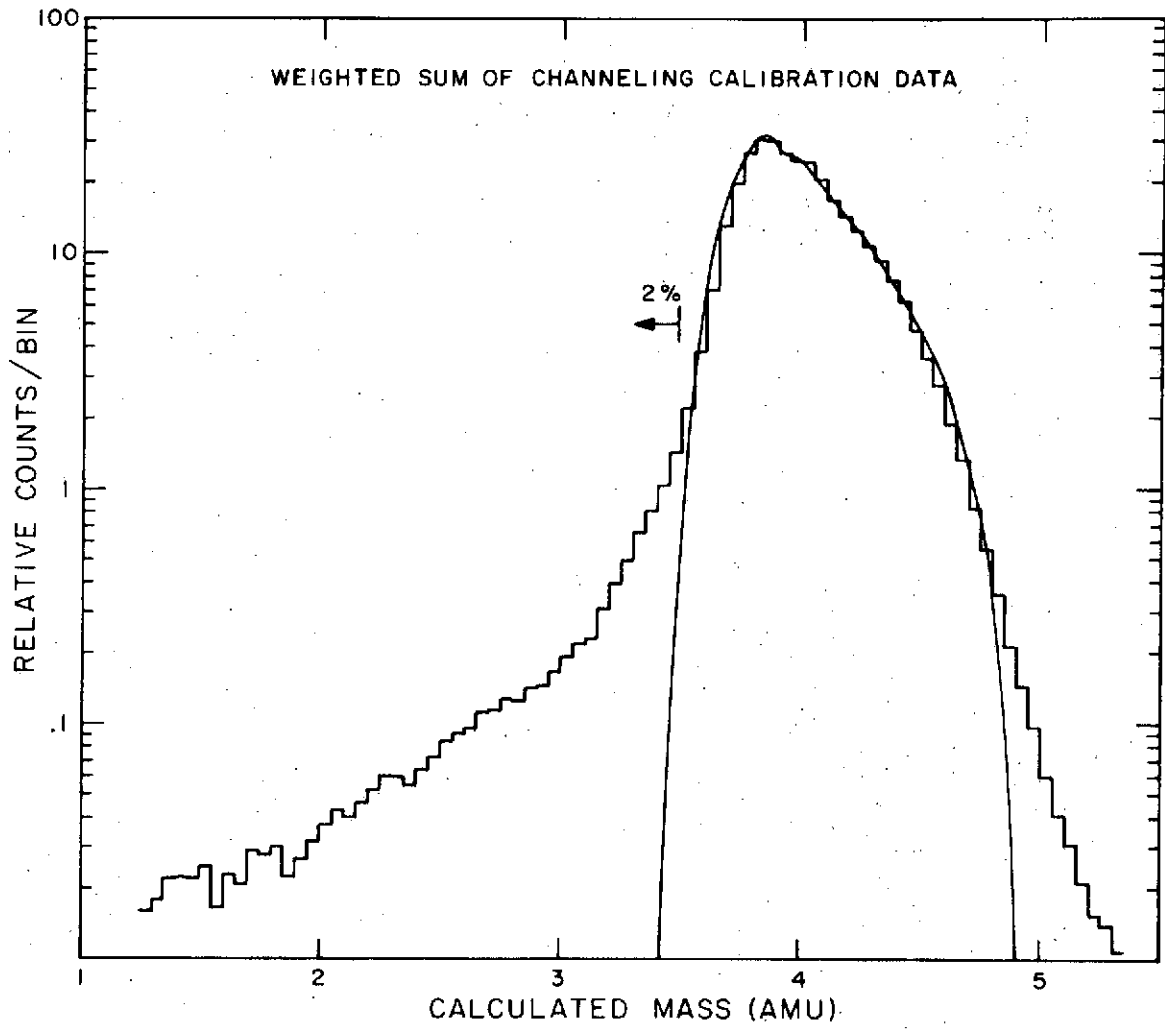
The role of this resolution difference can be evaluated by means of a Monte Carlo program which simulates the response of D' and D'' to incoming alphas, with due allowance paid to all the contributions to mass resolution outlined in Section II-D (except for channeling). The output is analagous to that of the experiment itself. Analyzing such data in an identical manner yields the smooth curve shown in Figure C-5. It is seen that except for the tails of the distribution, the mass response of the experiment is well understood. The high mass tail, containing  $\sim 10^{-3}$  of the total is due

Figure C-5

Weighted average of 11 mass histograms to simulate the D' - D'' response to an isotropic flux of 8.785 MeV alphas, with collimation similar to that provided by D0 and D4.

The smooth curve represents the expected response of the D' - D'' system allowing for all factors except channeling.

The low mass tail, containing about 2% of the total is due to channeling.



to elastic  $\alpha$  - Si nuclear collisions in D'. Since it does not affect the response below  $M = 4$ , it will not be considered further. About 2% of the particles have an abnormally low calculated mass (viz, low D' energy loss) due to channeling. This component, which dominates below  $M = 3.5$ , can be used directly to predict the channeling response of the D2-D5 system to an isotropic flux of alphas with energies near 8.785 MeV. Above  $M = 3.7$ , the channeling component can be neglected compared to other resolution mechanisms, and the response of the D2-D5 system can be adequately modelled by the Monte Carlo program.

While the alpha response for D25(H) events near  $M = 3$  is given by the channeling data in Figure C-5 for energies near 8.785 MeV, the channeling response to alphas of other energies cannot be established without either further calibration data or a model with which to determine the energy dependence of this response. While certain aspects of the energy dependence of the channeling process are well established,\* any model applicable to the D25(H) system must also include dechanneling effects.†

---

\* For example, the acceptance angle for planar channeling has an  $E^{-1/2}$  dependence on the energy of the incident ion (eg. Barrett, as reported in Chapter III of Morgan, 1973). For an isotropic flux this might be interpreted as the energy dependence of the channeling probability. Also Eisen et al. (1972) has shown that above  $\sim 5$  MeV, the ratio of the ionization energy loss rates for channeling and randomly oriented particles is only a weak function of energy.

† After traveling a distance, D, a channeling particle may dechannel (ie revert to random motion through the crystal). Several experimenters (eg. Campinsano et al., 1972, Davies et al., 1968) have established that the distribution of D is exponential with a characteristic half depth which is proportional to energy. For 10 MeV alphas, this half depth is  $\sim 10$  microns.

Although models of the energy dependence can be constructed on such a basis and normalized to Figure C-5 at 8.785 MeV, their application to alphas with energies as high as 51 MeV is not sufficiently accurate<sup>‡</sup> to justify their use for quantitative background subtraction. Further isotropic channeling experiments are necessary to determine the channeling response at other energies.

---

<sup>‡</sup>This is because of the inherent resolution of 0.25 amu in Figure C-5 and the lack of channeling response data above  $M = 3.5$ . While these limitations are not important near 8.785 MeV, they become significant when scaled to higher energies.

## APPENDIX D. ESTIMATE OF BACKSCATTERED PROTON AND ALPHA SPECTRA

In the R&K thick target model of  ${}^3\text{He}$  production, a primary beam of protons, alphas and CNO nuclei is incident on an ambient solar atmosphere of similar composition. They calculate the spectrum of  ${}^2\text{H}$  and  ${}^3\text{He}$  produced in the backward lab hemisphere from inelastic proton-alpha collisions. In this appendix, an estimate is made of the corresponding backscattered proton spectrum, produced by elastic scattering of incident protons by the ambient helium.

Following R&K, the production spectrum of secondary particles can be expressed as,

$$N_s(E_s) = (n_t/n_H) \int N(>E) \frac{\sigma(E)}{m_p} \cdot (dE/dx)^{-1} \cdot f(E, E_s) \cdot dE \quad (\text{D-1})$$

where  $(n_t/n_H)$  is the number fraction of 'target nuclei';  $N(>E)$  is the number of particles in the primary beam with energy greater than  $E$ , normalized to  $N(>30\text{MeV}) = 1$ ;  $\sigma(E)$  is the total cross section that results in backscattered protons, as a function of primary energy,  $E$ ;  $m_p$  is the proton mass;  $dE/dx$  is the rate of ionization energy loss; and  $f(E, E_s)$  is the probability in the lab frame that the energy of the secondary particle will be in  $dE_s$  around  $E_s$ . Implicit in this formulation is the well satisfied assumption that only a small fraction of incident particles suffer a nuclear collision.

To estimate  $N_s(E_s)$ , each term in Equation D-1 can be approximated as discussed below.

Meyer (1971) has summarized the differential cross section data for proton-alpha elastic collisions between 2 and 1000 MeV. From this summary the total cross section for scattering incident protons into the backward lab hemisphere has been found to decrease with increasing energy according to the relation,  $\sigma(\text{barns}) = 3.2 E^{-1.25}$  (MeV), which is accurate to within 20% between 2 and 30 MeV.

From classical kinematics, the energy,  $E_s$ , of the backscattered proton, is constrained to the range,  $0.36E \leq E_s \leq 0.76E$ . Meyer's differential cross section summary further shows that the average recoil energy is in the range,  $0.58E \leq (E_s) \leq .65E$  for  $2 < E < 30$  MeV. Therefore setting  $f(E, E_s)$  equal to  $\delta(E_s - 0.6E)$  eliminates the integral in Equation D-1 while preserving the average energy of the backscattered protons. The shape of the resulting spectrum is not seriously compromised since both the primary and backscattered spectra are expected to be smooth.

Using the Janni range energy data for neutral hydrogen\* (Janni, 1966),  $dE/dx$  can be set equal to  $684 E^{-0.82}$  (MeV/g/cm<sup>2</sup>) between 1 and 100 MeV. Finally  $n_t/n_H$  is set equal to 7% to complete the correspondence with the R&K model.

Substituting these numerical parameters into Equation D-1 results in

$$N_s(E_s) = 2.6 \times 10^{-4} E_s^{-0.43} N(> E_s/0.6) \quad (\text{D-2})$$

---

\* Although neutral hydrogen does not necessarily provide the most appropriate range-energy relation, it is used here in order to be consistent with the R&K model.

Thus the yield of backscattered protons at energy,  $E_s$ , is proportional to the integral flux of primary protons above energy,  $(E_s/0.6)$ . The results for specific functional forms of the primary spectrum are discussed in Chapter IV.

Similar estimates might also be made for the yield of backward moving alphas. In this case there are two processes which should be considered. The first is the elastic scattering of alphas from the ambient CNO nuclei. The cross sections for this process are characterized by numerous resonances (John et al., 1969, Marvin and Singh, 1972, Tollefsrud and Jolivet, 1970). The average value of  $\sim 0.7$  barns at  $2 \frac{1}{2}$  MeV/nuc incident energy is about the same as 1 barn for the corresponding proton-alpha elastic scattering cross section into the backward lab hemisphere. Compared to the proton backscattered yield at  $1 \frac{1}{2}$  MeV, the corresponding alpha yield can be written

$$\frac{\text{Backscattered alphas}}{\text{Backscattered protons}} = \frac{n_{\text{CNO}} \cdot \sigma_{\alpha\text{-CNO}} \cdot N(\alpha > 2 \frac{1}{2} \text{ MeV/nuc})}{n_{\text{He}} \cdot \sigma_{\text{p-}\alpha} \cdot N(\text{p} > 2 \frac{1}{2} \text{ MeV})} \quad (\text{D-3})$$

Substitution of the cross section values given above and the ambient abundance ratios,  $n_{\text{CNO}}/n_{\text{He}} = 0.001/0.07$  shows that the alpha-proton ratio in the backscattered beam at  $1 \frac{1}{2}$  MeV/nuc is about  $10^2$  lower than their integral ratio in the primary beam. Thus even in the extreme case of primary  $\alpha/\text{p} \sim 50\%$ , backscattered ratios of only  $\sim 1/2\%$  are possible from this mechanism. Note that this one point estimate is not sensitive to the primary spectral shape.

A second source of backward moving alphas is CNO(p, $\alpha$ ) reactions. The cross sections for this process is somewhat larger than that for CNO(p,  $^3\text{He}$ )\* but the yield of the latter is  $\sim 2$  orders of magnitude lower than that of proton-alpha reactions (Lingenfelter and Ramaty, 1967). Therefore the total yield of alphas from proton-CNO reactions will certainly be smaller than the total yield of  $^3\text{He}$ , and so be unimportant in most cases.

---

\* For example at 8 MeV,  $\sigma_{^4\text{He}} \sim 60$  mb (Dangle et al., 1964) compared to  $\sigma_{^3\text{He}} \approx 11$  mb (R&K).

## REFERENCES

- Anglin, J. D., W. F. Dietrich and J. A. Simpson, "Solar Flare Accelerated Isotopes of Hydrogen and Helium," High Energy Phenomena on the Sun Symposium Proceedings, edited by R. Ramaty and R. G. Stone, NASA SP-342, 315, 1973a.
- Anglin, J. D., W. F. Dietrich and J. A. Simpson, "Deuterium and Tritium from Solar Flares at  $\sim 10$  MeV per Nucleon," Ap. J., 186, L41, 1973b.
- Anglin, J. D., J. A. Simpson and R. Zamow, "Solar Flare  $^2\text{H}$ ,  $^3\text{H}$  and  $^3\text{He}$ ," Bull. Am. Phys. Soc., 19, 457, 1974.
- Biswas, S. "The Composition of Solar Particle Radiation," Proc. Intern. Conf. Cosmic Rays, Jaipur, December 1963, I, 43, 1964.
- Cameron, A. G. W., "Abundances of the Elements in the Solar System" Space Sci. Rev., 15, 121, 1973.
- Campinsano, S. U., G. Foti, F. Grasso, M. Lo Savio and E. Rimini, "Lindhard's Multiple Scattering Description Justifies Axial and Planar Dechanneling Data," Radiation Effects, 13, 157, 1972.
- Chupp, E. L., D. J. Forrest, P. R. Higbie, A. N. Suri, C. Tsai, and P. P. Dunphy, "Solar Gamma Ray Lines observed during the Solar Activity of August 2 to August 11, 1972." Nature, 241, 333, 1973.
- Dangle, R. L., L. D. Oppliger and G. Hardie, " $^{16}\text{O}(p,\alpha)^{13}\text{N}$  and  $^{16}\text{O}(p,p')^{16}\text{O}$  Differential Cross Sections," Phys. Rev., 133, B647, 1964.
- Davies, J. A., J. Denhartog and J. L. Whitton, "Channeling of MeV Projectiles in Tungsten and Silicon," Phys. Rev., 165, 345, 1968.
- Dietrich, W. F., "The Differential Energy Spectra of Solar Flare  $^1\text{H}$ ,  $^3\text{He}$  and  $^4\text{He}$ ," Ap. J., 180, 955, 1973.
- Eisen, F. H., G. J. Clark, J. Bottiger and J. M. Poate, "Stopping Power of Energetic Helium Ions Transmitted Through Thin Silicon Crystals in Channeling and Random Directions," Radiation Effects, 13, 93, 1972.
- Epstein, S. and H. P. Taylor, Jr., " $^{18}\text{O}/^{16}\text{O}$ ,  $^{30}\text{Si}/^{28}\text{Si}$ , D/H and C  $^{13}/\text{C}^{12}$  ratios in lunar samples," Proc. of the Second Lunar Science Conf., 2, (MIT Press, Cambridge, Mass.), 1421, 1971.
- Garrard, T. L., "Caltech Energetic Particles Experiments on IMP's H & J," Space Radiation Laboratory Internal Report #50, Calif. Inst. of Technology, 1974a.

- Garrard, T. L., "Abstraction of IMP Tapes," Space Radiation Laboratory Internal Report #52, Calif. Institute of Technology, 1974b.
- Garrard, T. L., "General Overview of IMP Data Processing," Space Radiation Laboratory Internal Report #59, Calif. Inst. of Technology, 1974c.
- Garrard, T. L., and G. J. Hurford, "IMP-H Experiment Tape Data Format," Space Radiation Laboratory Internal Report #43, Calif. Inst. of Technology, 1973.
- Garrard, T. L., and A. Petruncola, "STRIP Program User's Guide," Space Radiation Laboratory Internal Report #49, Calif. Inst. of Technology, 1973.
- Garrard, T. L., E. C. Stone and R. E. Vogt, "The Isotopes of H and He in Solar Cosmic Rays," High Energy Phenomena on the Sun Symposium Proceedings, edited by R. Ramaty and R. G. Stone, NASA SP-342, 341, 1973a.
- Garrard, T. L., E. C. Stone and R. E. Vogt, "The Isotopes of H and He in Solar Cosmic Rays," Conf. Papers 13th Int. Cosmic Ray Conf. Denver, 2, 1485, 1973b.
- Geiss, J., and H. Reeves, "Cosmic and Solar System Abundances of Deuterium and Helium-3," Astron. & Astrophys., 18, 126, 1972.
- Gemmell, D. S., "Channeling and Related Effects in the Motion of Charged Particles through Crystals," Rev. Mod. Phys., 46, 129, 1974.
- Grevesse, N., "Deuterium in the Solar Photospheric Spectrum," Mem. Soc. R. Sci. Liege, 19, 249, 1970.
- Hartman, S., "Geometrical Factors for IMP-H," Space Radiation Laboratory Internal Report #45, Calif. Inst. of Technology, 1973.
- Hsieh, K. C. and J. A. Simpson, "The Relative Abundance and Energy Spectra of  $^3\text{He}$  and  $^4\text{He}$  from Solar Flares," Ap. J., 162, L191, 1970.
- Hurford, G. J., "ATS-the Abstract Tape Summary Program," Space Radiation Laboratory Internal Report #58, Calif. Inst. of Technology, 1974a.
- Hurford, G. J., "IMP-H Tandem Calibrations," Space Radiation Laboratory Internal Report #60, Calif. Inst. of Technology, 1974b.
- Hurford, G. J., R. A. Mewaldt, E. C. Stone and R. E. Vogt, "The Energy Spectrum of 0.16 to 3 MeV Electrons during Solar Quiet Times," Conf. Papers 13th Int. Cosmic Ray Conf. Denver, 1, 324, 1973a.

- Hurford, G. J., R. A. Mewaldt, E. C. Stone and R. E. Vogt, "Observations of the Ratio of Low Energy Cosmic-Ray Positrons and Electrons during Solar Quiet Times," Conf. Papers 13th Int. Cosmic Ray Conf. Denver, 1, 330, 1973b.
- Hurford, G. J., R. A. Mewaldt, E. C. Stone and R. E. Vogt, "Measurements of the Flux of Low-Energy Solar Flare Positrons," Conf. Papers 13th Int. Cosmic Ray Conf. Denver, 2, 1613, 1973c.
- Hurford, G. J., R. A. Mewaldt, E. C. Stone and R. E. Vogt, "Observations of Low Energy Hydrogen and Helium Isotopes During Solar Quiet Times," Conf. Papers 13th Int. Cosmic Ray Conf. Denver, 1, 93, 1973d.
- Hurford, G. J., R. A. Mewaldt, E. C. Stone and R. E. Vogt, "Observations of H and He in Solar Cosmic Rays," talk presented at the Tucson Meeting of the American Physical Society, Dec. 6-8, 1973e.
- Hurford, G. J., R. A. Mewaldt, E. C. Stone, S. B. Vidor and R. E. Vogt, "The Isotopic Composition of 5 to 12 MeV/nucleon Cosmic Ray Nitrogen and Oxygen Nuclei," Bull. Am. Phys. Soc., 19, 433, 1974a.
- Hurford, G. J., R. A. Mewaldt, E. C. Stone and R. E. Vogt, "The Energy Spectrum of 0.16 to 2 MeV Electrons during Solar Quiet Times," Ap. J., 192, 541, 1974b.
- Janni, J. F., "Calculations of Energy Loss, Range, Pathlength, Straggling, etc.," Tech. Report AFWL-TR-65-150, 1966.
- John, J., J. P. Aldridge and R. H. Davis, "Phase Shift Analysis of  $^{16}\text{O}(\alpha,\alpha)^{16}\text{O}$  Scattering from 5 to 10 MeV," Phys. Rev., 181, 1455, 1969.
- Jung, M., Y. Sakamoto, J. N. Suren, C. Jacquot, L. Girardin and R. Schmitt, "Proton-Alpha-Particle Inelastic Channels at Medium Incident Energies," Phys. Rev., C7, 2209, 1973.
- Leighton, H. I. ed., Solar-Geophysical Data, vol. 338-358, U. S. Dept. of Commerce, Boulder, Colo., 1973-4.
- Lingenfelter, R. E. and R. Ramaty, "High-Energy Nuclear Reactions in Solar Flares," High-Energy Nuclear Reactions in Astrophysics, ed. B. S. P. Shen (W. A. Benjamin, Inc., New York), 99, 1967.
- Marshall, F., "Adiabatic Energy Loss of Solar-Cosmic-Ray Protons," Space Radiation Laboratory Internal Report #44, Calif. Inst. of Technology, 1974a.
- Marshall, F., "Varian Software for PACE System," Space Radiation Laboratory Internal Report #57, Calif. Inst. of Technology, 1974b.

- Marvin, T. P. and P. P. Singh, "Energy Levels of  $^{16}\text{O}$  between 10.0 and 17.1 MeV Excitation," Nucl. Phys., A180, 282, 1972.
- Mewaldt, R. A., E. C. Stone and R. E. Vogt, "The Time Variation of 5-11 MeV/nucleon Cosmic Ray Nitrogen and Oxygen Nuclei," Bull. Am. Phys. Soc., 19, 433, 1974.
- Mewaldt, R. A. and S. Vidor, "Electronic Calibrations of the IMP-H & J EIS," Space Radiation Laboratory Internal Report #56, Calif. Inst. of Technology, 1974.
- Meyer, J. P., "Deuterons and  $\text{He}^3$  Formation and Destruction in Proton Induced Spallation of Light Nuclei ( $Z \leq 8$ )," Astron. Astrophys. Suppl., 7, 417, 1972.
- Morgan, D. V., ed., "Channeling, Theory, Observation and Applications," John Wiley and Sons, New York, 1973.
- Murray, S. S., "Propagation of 1-10 MeV Solar Protons in Interplanetary Space," Ph.D. Thesis, Calif. Inst. of Technolgy, 1970.
- Northcliffe, L. C. and R. F. Schilling, "Range and Stopping-Power Tables for Heavy Ions," Nuclear Data Tables, A7, 233, 1970.
- Palmer, I. D., "Energy Losses of Solar Cosmic Rays in Interplanetary Space," Solar Physics, 30, 235, 1973.
- Ramaty, R. and B. Kozlovsky, " $\text{H}^2$ ,  $\text{H}^3$  and  $\text{He}^3$  Production in Solar Flares," GSFC Preprint # X-660-74-94, 1974.
- Roelof, E. C., "On the Measurement of Energetic Particle Flux Anisotropies With a Class of Spinning Detectors," J. Geophys. Res., 79, 1535, 1974.
- Rothwell, P. L., L. Katz, B. Sellers and F. A. Hansen, "Upper Limits to Flare-Produced Deuterium and Tritium," Phys. Rev. Lett., 31, 407, 1973.
- Schaeffer, O. A. and J. Zahringer, "Solar Flare Helium in Satellite Materials," Phys. Rev. Lett., 8, 389, 1962.
- Seltzer, S. M. and M. J. Berger, "Energy Loss Straggling of Protons and Mesons: Tabulation of the Vavilov Distribution," Studies in Penetration of Charged Particles in Matter, NAS-NRC-Publication 1133, 187, 1964.

Tollefsrud, P. B. and P. L. Jolivet, "<sup>18</sup>F States with Large Isospin Impurities," Phys. Rev., Cl, 398, 1970.

Vorona, J., J. W. Olness, W. Haerberli and H. W. Lewis, "Levels of P<sup>29</sup> from Si<sup>28</sup> (p, p) Si<sup>28</sup> and Si<sup>28</sup> (p, p') Si<sup>28</sup>," Phys. Rev., 116, 1563, 1959.

Waddington, C. J. and P. S. Freier, "Relative Abundances of Energetic Hydrogen Isotopes Produced in Solar Flares," Phys. Rev., 136, B1535, 1964.